TAMPERE UNIVERSITY OF TECHNOLOGY

KARINA MAGALY ESPEJO DELZO

RFID TAGS MOUNTABLE ON METALLIC SURFACE

Master of Science Thesis

Examiners: Adjunct Professor Leena Ukkonen and Professor Lauri Sydänheimo
Examiners and topic approved in the Computing and Electrical Department Council meeting on 8 September 2010.

ABSTRACT

TAMPERE UNIVERSITY OF TECHNOLOGY
Master's Degree Program in Radio Frequency Electronics
ESPEJO DELZO, KARINA MAGALY: RFID Tags Mountable on Metallic Surface.
Master of Science Thesis, 90 pages, 5 Appendix pages
October 2010
Major: Radio Frequency Electronics
Examiners: Adjunct Professor Leena Ukkonen and Professor Lauri Sydänheimo
Keywords: Radio frequency identification technology, RFID, tag antenna, surface wave, metal surface, patch antenna.

The Radio Frequency Identification (RFID) technology in the UHF band is a growing technology with a variety of applications in the market. The purpose of this technology is the identification of certain "object" or objects at longer distances, cheap cost and durability. This is achieved by attaching a tag antenna to the "object". Passive UHF tag antennas fulfill these requirements, mainly due to cheap fabrication and durability. Nevertheless, the identification distance is sensitive to the object material properties.

If this "object" is a metal surface, the tag antenna radiation properties change due to reflections that propagating wave under on metal surface. There is performance degradation in the tag antenna hence shorter identification range is achieved. Some proposals to overcome the metal surface effects over tag antennas are mentioned. Moreover, a survey of different UHF patch tag antenna design is reviewed and finally the appropriate tag patch antenna is chosen for design and construction.

It is one purpose of this thesis to introduce a new design of passive UHF patch tag antenna. The main design objective of this antenna is the immunity of operating frequency and radiation properties on metal surface. The dielectric constant, thickness, and dimensions of the proposed tag antenna are based on a compromise between bandwidth and radiation efficiency. This tag antenna is simulated in electromagnetic simulators HFSS and CEMS; and measured in anechoic chamber of RFID cabinet and by the read range technique. The simulation results between HFSS and CEMS shows good agreement. This enhances the reliability of the new tag antenna design.

Some parameters of the proposed tag antenna are measured and compared with the simulation results. This tag antenna placed on metal surface 200x200 mm^2 achieves a maximum read range of 18m and realized gain of 6 dBi at 935 MHz.

As future work an improvement in the size reduction should be explored.

PREFACE

This thesis work was done at Tampere University of Technology (TUT) in the Electronics Department. My research is based on the design of a patch tag antenna that works on metal surface for the ultra high frequency (UHF) band in the scope of the radiofrequency identification technology (RFID). This topic was introduced to me by my supervisors, Adjunct Professor Leena Ukkonen and Professor Lauri Sydänheimo. During January to August 2010, I worked on the simulation and measurement of an UHF patch tag antenna mountable on metal surface. This tag antenna is designed based on an electromagnetic simulator provided by the RFID Lab at TUT and by CEMS software provided by Professor Atef Elsherbeni from the department of Electrical Engineering of the University of Mississippi. The tag antenna is constructed in the Rauma Research Unit and measured in the RFID Lab at TUT.

I wish to acknowledge to my supervisors Leena Ukkonen and Lauri Sydänheimo for the continuous support and confidence during my work. The opportunity to work in a research group that is very active on RFID field; inspired me to learn intensive for my thesis. I express my sincere gratitude to Prof. Atef Elsherbeni for his valuable support in teaching the CEMS simulator and reviewing the thesis. His valuable feedback on the whole thesis stage motives me to continue improving my work. I also would like to acknowledge and thanks two of my main teachers in the master program: Olli-Pekka Lundén and Jari Kangas, for transmitting your knowledge, patient and support as teachers and friends.

I would like thanks to Toni Björninen for reviewing also my thesis and answer many of my doubts related to RFID technology. Thanks Juha Virtanen for teaching me how to use HFSS software, for supporting in any enquiry and for some funny comments you always have in mind. Special thanks to Ali Babar, for helping me in the construction of the tag antenna. And huge thanks to all the RFID group for the collaboration, feedback and friendship during this work: Nebiat Awano, Anabel Perez, Karolina Koski and Evelina Koski. I also would like thank to all my friends of the master's program for having a great time during these two years!

Finally, my sincere gratitude to God for let me achieve this dream, thanks to my parents Juan and Nelly, my brothers Chavito and JC; and to my beloved Gustavo for your love, support and comprehension every day.

Enjoy it!

Tampere, September 2010

KARINA ESPEJO DELZO
caphri@hotmail.com

CONTENTS

1. INTRODUCTION 1
1.1 Scope of the thesis 1
1.2 Outline of the thesis 2
2. THE RFID TECHNOLOGY 4
2.1 Common RFID implementation 4
2.2 Classification of RFID systems 5
2.3 Radio regulations and standards 7
2.4 Near-field and far-field RFID 9
3. ELECTROMAGNETIC THEORY 10
3.1 The Maxwell laws 10
3.1.1 The constitutive properties of the medium 11
3.1.2 Boundary conditions of electromagnetic fields 12
3.2 Power flow and poynting vector 13
3.3 The uniform plane waves 15
3.3.1 Lossless media and lossy media 15
3.3.2 Effective permittivity and effective conductivity 16
3.3.3 Skin depth 17
3.3.4 Polarization of uniform plane waves 17
3.3.5 Propagation of uniform plane waves at boundary surface 18
3.4 Perfect electric and magnetic conductor 21
3.5 Surface waves 22
3.6 The rectangular waveguide 23
4. RECTANGULAR PATCH ANTENNA 25
4.1 Fundamental parameters of antenna 25
4.1.1 The effective aperture and radar cross section 28
4.1.2 Radar range equation 28
4.2 Analysis models for a rectangular microstrip antenna 29
4.2.1 The transmission line model 31
4.2.2 The cavity model 33
4.3 Electromagnetic modeling simulators 34
4.4 Design considerations for a rectangular patch antenna 41
5. PASSIVE FAR FIELD RFID TAG 43

5.1 Operation of far field RFID system 43
5.2 Matching Impedance and Power Reflection Coefficient 45
5.3 Link budget applied to measurement setup 49
6. METAL SURFACE EFFECTS ON UHF PATCH TAG ANTENNA 53
6.1 Solution proposals 53
6.2 Review of different RFID patch tag antenna designs 57
7. EXPERIMENTAL UHF PATCH TAG ANTENNA 66
7.1 Antenna Design Process 66
7.2 Simulation results in CEMS and HFSS 70
7.3 Simulation and measurement results 74
7.3.1 Transmitted power and read range measurement 74
7.3.2 Realized gain and radiation pattern result 78
8. CONCLUSIONS 82
REFERENCES 84
APPENDIX 1: Survey of different patch antenna mountable on metallic objects 91
APPENDIX 2: The problem parameter definition in CEMS. 92
APPENDIX 3: UHF Patch tag antenna measured with linear and circular polarized antenna 94
APPENDIX 4: Simulation performance result from HFSS of patch tag antenna in free space and on metal surface 95

SYMBOLS

$\boldsymbol{E}$	Electric field intensity (V/m)
$\boldsymbol{D}$	Electric flux density (C/m^2)
$\boldsymbol{P}$	Polarization vector (C/m^2)
$\boldsymbol{H}$	Magnetic field intensity (A/m)
$\boldsymbol{B}$	Magnetic flux density (T or Wb/m^2)
$\boldsymbol{M_p}$	Magnetic polarization vector (A/m)
$\boldsymbol{M}$	Magnetic current density vector (V/ m^2)
$\boldsymbol{M_c}$	Conductive magnetic current density (V/ m^2)
$\boldsymbol{M_i}$	Impressed or source magnetic current density (V/ m^2)
$\boldsymbol{J}$	Electric current density vector (A/m^2)
$\boldsymbol{J_c}$	Conduction current density vector (A/m^2)
$\boldsymbol{J_i}$	Impressed or source current density vector (A/m^2)
J_{sn}	Surface current density normal to a surface (A/m)
n_{pml}	Order of propagation
k_{ei}	Propagation constant factor, electric and along “i” direction
k_{mi}	Propagation constant factor, magnetic and along “i” direction
k_{max}	Maximum propagation constant factor
σ_{pei}	Conductivity factor, electric and along “i” direction
σ_{mei}	Conductivity factor, magnetic and along “i” direction
σ_{max}	Maximum conductivity scaling, for CPML definition
σ_{factor}	Conductivity factor, for CPML definition
σ_{opt}	Optimum conductivity, for CPML definition
α_{ei}	attenuation factor, electric and along “i” direction
σ_{mei}	Attenuation factor, magnetic and along “i” direction
α_{min}	Minimum attenuation factor for CPML
α_{max}	Maximum attenuation factor for CPML
ρ	Electric Charge density (C/ m^2) ; distance from the computational domain-CPML to the position of the field components (m)
ρ_e	Electric charge density (C/ m^2 or C/ m^3)
ρ_m	Magnetic charge density (Weber/ m^3)
ρ_s	Surface charge density(C/m^2)
μ	permeability (H/m)
μ_{r}	Relative permeability (H/m)
μ_0	Permeability in free space (H/m)
χ_m	Magnetic susceptibility
χ_e	Electric susceptibility

ε	Permittivity (F/m), in general refer to electric permittivity
$\hat{\varepsilon}$	Complex permittivity (F/m)
$\varepsilon^{'}, \varepsilon_{eff}$	Effective permittivity (F/m)
ε_0	Permittivity in free space (F/m)
ε_r	Relative permittivity (F/m)
χ_e	Electric susceptibility
σ^e, σ	Electric conductivity(S/m)
σ^m	Magnetic conductivity (Ω/m)
σ	Electric conductivity (S/m) or radar cross section (m^2)
ω	Radial frequency (rad/s)
S_{ei}	Electric complex stretching value in "i" direction
S_{mi}	magnetic complex stretching value in "i" direction
$\boldsymbol{a}_n$	Unitary vector normal to the surface
$\boldsymbol{S}$	Poynting vector (W/m^2)
$\boldsymbol{S}_r$	Poynting vector in radial direction(W/m^2)
$\boldsymbol{S_{av}}$	Average power density (W/m^2)
$\boldsymbol{S}_0$	Average power density of an isotropic radiator (W/m^2)
$P_{radiated}$	Power radiated by a source (W)
P_rad	Average power radiated by a source (W)
$\hat{\boldsymbol{x}}$	Unit vector along the "x" direction.
$\hat{\boldsymbol{y}}$	Unit vector along the "y" direction.
$\hat{\boldsymbol{z}}$	Unit vector along the "z" direction.
$\boldsymbol{E}_x$	Electric field vector in the $\hat{\boldsymbol{x}}$ direction (V/m)
$\boldsymbol{H}_y$	Magnetic field vector in the $\hat{\boldsymbol{y}}$ direction (V/m)
E_m^+	Amplitude of the electric field in positive $\hat{\boldsymbol{x}}$ direction (V/m)
H_m^+	Amplitude of magnetic field in positive $\hat{\boldsymbol{y}}$ direction (A/m)
γ	Propagation constant
α	Attenuation constant (Np/m)
α_2	Attenuation factor in medium 2 (Np/m)
$\hat{n}$	Complex intrinsic impedance (Ω)
$tan\delta$	Loss tangent
δ	Skin depth (m) , thickness of the CPML layer
β	Phase constant (rad/m)
θ	Phase angle (rad)
ɯ	Phase velocity (m/s)
λ	Wavelength (m)
θ_i	Angle between incident wave and normal of the boundary (degree)
θ_r	Angle between reflected wave and normal of the boundary (degree)
θ_t	Angle between transmitted wave and normal of the boundary (degree)

θ_c	Critical angle (degree)
$\hat{\Gamma}$	Reflection coefficient, expressed in phasor form
m, n	Order modes of propagation
R	Radio of a sphere (m)
r	Distance from the transmitted antenna (m)
d	Distance from the antenna to the metal surface (m)
e_0	Antenna efficiency
e_{cd}	Antenna radiation efficiency
e_r	Antenna reflection efficiency
$U(\theta, \phi)$	Radiation intensity (W)
U_0	Isotropic radiation intensity (W)
$D(\theta, \phi)$	Directivity of an antenna in a given direction
D_{max}	Maximum directivity of an antenna for the maximum direction of the radiation pattern.
$G(\theta, \phi)$	Gain of an antenna in a given direction (dBi)
G_r	Realized gain (dBi)
A_e	Antenna effective aperture (m^2)
$\widehat{\boldsymbol{\rho}}_{\boldsymbol{w}}$	Direction of polarization of an arbitrary traveling wave
$\widehat{\boldsymbol{\rho}}_{\boldsymbol{a}}$	Direction of polarization of an antenna
ψ_p	Angle formed by the unitary vectors $\widehat{\boldsymbol{\rho}}_{\boldsymbol{w}}, \widehat{\boldsymbol{\rho}}_{\boldsymbol{a}}$ (rad)
P_t	Transmitted power (W)
P_r	Power delivered to the load in receiver antenna (W)
h	Dielectric thickness
L	Length of the antenna
L_e	Total electrical length of a microstrip antenna
W	Width of the antenna
$\Delta x, \Delta y, \Delta z$	Cell size of a cube in the x, y and z direction
Δt	Time step
Z_{IC}	Equivalent impedance of the integrated chip.
Z_{state2}	Equivalent impedance in other state of the integrated chip.
f_o	Operating frequency (Hz)
Q	Quality factor
e	Complex stretching value / Neper number

ABBREVIATIONS

ABC	Absorbing Boundary Condition. Artificial boundary to simulate the solution in an open domain.
ASK	Amplitude Shift Keying. It is a modulation that represents digital data as variations in the amplitude of a carrier wave.
CDMA	Code Division Multiple Access. It is a radio channel access method used in a radio communication.
CEMS	Computational Electromagnetic Simulator. Software developed by the University of Mississipi
CPML	Convolutional Perfect Match Layer. Extension of Perfect Match Layer.
CW	Continuous Wave. An electromagnetic wave with constant amplitude and phase
CPW	Coplanar waveguide
DSB	Double Side Band. It is an amplitude modulation in which the modulated wave is composed of carrier, upper sideband and lower sideband.
EAN	Equivalent Admittance Network. It represents the equivalent circuit of the fringing field.
EIRP	Equivalent Isotropic Radiated Power. It is the amount of power that theoretical isotropic antenna should radiate in order to radiate with the peak power density observed in the direction of maximum antenna gain
ERP	Equivalent Radiated Power. It is a standardized theoretical measurement of radio frequency energy.
EPC	Electronic Product Code. It is a family of coding schemes for use with RFID tags created as a complement to the barcode.
EPCglobal	It is an organization set up to achieve worldwide adoption and standardization of EPC technology.
ETSI	European Telecommunications Standards Institute. It is an institution that produces globally-applicable standards for information and communication technology (ICT), including fixed, mobile, radio, converged, broadcast and internet technologies.
EBG	Electromagnetic Band Gap. Material designed to prevent the propagation of a designed bandwidth of frequencies

FCC	Federal Communication Commission. It is an independent United States government agency in charged with regulating interstate and international communications by radio, television, wire, satellite and cable.
FM0	Bi-phase space. It is a coding scheme used in RFID system
FEM	Finite Element Method. It is a numerical technique that solves the integral form of Maxwell's equation in frequency domain
FDTD	Finite Difference Time Domain. It solves the differential time domain Maxwell's equations.
HFSS	High Frequency Simulator Solver
HIS	High Impedance Surface. It prevents the propagation of radio frequency surface current within the band gap.
IC	Integrated circuit. It is a miniaturized electronic circuit that holds information to which it is attached. It is the responsible for the communication from tag to reader.
IEC	International Electronical Commission. It is the organization that prepares and publishes International Standards for all electrical, electronic and related technologies.
ISM	Industrial Scientific Medical radio band.
ISO	International Organization for Standardization. It is the world largest developer and publisher of international standards.
IFA	Inverted F-Antenna
IEEE	Institute of Electrical and Electronics Engineers
MMS	Miller Modulated Subcarrier. It is a method of encoding serial data.
PIE	Pulse Interval Encoding. It's a coding method used prior to data modulation in a RFID system.
PLF	Polarization Loss factor. It is the angle mismatch formed by two different polarized electric fields.
PML	Perfect Match Layer. Artificial absorbing layer for wave equations.
PIFA	Planar Inverted F-Antenna
PEC	Perfect Electric Conductor. Ideal material with infinite conductivity
PMC	Perfect Magnetic Conductor. Ideal material with infinite permeability
QAM	Quadrature Amplitude Modulation. It is an analog or

	digital modulation. In the digital sense, it uses ASK to modulate two digital bit streams and summed them with 90 degree phase shift.
RFID	Radio Frequency Identification. It is a technology for the identification of objects.
RCS	Radar Cross Section. It is visibility area of an object for radar.
SAW	Surface Acoustic Wave. It is a passive UHF RFID system in which the reader sends an acoustic wave and the tag responses by reflecting the wave multiple times.
SSB	Single Side Band. It is an amplitude modulation in which the modulated wave is composed of carrier, upper sideband or lower sideband.
TM	Transverse magnetic. No magnetic field in the direction of propagation.
TE	Transverse electric. No electric field in the direction of propagation.
TEM	Transverse ElectroMagnetic. Nor electric nor magnetic field in the direction of propagation.
UHF	Ultra High Frequency. It ranges from 300MHz to 3GHz

1. INTRODUCTION

The Radio Frequency Identification (RFID) system is a technology in expansion due to the growth of emerging applications.

An RFID system is mainly based on the reader and tag antenna. The reader is the responsible to generate the information to be sent to the tag antenna. The tag antenna is the device attached to an object for an identification purpose. There are different RFID system based on the frequency band, operational mode and energy source delivered to the tag antenna. In this thesis, it is of main interest to work in the Ultra High Frequency (UHF) band and passive tag antenna.

Based on the object material property and the tag antenna radiation characteristic attached to the object, it is possible to success in the identification process. If the desired object to be identified is a metal surface; the tag antenna, attached to this object, degrades its radiation characteristic performance. The object risks to be identified or the identification distance is shorter compared if the object is working on free space.

Nevertheless, many UHF-RFID applications are based on the identification of metal surface objects like box of cans, containers, package of cigarettes, etc. Under this adversity, there is a necessity to study the reason that metal surface affects tag antenna performance; suggest options to diminish the degradation of tag radiation; and review the latest tag antenna designs used for metal surface immunity.

This thesis introduces a new design of passive UHF patch tag antenna that overcomes its radiation performance on metal surface. The study of patch antenna and the necessity of metal surface to operate are part of this thesis. The designed patch antenna is simulated in the electromagnetic software HFSS and CEMS; and comparison between both software is done through simulation results of the tag antenna impedance, total gain and power reflection coefficient.

This new tag antenna design is measured in a special RFID cabinet. It is measured the minimum transmitted power necessary to read the tag antenna. The maximum read range is calculated when the transmitted power is equal to the allowed European EIRP power. Besides, the realized gain is compared between HFSS simulation and measurement results.

1.1 Scope of the thesis

This thesis is based on the study of passive far field UHF RFID patch tag antenna. The reader is the generating of source and starts the communication. However, no detail

information related to the software or hardware is described during the thesis about the reader.

The patch tag antenna is studied and constructed as a passive device. The advantage of a passive antenna over active and semi-passive antenna is the cheaper investment in the construction, ideal durability and simplicity.

The study, design and measurement of the patch tag antenna are based on the UHF RFID band. The UHF band ranges from 300 MHz to 3GHz, and the UHF RFID band ranges from 860MHz up to 960MHz. However, the tag antenna is not designed for a specific country or region frequency band.

The air interface communication between reader and tag antenna is based on the standard ISO/IEC 18000. This global air interface standard sets the rules for communication between reader and tag antenna.

1.2 Outline of the thesis

This thesis consists of eight chapters and two appendixes.

An introduction to the general RFID technology is described in Chapter 2. The basis of the electromagnetic theory is described in Chapter 3 and the effects of metal surface through surface waves are also analyzed. The analysis for patch antenna is introduced in Chapter 4. Specific passive UHF RFID system is described in Chapter 5. The review of different patch tag antenna designs is included in Chapter 6 as well as a list of possibilities to overcome the metal surface. The design, construction and measurement results of the new patch tag antenna are described in Chapter 7. Finally, some remarkable conclusions are also mentioned in this thesis. The outline of each chapter is described below.

Chapter 2 named “The RFID technology” describes common RFID implementations, classification, radio regulations, standards and far field in RFID system. The implementation of RFID technology is commonly based on a reader and tag antenna. The classification of RFID system is based on the 3 parameters: the frequency allocation, operation principle and energy source delivered to tag antenna. An overview of each type of classification is covered. Besides, radio regulations and standards rule the maximum transmitted power limit and the communication between reader and tag. Radio regulations and frequency allocation vary from country and region. They are listed in a single overview table. A brief resume of the air interface standard in UHF RFID is introduced. This standard sets the rules in for the communication between the reader and tag.

Chapter 3 named “Electromagnetic theory” gives a review of some important laws, formulations and theory of the electromagnetic waves. Maxwell’s laws and the application to the boundary conditions are reviewed. Besides, uniform plane wave, which is a special type of propagating wave, is described. The behavior of this kind of wave depends on type of medium in which it is propagating. This chapter solidifies the required electromagnetic theory to face the tag antenna performance under metal

surface. Furthermore the performance of traveling wave under metal surface effect through surface waves is also described.

Chapter 4 named “Rectangular patch antenna” makes an analysis of patch antennas. An introduction to the theory of the methods: FEM (Finite Element Method) and FDTD (Finite Discrete Time Domain) is described. Those numerical methods are used for solving the Maxwell’s equation and applied in the electromagnetic simulators CEMS and HFSS, respectively. The chapter begins with the fundamental parameters of the antenna, the effective aperture and radar cross section of the antenna. The importance of those parameters lies in the application for link budget of passive RFID system and in the measurement of tag antenna.

Chapter 5 named “Passive far field RFID tag” describes the operation and link budget in passive UHF RFID system. Besides, the power reflection coefficient term is defined as a measure of matching impedance between the e equivalent circuit of the tag antenna and the integrated circuit.

Chapter 6 named “Metal surface effects on UHF patch tag antenna” gives some alternatives to overcome the metal surface effect on tag antenna. Some tag antenna designs that need a metal surface to operate are also review. These different designs are classified according to the structure and properties of operation.

Chapter 7 named “Experimental UHF patch tag antenna” describes the new UHF patch tag antenna design. The simulation process in two different software and the achieved measurement results of this tag antenna are explained in this chapter.

Finally, some conclusions of this thesis and recommendation for future work are also mentioned.

2. THE RFID TECHNOLOGY

The Radio Frequency Identification (RFID) technology is a continuous growing technology in commercial and military applications. In this chapter common RFID implementation, classification, regulation and standard of the RFID technology are introduced. A common RFID system is based on a reader and tag; and the communication between them is based on the same frequency band, operational principle and energy source delivered to the Integrated Circuit (IC). In the UHF RFID system, the frequency allocation and maximum allowed power are regulated by the own regions or countries while the interface communication protocols that govern the communication between reader and tag is unique and ruled by the ISO/IEC 18000 [1].

2.1 Common RFID implementation

All RFID systems are implemented with two basic components, a reader and a tag [2]. The RFID reader has also two separate components, the transmitter hardware and receiver hardware, which may use a single antenna for transmitting and receiving the signal. The transmitter and receiver hardware can also be two separate entities located at different positions or they both can be integrated in a same device.

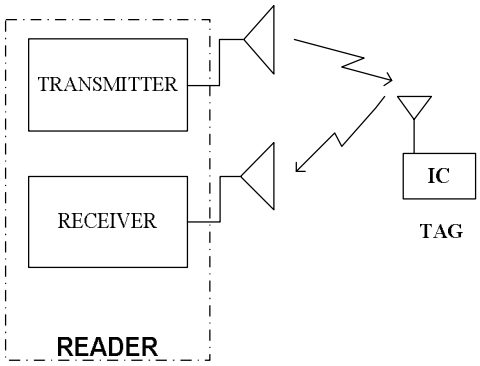

Figure 2.1. *Typical UHF RFID system components, the reader contains the transmitter and receiver hardware; and, the tag which contains the antenna and IC working in the same frequency band of the reader.*

The tag has also two basic components, the tag antenna and the IC. They are not independent components; the tag antenna design depends on matching properly to the IC equivalent circuit. The single tag antenna receives and transmits the signal. The IC holds information about the object to which it is attached. It is the brain of the tag because it encodes and modulates the received information from the reader furthermore

it is the responsible for the communication to the reader. The IC switches its impedance between two states and modulates the incoming RF field.

2.2 Classification of RFID systems

An RFID system is mainly classified by the frequency band; operational principle and energy source delivered to the IC. Fig. 2.2 describes in a single graph the RFID classification and tendencies based in the state of art of the RFID technology [3].

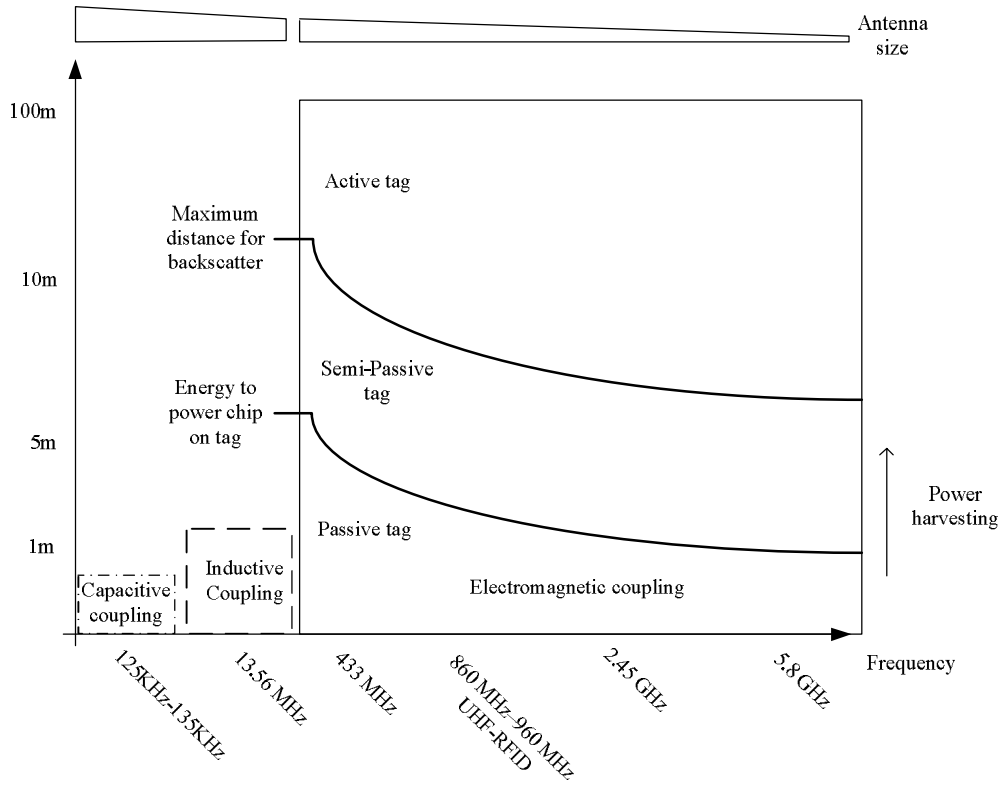

Figure 2.2. *Tendencies of the RFID system classification [3].*

The frequency band allocation varies for region or country and it usually ranges from LF (Low Frequency) and HF (High Frequency) versus UHF and microwave bands.

The operational principle refers to how the reader delivers energy to the tag antenna for the communication between them. Some principles are the coupling methods and surface acoustic wave (SAW). SAW system is a passive UHF RFID system in which the reader sends an acoustic wave and the tag responses by reflecting the wave multiple times [3]. This system has special properties like: high temperature resistance (400 ^{o}C), high velocity reading (420 Km/h), and long read range (10m. passive), etc. However, this thesis focus on one of the coupling methods for the RFID system described below.

There are three main coupling methods used in RFID systems: capacitive (electric) coupling, inductive (magnetic) coupling, and electromagnetic coupling (backscattering). Capacitive and inductive coupling methods work in the near field. Electromagnetic

coupling, which works in the far field, is the most used method for the UHF-RFID system because of its longer read range achievement.

Inductive coupling uses the magnetic field for operation and communication between the reader and tag antenna. The frequency band is usually allocated for high frequency (HF). Shorter read range (<1m) is achieved by using inductive coupling because the field strength path of a magnetic antenna falls as cube of distance in the near field. However, upon the transition to the far field, the decaying path flattens out [4; 5].

Electromagnetic coupling is mainly above 40MHz [3]. The antenna dimension gets smaller due to lower wavelengths (<30 cm). This operating mode achieves longer read ranges because the communication between reader and tag can be held in the far field region. The maximum allowed transmitted power is higher than previous operation modes, and the signal strength from the reader decays as square of distance.

The energy source provided to activate the IC for the communication between reader and tag is classified as passive, semi-passive and active. In passive system, the IC is power up by harvesting energy emitted by the reader in the operational frequency. The communication from tag to reader is also held by harvesting energy from the reader. The tag modulates its information by switching the reflected signal back to the reader. The reflection of the signal depends on the matching impedance between the tag antenna and the IC. The impedance of the IC is switched between two states depending on the information of the IC. This communication process is known as backscattering modulation and it is described in chapter 5.

In semi-passive system or battery assisted passive tags, the IC has its own energy source, like a battery for additional tag functions that need continuous supply. The semi-passive tag uses the energy emitted from reader for the backscattering communication but use internal power source for the operation of the IC.

In active system, the IC is powered up by an internal energy source. The tag has also a conventional transmitter. This enables the tag, the ability to communicate with the reader in the presence of other tags by using different frequency channels. The tag has the possibility to use robust modulation of the information and high code rates to access the radio channel like Quadrature Amplitude Modulation (QAM) and Code Division Multiple Access (CDMA), respectively. Those provide higher efficiency of spectrum availability to users, superior noise robustness and reuse of the same frequency band by multiple tags [8].

The advantage of a passive, semi-passive and active system depends on the RFID system application. Active system offers reliable communication link for obstructed environments and longer read ranges. However, the cost of using an active system is the increase of the size tag, the price, the maintenance budget of the system itself, and radio regulations requirements for working as a transmitter, etc. Passive system instead is sensitive to environment, especially when it is attached to metal surface. It offers shorter read range compared to active system because its operation depends on harvesting

energy from the transmitter. Nevertheless, the cost of passive tags are really cheap and theoretically they have unlimited life [8].

2.3 Radio regulations and standards

RFID system uses the electromagnetic spectrum for the communication. RFID system is allocated in frequency and power in order to preserve the harmony with other RF application systems. The frequency range and maximum transmitted power limit are regulated in each region or country.

The licensing regulations vary from region or country. The Federal Communications Commission (FCC) regulates the license for USA region; whereas the European Telecommunications Standards Institute (ETSI) for Europe [6; 7; 9]. The FCC is an independent United States government agency; it is in charged with regulating interstate and international communications by radio, television, wire, satellite and cable [11]. The ETSI is a European institution that produces globally-applicable standards for information and communication technology (ICT), including fixed, mobile, radio, converged, broadcast and internet technologies [10].

There is not a global band for UHF RFID application but it uses the classified worldwide ISM (Industrial-scientific-medical) frequency ranges. The ISM radio bands were originally reserved internationally for the use of RF electromagnetic fields for industrial, scientific and medical purposes other than communication. The equivalent isotropic radiated power (EIRP) is the amount of power that theoretical isotropic antenna should radiate in order to radiate with the peak power density observed in the direction of maximum antenna gain [4; 8]. EIRP is often either explicitly or implicitly used as a regulatory limitation on radio operations. The equivalent radiated power (ERP) is referenced to half-wave dipole antenna and the relation between ERP and EIRP (EIRP=1.64 ERP).

Table 2.1. *UHF RFID Radio Regulations in different regions around the world [6].*

Country/ region	UHF RFID spectrum allocation frequency (MHz)	Max. TX power limit in (ERP)	Regulation
Europe	869.4-869.65	0.5 W	EN300 200 [10]
Europe	865-868	2.0 W	EN302 208 [10]
USA	902-928	2.4 W	FCC Part 15 [11]
Korea	908.5-914	2.4 W	
Japan	952-954	2.4 W	
China	840.25-844.75	2.0 W	
China	920.25-924.75	2.0 W	
Brazil	902-907.5	2.4 W	
Brazil	915-928	2.4 W	
South Africa	865.6-867.6	2 W	
South Africa	917-921	2.4 W	

Table 2.2. *Parameters of some air interface standards and protocol for the UHF RFID.*

Parameters	Standard / Protocol		
	ISO/IEC 18000-6A [1]	ISO/IEC 18000-6B [1]	ISO/IEC 18000-6C EPC class1 Gen2[9]
Forward link modulation	ASK	ASK	DSB-ASK SSB-ASK PR-ASK
Forward link encoding	PIE	Manchester	PIE
Return link modulation	ASK	ASK	ASK PSK
Return link encoding	FM0	FM0	FM0 MMS
Collision arbitration	ALOHA	Binary tree	Random slotted
Forward link bit rate	33kbps(mean)	10kbps to 40kbps (depends on local regulations)	26.7kbps-128kbps
Return link bit rate	40kbps-160kbps	160kbps	FM0:40kbps-640kbps MMS: 5kbps-320kbps

ASK: Amplitude Shift Keying
DSB: Double Side Band
MMS: Miller Modulated Subcarrier
PIE: Pulse Interval Encoding
SSB: Single Side Band
PR-ASK: Phase reversal ASK
FM0: Bi-phase space

The standardization of the air interface in the RFID System is intended to allow compatibility and to encourage interoperability between different providers of RFID readers and tags in the market. For example, it is possible to read any EPC Gen2 tag with any Gen 2 reader.

The air interface protocol is a set of rules governing communication between tag and reader. This is issued in the UHF RFID air interface standards; which is supported by ISO (International Organization for Standardization) and EPCglobal in ISO/IEC 18000-6 and EPC class 1 Gen 2, respectively. These two standards cover the physical layer of the UHF RFID system like modulation and bit encoding rules, anti-collision protocol, commands for reading, writing, etc [5]. “Both standards are identical, except for a few application identifier bits in the transponder memory mapping” [9].

Regarding to the standard organizations that take part in defining the air interface protocol; they are introduced as follows. The ISO is the world largest developer and publisher of international standards; and the International Electronical Comission (IEC) is the organization that prepares and publishes International Standards for all electrical, electronic and related technologies. The EPCglobal is an organization set up to achieve worldwide adoption and standardization of EPC technology. Where the EPC (Electronic Product Code) is a family of coding scheme for use of RFID tags created as a complement to the barcode. The ISO and IEC together defined the standard protocol for air interface communication between the reader and tag.

The protocol EPC class 1 Gen2 establishes a single global standard with some advantages with respect to the previous air interface UHF RFID standards, like more robust performance in dense reader environments, enhance security, etc. This protocol is supported since 2006 as the standard ISO/IEC 18000-6C [5]. A summary of air interface parameters for the three standards are listed in Table 2.2. EPC Class1 Gen 2 is the actual

standard used in UHF-RFID communication and that will be used in this thesis for the tag design and measurement setup.

2.4 Near-field and far-field RFID

An inductive and capacitive coupling RFID system operates mainly at low frequencies; and in the near field because the tag antenna is placed at distance much shorter than antenna dimension. The large wavelength of near-field systems makes the tag antenna very efficient regardless of what is attached them. The signal travels through many non-metallic substances without much loss, and it travels around most non-penetrable substances such as water and metal. This makes near field RFID very attractive option if the application can survive with read distance under one meter [2].

Far-field RFID uses electromagnetic waves or electromagnetic coupling for the communication link between reader and tag. Far field is generally defined as the area where travelling waves can be modeled as plane waves. Travelling waves are used to send and receive information. Far-field RFID system is implemented at high frequencies (UHF, microwave); however, at those frequencies, the tag antennas are very susceptible to material attachment. The challenging in designing a tag antenna on metal surface increases due to tag antenna undergoes degradation of its radiation performance.

3. ELECTROMAGNETIC THEORY

This chapter is a review of some electromagnetic concepts that should be well solidified for the thesis. Those concepts lead to understand the effect of metal surface on tag antenna performance and how it may be avoided or overcome. Electromagnetic theory is based on Maxwell's laws, which establish the propagation of waves in space and time. A special and simple type of wave propagation is the uniform plane waves whose properties of propagation and boundary effects are also reviewed. Finally, rectangular waveguide is briefly introduced since its propagation behavior, which is used in microstrip antennas, is not exactly uniform plane wave, but it is similar to guided wave behavior.

3.1 The Maxwell laws

Maxwell laws govern the electromagnetic field behavior and they are the result of combining Faraday's law (3.1), Ampere's law (3.2), and Gauss' laws (3.3), (3.4). Although these equations had not been completely derived analytically, they are reasonable and no experiments shown them to be invalid. These equations are well explained in [12; 13; 22].

These equations are applicable to macroscopic model. For a linear, homogeneous and isotropic medium, the Maxwell's laws in the phasor form are expressed as

$$\nabla \times \boldsymbol{E} = -j\omega\mu\boldsymbol{H} - \boldsymbol{M} \tag{3.1}$$

$$\nabla \times \boldsymbol{H} = (\sigma^e + j\omega\varepsilon)\boldsymbol{E} + \boldsymbol{J_i} \tag{3.2}$$

$$\nabla \cdot \boldsymbol{D} = \rho_e \tag{3.3}$$

$$\nabla \cdot \boldsymbol{B} = \rho_m \tag{3.4}$$

where $\boldsymbol{E}$ denotes the electric field intensity (V/m), $\boldsymbol{H}$ is the magnetic field intensity (A/m), $\boldsymbol{D}$ is the electric flux density (C/m^2), $\boldsymbol{B}$ is the magnetic flux density (T or Wb/m^2), μ is permeability (H/m), ε is the permittivity (F/m). σ^e is the electric conductivity (S/m). ρ_e is the electric charge density (C/ m^2 or C/ m^3) and ρ_m is the magnetic charge density (Weber/ m^3). ω is the radial frequency (rad/s).

"The electric current density $\boldsymbol{J}$ is the sum of the conductor current density $\boldsymbol{J_c} = \sigma^e \boldsymbol{E}$ and the impressed or source current density $\boldsymbol{J_i}$ as $\boldsymbol{J} = \boldsymbol{J_c} + \boldsymbol{J_i}$. The magnetic current density, $\boldsymbol{M} = \boldsymbol{M_c} + \boldsymbol{M_i}$, where $\boldsymbol{M_c} = \sigma^m \boldsymbol{E}$ " expressed in [22]. σ^m is the magnetic conductivity (Ω/m). The displacement current density ($-j\omega\varepsilon\boldsymbol{E}$) is perhaps Maxwell's most important contribution; it is the rate of change of electric flux [12].

The notation of electric and magnetic field will be used along this chapter.

3.1.1 The constitutive properties of the medium

The constitutive properties refer to the type of material medium and it is defined by the permittivity (ε), permeability (μ) and conductivity (σ) of the medium. The material medium can be classified as linear, homogeneous and isotropic [13]. For a simple media, the scalars ε, μ, σ are assumed to be constants.

$$\boldsymbol{D} = \varepsilon \boldsymbol{E} \quad , \tag{3.5}$$

$$\boldsymbol{B} = \mu \boldsymbol{H} \, , \tag{3.6}$$

$$\boldsymbol{J_c} = \sigma^e \boldsymbol{E} \, , \tag{3.7}$$

where $\boldsymbol{J_c}$ is the conduction current density vector (A/m^2).

In a linear medium, the constitutive properties are field independent magnitude. A ferromagnetic material is an example of nonlinear media, in which $\boldsymbol{B}$ and $\boldsymbol{H}$ are related by a nonlinear, hysteresis curve instead of a constant scalar μ. An isotropic medium exhibit the same properties in all directions. But, an anisotropic dielectric exhibits constitutive parameters as a matrix. A homogeneous medium has the same medium properties at all points in the medium. But, in an inhomogeneous medium, the constitutive properties are functions of the spatial coordinates.

Under electric polarization and magnetic polarization, equations (3.5) (3.6) are updated to (3.8) and (3.9), respectively. The electric flux density ($\boldsymbol{D}$) and the magnetic field intensity ($\boldsymbol{H}$) consist in the superposition of contributions in free space; and electric and magnetic dipoles. The properties of linearity, isotropic and homogeneous of a medium are now related to the electric polarization vector ($\boldsymbol{P}$) and magnetic polarization vector ($\boldsymbol{M_p}$)

$$\boldsymbol{D} = \varepsilon_0 \boldsymbol{E} + \boldsymbol{P} \, , \tag{3.8}$$

$$\boldsymbol{H} = \frac{\boldsymbol{B}}{\mu_0} + \boldsymbol{M_p} \, . \tag{3.9}$$

Where electric polarization is equal to the product of the electric susceptibility (χ_e), the permittivity in free space (ε_0) and the electric field ($\boldsymbol{E}$). The magnetic polarization is

equal to product of the magnetic susceptibility (χ_m) and the magnetic field strength ($\boldsymbol{H}$). Here, μ_0 is the permeability in free space.

3.1.2 Boundary conditions of electromagnetic fields

The boundary conditions describe the relations between the electromagnetic field at the boundary between two different media, as it is well explained in [12].

Figure 3.1 describes the behavior of fields at the boundary of medium 1 and medium 2, tangential and normal components are denoted by subscript "t" and "n", respectively. J_{sn} is the electric surface current density normal to the interface, and ρ_s is the electric surface charge density at the boundary. For this analysis, it assumed that there is not impressed current density and not magnetic charge density in any of the mediums, besides the magnetic current density is zero.

The boundary condition for the tangential electric field states the continuity across the boundary from medium 1 to medium 2 ($E_{t1} = E_{t2}$). This is expressed in equation (3.10). In other hand, there is no continuity at boundary between the tangential components of the magnetic field. The difference between two different magnetic fields at the boundary is equal to the conductive surface current density normal to the interface($H_{t2} - H_{t1} = J_{sn}\ A/m$). $\boldsymbol{H}_2$ and $\boldsymbol{H}_1$ are the magnetic field intensity vectors at the interface. The quantity $\boldsymbol{a}_n \times (\boldsymbol{H}_2 - \boldsymbol{H}_1)$ gives the net resultant magnetic field tangent to the boundary, which is numerically equal to the vector conductive surface current density $\boldsymbol{J}_s$ at the boundary.

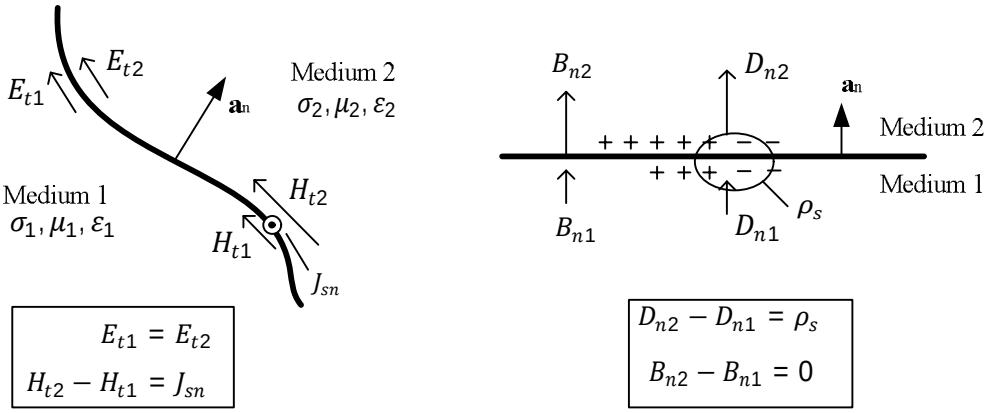

Figure 3.1. *Boundary conditions relating the tangential (left) and normal (right) components of the field vectors at the interface [12].*

The boundary condition for the normal components of $\boldsymbol{D}$ and $\boldsymbol{B}$ are based on Gauss' law. Equation (3.12) refers that the net electric flux that is normal to and directed away from the boundary is equal to the electric surface charge density at the boundary ($D_{n2} - D_{n1} = \rho_s\ c/m^2$). The normal component of $\boldsymbol{B}$ is continuous across the boundary ($B_{n2} - B_{n1} = 0$ A/m) as expressed in (3.13).

$$\boldsymbol{a}_n \times (\boldsymbol{E}_2 - \boldsymbol{E}_1) = \boldsymbol{0} \tag{3.10}$$

$$\boldsymbol{a}_n \times (\boldsymbol{H}_2 - \boldsymbol{H}_1) = \boldsymbol{J}_s \tag{3.11}$$

$$\boldsymbol{a}_n \cdot (\boldsymbol{D}_2 - \boldsymbol{D}_1) = \rho_s \tag{3.12}$$

$$\boldsymbol{a}_n \cdot (\boldsymbol{B}_2 - \boldsymbol{B}_1) = 0 \tag{3.13}$$

The boundary conditions for the normal components of ***D, B*** and the tangential components for ***E, H*** are derived from Maxwell's laws which are not independent of each other. Hence, for the time varying case, the condition on tangential ***E*** is equivalent to the condition on normal ***D*** and similarly the condition on tangential ***H*** is equivalent to the condition on normal ***B***.

Special cases of boundary condition emerge if the medium is perfect conductor, finite conductor and perfect dielectric.

A *perfect conductor* medium is a hypothetic material that has infinite electric conductivity ($\sigma = \sigma^e = \infty$) or zero resistance to the flow of charges. In a perfect conductor medium all the time varying fields are zero and also the static electric fields are zero. This is demonstrated also in [12]. How? Since $\sigma = \infty$; permeability and permittivity μ, ε are finite. Then, $\boldsymbol{J}_c = \sigma\boldsymbol{E}$, ***E*** must be zero because an infinite ***J*** means that an infinite amount of charge is transported in a finite amount of charge or that a finite amount of charge is transported in zero time. Hence $\boldsymbol{D} = \varepsilon\boldsymbol{E} = \boldsymbol{0}$ for a finite dielectric constant. Then, applying ***E***=0 to the faraday's law, this reduces to $\frac{\partial \boldsymbol{B}}{\partial t} = 0$. ***B*** is time independent and it can be constant or zero. Experiments have shown that a static magnetic field cannot exit inside a superconductor [12], so ***B***=0 and $\boldsymbol{H} = \frac{\boldsymbol{1}}{\mu}\boldsymbol{B} = \boldsymbol{0}$. If medium 1 is a perfect conductor ($\sigma_1 = \infty$) then all the fields inside the medium are zero ($\boldsymbol{E}_1 = 0, \boldsymbol{H}_1 = 0, \boldsymbol{D}_1 = 0, \boldsymbol{B}_1 = 0$).

A *material media*; if both mediums have finite conductivity (σ_1, σ_2 finite), the electric current not exist on the boundary because it will penetrate into the media. Thus, an isolated electric current density on the boundary between the two media cannot exist and only equation (3.11) turns to be $\boldsymbol{a}_n \times (\boldsymbol{H}_2 - \boldsymbol{H}_1) = 0$. If both mediums are ideal dielectrics ($\sigma_1 = 0, \sigma_2 = 0$) then free electric surface charge density is zero and normal component of the electric density is continuous.

3.2 Power flow and poynting vector

The cross-product of vectors ***E*** (V/m) and ***H*** (A/m) implies a distribution of power (W/m^2) in the field over some surface area. The poynting vector ***S*** is defined as the cross product of these vector fields, ***S*** is also known as the power density vector [12]. It indicates the magnitude and direction of power flow. The direction of ***S*** is perpendicular to the plane containing ***E*** and ***H***.

$$\boldsymbol{S} = \boldsymbol{E} \times \boldsymbol{H} \ \text{W/m}^2 \tag{3.14}$$

If $\boldsymbol{S}$ is integrated over a closed surface, it will be obtained the power dissipated and the rate of change of stored energy in the region enclosed by that surface [15].

The direction of poynting vector for an isotropic antenna ($\boldsymbol{S}_r$) is radial. See Fig. 3.2. The electric and magnetic fields produced by the antenna at radial distance R are $\boldsymbol{E}_\theta$ and $\boldsymbol{H}_\phi$, respectively. Those fields are orthogonal with the poynting vector in radial direction ($\boldsymbol{S}$=$\boldsymbol{S}_r$=$\boldsymbol{E}_\theta \times \boldsymbol{H}_\phi$). The determination of dissipated power by antenna is a clear application of poynting vector. The power radiated ($P_{radiated}$) or the power leaving the antenna is obtained by integrating the poynting vector over a closed surface "$\boldsymbol{s}$". It is calculated as

$$P_{radiated} = \int_{\phi=0}^{2\pi} \int_{\theta=0}^{\pi} \boldsymbol{S} \cdot d\boldsymbol{s}.$$

The sphere surface of radius R is an appropriate surface for the integration of the pointing vector. The average power radiated (P_{rad}) is obtained by time averaging the power radiated over one period of the sinusoid. Actually, it is a practical term used for the description of energy in antenna theory.

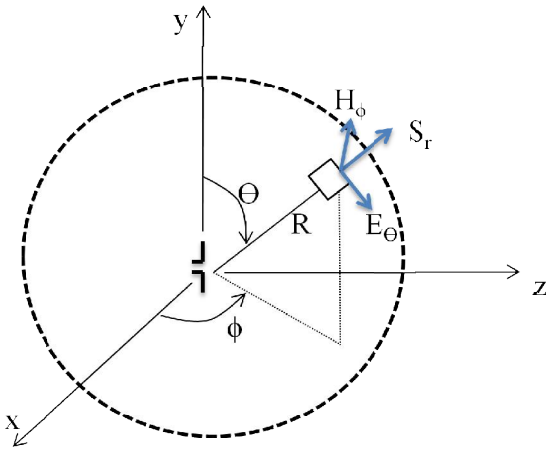

Figure 3.2. *Poynting vector and power flow for an isotropic antenna [12].*

$$P_{rad} = \frac{1}{T} \int_0^T P_{radiated} dt \tag{3.15}$$

The average power density denoted by $\boldsymbol{S}_{\boldsymbol{av}}$ is defined by equation (3.16), considering $\boldsymbol{E}, \boldsymbol{H}$ in phasor form

$$\boldsymbol{S}_{\boldsymbol{av}} = \frac{1}{2} \Re\{\boldsymbol{E} \times \boldsymbol{H}^*\}. \tag{3.16}$$

And the average power radiated can also be obtained by using the previous equation; such that:

$$P_{rad} = \int_{\phi=0}^{2\pi} \int_{\theta=0}^{\pi} \boldsymbol{S}_{\boldsymbol{av}} \cdot d\boldsymbol{s} \ . \tag{3.17}$$

3.3 The uniform plane waves

One important implication of Maxwell's equations is the prediction of electromagnetic energy propagation in form of waves. Uniform plane waves are the simplest form of electromagnetic wave propagation. Many properties and characteristic of uniform plane waves have close parallels in the wave propagated on transmission line and within hollow waveguide, as it is explained in [12; 13].

The wave equation that governs the propagation of electromagnetic waves is derived by applying Maxwell's laws to simple medium (linear, isotropic, and homogeneous). It assumes zero net free charge ($\rho = 0$) and the existence of only conduction current ($\boldsymbol{J} = \sigma \boldsymbol{E}$) in the region.

The term plane means that field vector $\boldsymbol{E}$ and $\boldsymbol{H}$ at each point in space lie in a same plane. Uniform means the phasor field vectors are independent of position in each of these planes. Therefore $\boldsymbol{E}$ and $\boldsymbol{H}$ for a uniform plane wave are orthogonal and the poynting vector is in the direction of $\boldsymbol{E} \times \boldsymbol{H}$.

The propagation of uniform plane waves is illustrated in Fig. 3.3; the electric and magnetic fields for this case are expressed in phasor form in equation (3.18) and (3.19)

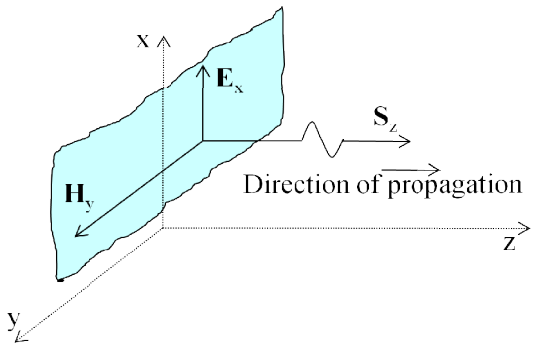

Figure 3.3. *Propagation of uniform plane waves.*

$$\boldsymbol{E}_x = E_m^+ e^{-\gamma z}\, \hat{\boldsymbol{x}} \tag{3.18}$$

$$\boldsymbol{H}_y = H_m^+ e^{-\gamma z} \hat{\boldsymbol{y}} \tag{3.19}$$

Where E_m^+ is the amplitude of the electric field in positive $\hat{\boldsymbol{x}}$ direction ($\boldsymbol{E}_x$), H_m^+ is the amplitude of magnetic field in positive $\hat{\boldsymbol{y}}$ direction ($\boldsymbol{H}_y$). The propagation constant is denoted by γ ; and z is the distance in the direction of propagation. The negative sign means that the uniform plane wave is propagating in along the direction of propagation which is the positive $\hat{\boldsymbol{z}}$ direction.

3.3.1 Lossless media and lossy media

The conductivity is zero for a lossless media ($\sigma = 0$), and non-zero for a lossy media ($\sigma \neq 0$). A dielectric is a hypothetical lossless medium because electromagnetic waves

do not attenuate inside the medium. A metal plate or a conductor is lossy media since conductivity is infinite. There are two main differences between a lossless media and lossy media. First, the attenuation constant (α Np/m) is zero for lossless media and the amplitude of field vectors (E_m^+) is constant over the propagation. However, for a lossy media, α is different to zero and the amplitude of field vector ($E_m^+ e^{-\alpha z}$) is exponential decreased over the propagation direction. Second, since $\sigma \neq 0$ for a lossy media, the intrinsic impedance ($n\angle\theta$) is an imaginary parameter with magnitude (n) and phase (θ). The fields $\boldsymbol{E}$, $\boldsymbol{H}$ are out of phase by θ for a lossy media. For a lossless media, $\boldsymbol{E}$ and $\boldsymbol{H}$ are in phase since the intrinsic impedance is positive constant.

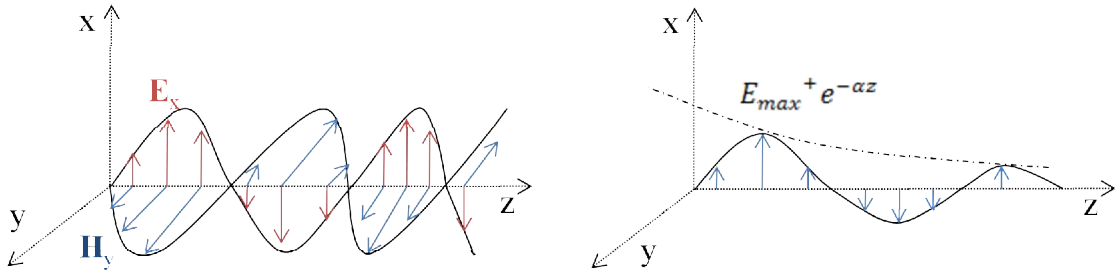

Figure 3.4. *Individual forward traveling waves as a function of position in a lossless media (left) and lossy media (right) [12].*

3.3.2 Effective permittivity and effective conductivity

The effective permittivity of a material emerges when a high frequency electric field is applied to the medium. The permanent dipoles and induced dipoles of any material tend to align under the direction of sinusoidal varying electric field, but as the frequency of the applied field increases, the alignment of dipoles lags due to atomic and molecular restoring sources prevent an instantaneous alignment [12]. A complex permittivity $\hat{\varepsilon}$ represents this physical characteristic of the material because permittivity gives a measure of polarizability of a material and it is defined by (3.20).

$$\hat{\varepsilon} = \varepsilon' - j\varepsilon'' \tag{3.20}$$

From (3.20) into (3.2) and in the absence of impressed current density, the equation results in $\nabla \times \boldsymbol{H} = (\sigma + \omega\varepsilon'')\boldsymbol{E} + j\omega\varepsilon'\boldsymbol{E}$. Observe that $\sigma + \omega\varepsilon''$ is the effective conductivity and ε' is the effective permittivity and they both depend on frequency.

The loss tangent ($tan\delta$) is a measure of the lossy nature of the material. It is defined as the ratio between the effective conductivity with respects to the effective permittivity multiplied by the angular frequency ω.

$$tan\delta = \frac{\sigma + \omega\varepsilon''}{\omega\varepsilon'} \tag{3.21}$$

Loss tangent also express the relation between the energy loss mechanism and the energy storage for a material. So, it is a term that classifies lossless or lossy materials. For good dielectrics $tan\delta \ll 1$; whereas for good conductor $tan\delta \gg 1$.

3.3.3 Skin depth

The skin depth denoted by δ or depth of penetration is the distance at which the field amplitude is attenuated by 1/e [13]. Here e is the neper number and α is the attenuation constant (Np/m).

$$\delta = \frac{1}{\alpha} \tag{3.22}$$

If the frequency of the electromagnetic wave, which impinges a conductor surface, increases, the skin depth decreases. In order to attenuate undesired signals inside the medium, a conductor surface with higher thickness than the skin depth should edge all around the medium [12]. For example, an anechoic chamber is constructed with a metal whose thickness is thicker than skin depth so any signal impinging on it will be attenuated.

3.3.4 Polarization of uniform plane waves

Polarization describes the amplitude relation of field vectors at a point in space and for every time in a plane perpendicular to the direction of propagation [12].

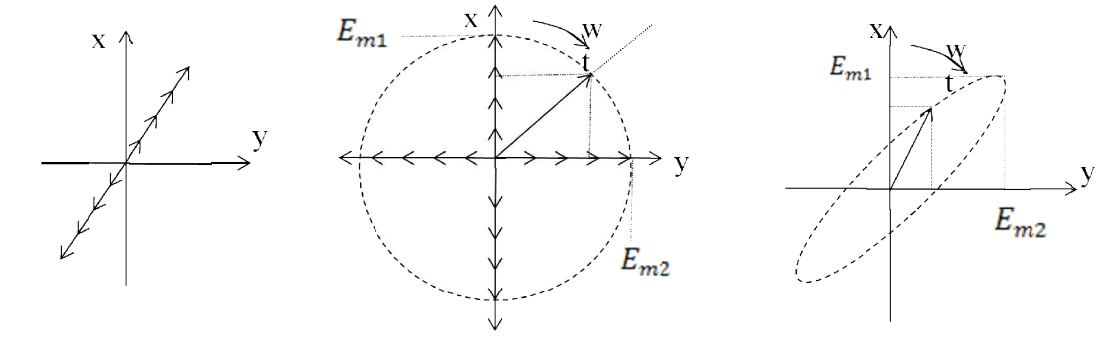

Figure 3.5. *Polarization of uniform plane waves in the direction of propagation as a function of time, view z=0. z is the direction of propagation.*

The wave draws an arbitrary shape in the plane of propagation. This arbitrary shape is usually an ellipse, circle, and/or line. Fig. 3.5 gives an illustration of those cases. Linear and circular polarizations are special cases of elliptical polarization. The difference among them resides on the phase angle (θ rad) and on the amplitude relation of the fields. The electric field with respect to time is expressed in (3.23). In linear

polarization, there is no phase angle and the amplitude of electric fields could be equals or different. In circular polarization, the amplitude of the electric field is constant but phase angle is $\pi/2$. In the general case is the elliptical polarization; in which the amplitude of the electric field is not constant and there is also a phase angle of $\pi/2$.The phase constant is denoted by β.

$$\boldsymbol{E}_{(t)} = E_{m1}\cos(\omega t - \beta z)\,\hat{\boldsymbol{x}} + E_{m2}\cos(\omega t - \beta z + \theta)\,\hat{\boldsymbol{y}} \tag{3.23}$$

3.3.5 Propagation of uniform plane waves at boundary surface

When the incident electric and magnetic fields $\boldsymbol{E}_i, \boldsymbol{H}_i$, respectively from medium 1 impinge the boundary; part of the field is transmitted ($\boldsymbol{E}_t, \boldsymbol{H}_t$) to medium 2 and the rest is reflected ($\boldsymbol{E}_r, \boldsymbol{H}_r$) to medium 1. The material properties of medium 1 and medium 2 are $\varepsilon_1, \mu_1, \sigma_1$ and $\varepsilon_2, \mu_2, \sigma_2$; respectively.

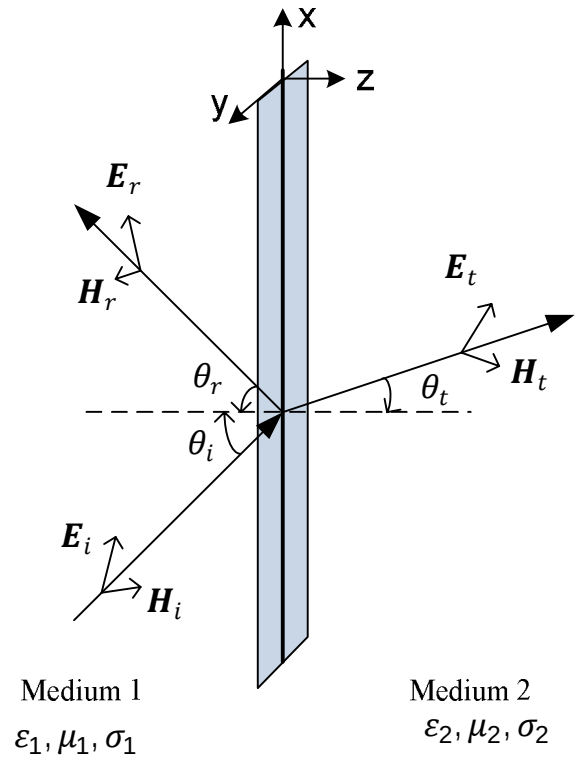

Figure 3.6. *Incidence of a uniform plane wave on a plane boundary showing incident, reflected, and transmitted waves for an arbitrary angle of incident.*

At the boundary z=0, the tangential electric and magnetic field's components are continuous; then it is demonstrated the phase matching as

$$\theta_i = \theta_r\,,$$
$$\gamma_1 \sin\theta_i = \gamma_2 \sin\theta_t. \tag{3.24}$$

This uniform plane wave is incident at arbitrary angle of incidence, Fig.3.6 illustrates this general scenario. The boundary between the two media lies in the *xy* plane. The pointing vectors of the incident, reflected and transmitted waves are assumed to lie in the *xz* plane; also known as the plane of incidence. The angle of incident of the incident wave is measure respect to the normal of the surface θ_i; similarly, it is measured the angle of reflection θ_r and the angle of transmission θ_t.

If both media are lossless, the incident and reflected angles depend only on the material properties of the medium. This is known as Snell law:

$$\frac{\sin\theta_i}{\sin\theta_t} = \sqrt{\frac{\mu_2\varepsilon_2}{\mu_1\varepsilon_1}} \tag{3.25}$$

An arbitrary polarization can be discomposed in two linearly polarized and orthogonal electric fields and the general result will be the superposition of these two results, as it is also explained in [12; 13]. The polarizations respects to the plane of incident are perpendicular and parallel polarization. The plane of incident (*XZ* plane) is the plane containing the propagation vector of the incident wave and the normal to the boundary. For perpendicular polarization, the incident electric field vector is perpendicular to the plane of incident and for parallel polarization; the incident electric field vector is parallel to the plane of incident.

The reflection coefficient indicates the relation between the magnitudes of reflected electric field respect to the incident electric field at the boundary (z=0).

$$\hat{\Gamma} = \left.\frac{E_r}{E_i}\right|_{z=0}$$

I.e. when the wave incident normal to the boundary, this means the incident angle equals to zero $\theta_i = 0$, then reflection coefficient is reduced to

$$\hat{\Gamma} = \left.\frac{E_r}{E_i}\right|_{z=0} = \frac{\hat{n}_2-\hat{n}_1}{\hat{n}_2+\hat{n}_1},$$

where $\hat{n} = \sqrt{\frac{j\omega\mu}{\sigma+j\omega\varepsilon}}$ is the intrinsic impedance of the respective medium.

A particular choice of the angle of incidence leads to reflection coefficient zero. So there is no reflected wave and total wave is trasmitted. This particular angle of incidence is called the Brewster angle. The reflection coefficient is analyzed for perpendicular and parallel polarization in [12] and it is observed that the Brewster angle does not exist for perpendicular polarization if both two materials are not magnetic. However, the Brewster angle may exist in parallel polarization for typical dielectric materials.

Oblique incidence on Perfect electric conductor:

The wave is traveling in a lossless medium and impinges oblique on the surface of a perfect conductor ($\sigma_2 \to \infty$). The incident electric field is discomposed in parallel and perpendicular polarization.

The intrinsic impedance of a perfect conductor is zero. The reflection coefficient at the boundary for any of the two polarizations is -1 so the amplitude of the reflected electric field is equal in magnitude but negative to the amplitude of the incident electric field [12]. The incident wave is completely reflected with phase shift.

$$\hat{\Gamma} = -1$$

For any of the two polarizations, the electric and magnetic fields form a standing wave pattern in the *z* direction and a traveling wave in the *x* direction. The fields forming the standing wave are 90^o out of phase then the time-average power flow is zero in the z direction [12]. The traveling wave in the x direction has time –average power flow in x direction; however, this is a non-uniform plane wave since the magnitude varies with z according to $\sin(\beta_1 \cos\theta_i z)$. I.e. for parallel polarization, the electric field in the x component is zero in medium 1 along z at certain distance, so that

$E_1^{\mathrm{x}} = 0$, then

$\sin(\beta_1 \cos\theta_i z) = 0$, then $\beta_1 \cos\theta_i z = -m\pi$

$\rightarrow z = -\frac{m\lambda_1}{2\cos\theta_i}$, m=1,2,3.. (3.26)

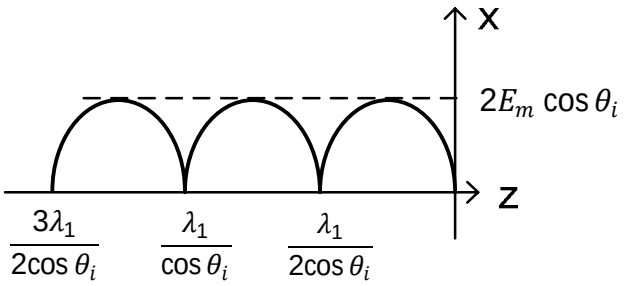

Figure 3.7. *Standing wave for parallel polarized electric field [12].*

Fig.3.7 illustrates the points were the electric field is zero respect to z for a parallel polarization. It is observed that the peak magnitude of total electric field in medium 1 is twice the magnitude of the magnitude of the incident electric field (E_m) multiplied by the factor $\cos\theta_i$.

Perfectly conductor planes could be intersected at these points $z = -\frac{m\lambda_1}{2\cos\theta_i}$ without affecting the solution. Furthermore, perfectly conducting surface supports surface current density from the boundary condition ($\hat{\boldsymbol{a}}_n \times \boldsymbol{H}_1 = \boldsymbol{J}_s$).

3.4 Perfect electric and magnetic conductor

Perfect electric conductor (PEC) is an ideal material with infinite conductivity. It can be defined as a material in which electric field and magnetic flux density vectors vanish; but there is not condition for the magnetic field and electric flux density.

$$\boldsymbol{E} = 0\,,\ \boldsymbol{B} = 0$$

$$\boldsymbol{a}_n \cdot \boldsymbol{B} = \boldsymbol{0}\,,\ \boldsymbol{a}_n \times \boldsymbol{E} = \boldsymbol{0} \tag{3.27}$$

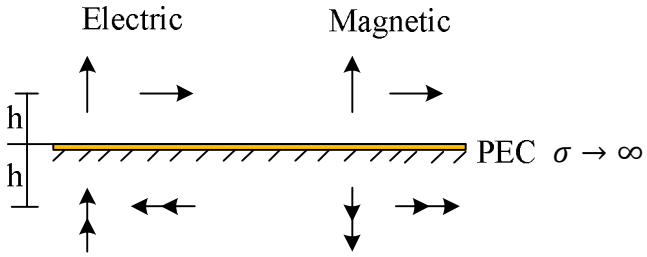

Figure 3.8. *Behavior of the polarized fields under Perfect Electric Conductor [15].*

Fig.3.8 summarized the PEC effect on the fields with vertical and horizontal polarization. PEC is a good reflector. In the boundary, the radio of the tangential component of the fields is equivalent to the surface impedance [78]. A smooth conducting plane has small surface impedance furthermore PEC would have zero surface impedance because tangential electric field is zero at the boundary. Thus when the antenna is placed near a metal surface, it changes the radiation properties.

$$\frac{E_t}{H_t} \propto Z \ \ (\Omega/\text{square}) \tag{3.28}$$

By incorporating a special texture on the smooth conductive surface, the quality of this new effective structure would depend only on the impedance. Indeed, this impedance is High Surface Impedance (HIS) that blocks the wave propagation at certain frequencies. Different proposed texture for HIS are described in [78; 54; 61].

Perfect magnetic conductor (PMC) is an ideal material with infinite permeability. Contrary to the PEC, in this medium, the magnetic field and electric flux density vanish while there is no condition for the other two fields.

$$\boldsymbol{H} = 0\ \ \boldsymbol{D} = 0$$

$$\boldsymbol{a}_n \cdot \boldsymbol{D} = \boldsymbol{0}\,,\ \boldsymbol{a}_n \times \boldsymbol{H} = \boldsymbol{0} \tag{3.29}$$

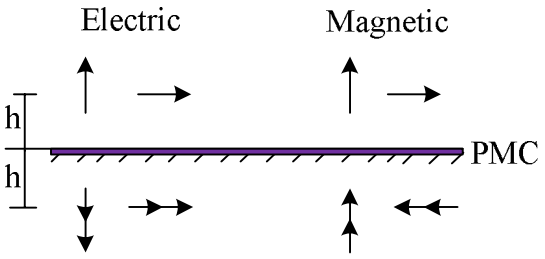

Figure 3.9. *Behavior of the polarized fields under Perfect Magnetic Conductor [15].*

If one of the media is a perfect magnetic conductor (PMC), the electric field reflects without phase reversal so there is constructive interference. However, the magnetic field reflects with phase reversal ($\boldsymbol{a}_n \times \boldsymbol{H} = 0$). This type of boundary is used theoretically to counteract the effect of conductive material in antenna performance.

3.5 Surface waves

Surface wave is a non uniform plane wave propagating along the boundary of propagation, the field is not constant over a plane of wave perpendicular to the direction of propagation but it is attenuated exponentially away from the boundary [12; 78].

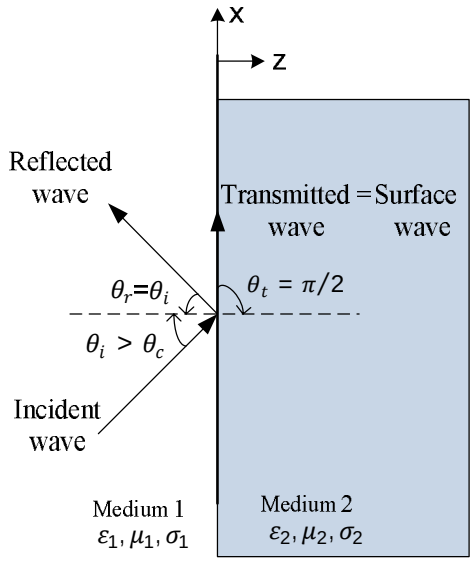

Figure 3.10. *Surface wave*

Surface waves originate at certain incident angle and for certain material properties. There is a critical angle of incident (θ_c) in which the transmitted angle is $\theta_t = \pi/2$. When the incident angle (θ_i) is greater than the critical angle of incident, θ_t takes imaginary values and the transmission electric field is expressed as

$$\boldsymbol{E}_t = E_m^t e^{-\alpha_2 z} e^{-j\beta_2 \sin\theta_i x}\,, \tag{3.30}$$

where $\alpha_2 = \beta_2\sqrt{\frac{\varepsilon_1}{\varepsilon_2}\sin^2\theta_i - 1}$. So the factor $e^{-\alpha_2 z}$ means that the transmitted electric field decays rapidly to zero away from the interface. The wave is tightly bound to the surface of the interface if α_2 is large. I.e. if medium 2 is a perfect electric conductor, dielectric constant is zero ($\varepsilon_2 = 0$) and $\alpha_2 \to \infty$. Perfect dielectric conductor contains surface current density and originates surface waves.

Metal surface supports surface waves. These waves are propagating electromagnetic waves bound to the surface between the metal surface and free space. At microwave frequency, surface wave are normal AC current that occur in any electrical conductor [78]. For smooth metal plane, surface waves does not couple to external wave but they will radiate and scatter if there is bend, discontinuities or surface texture. Any break in the continuous, flat metal surface allows the current to radiate and the result is a kind of multipath interference that cause ripples in the far field radiation pattern.

Bound surface wave does not exist on ideal PEC since in the limit of finite conductivity, the fields associated with the surface current extends and infinite distance into space [78]. Thus on an infinite large ground plane the surface current would be evident only as a slight reduction in radiation efficiency.

Discontinuities in the metal surface produce scattering/radiation from the metal surface into the free space. This apparent disadvantage could be used as an approach if the smooth metal plane is transformed into a special texture that creates constructive interference when the plane impinges into this new texture of metal surface. As introduced previously, this kind of structure are called HIS. If the protrusions of the special texture are small compared to the wavelength, the electromagnetic properties can be described using lumped circuit elements (capacitor, inductor). This equivalent circuit behaves as an electric filter to block the flow of currents along the metal surface [78]. This approach is used in the construction of tag antenna with HIS structure in order to immune the metal surface effect and size reduction of the design.

3.6 The rectangular waveguide

The waveguide is a structure in which other modes (TM, TE modes) can propagate in addition to the TEM field. These higher order modes of the field structure start to propagate when excitation frequency becomes large enough such that the cross section of the line, for example, conductor separation, becomes a significant portion of wavelength [12].

The transversal magnetic TM mode refers that the magnetic field in the direction of propagation equals zero $\boldsymbol{H}_Z = 0$ and the transversal electric TE mode refers that the electric field in the direction of propagation equals to zero $\boldsymbol{E}_Z = 0$. Updated formulas for phase constant (β), phase velocity (ɯ), and wavelength (λ) emerge as a result and they may be found in [12].

Rectangular waveguide behaves as a resonant circuit with high quality factor “Q”. A resonant circuit can be constructed of lumped components. But, lumped components

have non-ideal behavior and their losses increases at higher frequencies. The cut-off frequency $f_{c,mn}$ defines the frequency modes that may exist inside the waveguide. The permeability and permittivity inside the waveguide μ, ε are constant known values; *m* and *n* are the modes which are integer value (0, 1, 2…). The frequencies modes inside a rectangular waveguide depend only on the dimensions of the rectangular waveguide (*a*, *b*).

$$f_{c,mn} = \frac{1}{2\pi\sqrt{\mu\varepsilon}}\sqrt{\left(\frac{m\pi}{a}\right)^2 + \left(\frac{n\pi}{b}\right)^2} \tag{3.31}$$

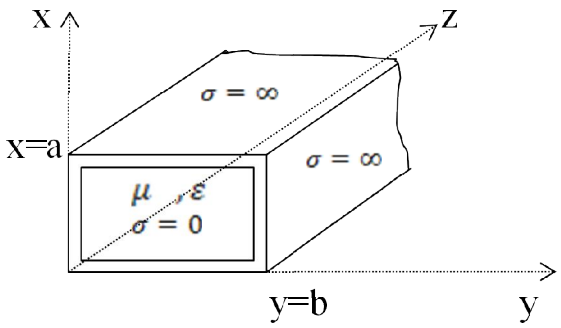

Figure 3.11. *Rectangular waveguide, parameter definition.*

Rectangular waveguide resembles the propagation case in microstrip antennas, which is the main topic of the next chapter.

4. RECTANGULAR PATCH ANTENNA

This chapter describes the fundamental parameters of the antenna for designing the microstrip antenna. Effective aperture and radar cross section are also introduced since both parameters are used for the link budget in a passive UHF-RFID communication. Besides, the microstrip antenna design parameters and radiation characteristic analysis are explained through the transmission line model and cavity model in this chapter. The accuracy of microstrip antenna analysis is improved by full wave analysis despite increasing the solution difficulty and memory capacity. Electromagnetic simulators use the full wave analysis and solve computationally Maxwell's equations. Two numerical methods: FEM (finite element method) and FDTD (finite difference time domain) are introduced. Both methods are used by the electromagnetic software: HFSS (High Frequency Simulator Software) and CEMS (Computational Electromagnetic Simulator), respectively for designing the microstrip patch tag antenna. Finally, design considerations based on microstrip antenna parameters (thickness, dielectric constant, dimensions) determine the radiation parameter behavior (bandwidth, radiation efficiency, directivity). The relation between them is also explained in this chapter.

4.1 Fundamental parameters of antenna

The definitions of antenna parameters are based in IEEE standard [14]; they are valid for all antennas.

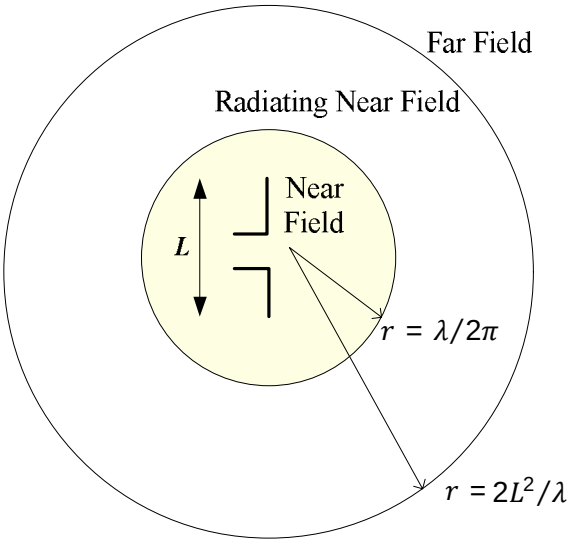

Figure 4.1. *Near Field and far field radiation region of the antenna in general.*

The antenna is defined as "that part of the transmitted or received system which is designed to radiate or receive electromagnetic wave" [14]. The radiation regions of the antenna depend on the distance (r) from the antenna to the testing point as it is expressed in Fig. 4.1. The near field region and far-field region is the energy zone originated by the antenna where energy is stored or radiated, respectively. The near field region is limited at distance $r \ll \lambda/2\pi$, where λ is the wavelength of the field. In the far field region, the radiation pattern is well formed and it starts at distance where: $r \gg \max(\lambda/2\pi, 2L^2/\lambda)$. For UHF-RFID antenna, the measurements are taken in the far field region.

The simple equivalent circuit of an antenna is formed by resistance (radiation resistance and losses resistance) and reactance. The antenna as an equivalent circuit of resistance and reactance is explained in [15]. The radiation resistance originates radiation power or scattering power when the antenna is operating in transmitting mode or receiving mode, respectively. The antenna losses as heat are represented by the losses resistance. The antenna can be connected to arbitrary load impedance; and the antenna starts to transmit/receive when energy source is applied to the antenna at certain frequency or range of frequencies. The maximum power transfer occurs when antenna impedance equals to the complex conjugate of the load impedance. This circuit scenario is practical for the comprehension of any antenna parameters.

The ***antenna efficiency*** (e_0) is an antenna parameter that "takes into account the reflection, conduction, and dielectric losses" [15]. It is obtained by multiplying the antenna radiation efficiency(e_{cd}) and the reflection efficiency (e_r). The reflection efficiency denotes the level of transmission coefficient ($1 - |\hat{S}|^2$). Where $\hat{S}$ is power wave reflection coefficient due to impedance mismatch between antenna impedance and arbitrary load impedance connected to the antenna.

The conduction-dielectric losses of an antenna are a joint parameter difficult to separate even by measurement. They are joined to express the antenna radiation efficiency (e_{cd}). The antenna radiation efficiency is the radio of radiated power of the antenna (P_{rad}) respect to total accepted power of the antenna (P_{in}). Radiation efficiency is equal to one for a lossless antenna.

The ***average radiated power***(P_{rad}) is obtained by integrating the average power density ($\boldsymbol{S_{av}}$) over the sphere area of radius R. Recall that $P_{rad} = \int_{\phi=0}^{2\pi}\int_{\theta=0}^{\pi} \boldsymbol{S_{av}} \cdot d\boldsymbol{s}$ from (3.17).

The ***radiation intensity*** $U(\theta, \phi)$ in a given direction is defined as the "power radiated from an antenna per unit solid angle" [14]. It is a far field parameter and it denotes (4.1).

$$U(\theta, \phi) = R^2 S_{av} \tag{4.1}$$

An isotropic radiator is an ideal source that radiates equally in all directions. The average power density of an isotropic radiator ($\boldsymbol{S}_0$) expressed in (4.2); depends only on distance ratio R and it is directed in radial direction $\widehat{\boldsymbol{a}_r}$. The isotropic radiation intensity (U_0) is expressed in (4.3).

$$\boldsymbol{S}_0 = \frac{P_{rad}}{4\pi R^2}\widehat{\boldsymbol{a}_r} \tag{4.2}$$

$$U_0 = R^2 S_0 = \frac{P_{rad}}{4\pi} \tag{4.3}$$

The ***directivity*** in a given direction is "the ratio of the radiation intensity in a given direction from the antenna respect to the radiation intensity averaged over all directions" [14]. This average radiation intensity is considered as the radiation intensity of an isotropic antenna.

$$D(\theta,\phi) = \frac{U(\theta,\phi)}{U_0} = 4\pi\frac{U(\theta,\phi)}{P_{rad}} \tag{4.4}$$

Hence, the maximum directivity (D_{max}) is defined for the maximum direction of the radiation pattern as

$$D_{max} = \frac{U(\theta,\phi)_{max}}{U_0} = 4\pi\frac{U(\theta,\phi)_{max}}{P_{rad}}$$

The ***gain*** is defined as "the ratio of the radiation intensity in a given direction, to the radiation intensity that would be obtained if the power accepted (P_{in}) by the antenna were radiated isotropically" [14] and it is expressed in (4.5).

$$G(\theta,\phi) = \frac{U(\theta,\phi)}{(P_{in}/4\pi)} \tag{4.5}$$

From (4.4), (4.5) and considering $P_{rad} = e_{cd}P_{in}$. The gain and directivity are related by the antenna radiation efficiency $G(\theta,\phi) = e_{cd}D(\theta,\phi)$.

Gain does not include losses arising from impedance and polarization mismatches. The realized gain (G_r), expressed in (4.6) includes the losses due to impedance mismatch between the antenna impedance and load impedance. Realized gain is the main parameter compared between simulation and measurement of tag antenna design. The impedance mismatch between the antenna and load is known as the power wave reflection coefficient ($\hat{s}$). This expression is explained in more detail in Chapter 5 and well explained in [26; 27].

$$\hat{s} = \frac{Z_{load} - Z_{antenna}^{*}}{Z_{load} + Z_{antenna}} \tag{4.6a}$$

$$G_r(\theta,\phi) = G(\theta,\phi)(1 - |\hat{s}|^2) \tag{4.6b}$$

The ***polarization loss factor*** (PLF) is the polarization mismatch between the antenna and the incoming incident wave [15]. The incoming incident wave ($\boldsymbol{E_i}$) is polarized in the direction ($\widehat{\boldsymbol{\rho}_w}$) and expressed as $\boldsymbol{E_i} = \widehat{\boldsymbol{\rho}_w}E_i$. The polarization of the antenna is along the direction ($\widehat{\boldsymbol{\rho}_a}$) and the electric field is expressed as $\boldsymbol{E_a} = \widehat{\boldsymbol{\rho}_a}E_a$. Then, the angle ($\psi_p$) formed by the incoming incident electric wave and the antenna polarization is known as the polarization loss factor

$$PLF = |\widehat{\boldsymbol{\rho}}_{\boldsymbol{w}} \cdot \widehat{\boldsymbol{\rho}}_{\boldsymbol{a}}|^2 = \left|\cos\psi_p\right|^2. \quad (4.7)$$

4.1.1 The effective aperture and radar cross section

The antenna equivalent areas like scatter area, loss area and effective area describe capturing characteristic of the antenna when a wave impinges on it. The mismatch impedance between the antenna impedance and the load impedance is represented by the power wave reflection coefficient ($\hat{s}$). This parameter influences the antenna effective aperture and radar cross section of an antenna.

The ***antenna effective aperture*** (A_e) is the area which multiplied by the incident power density gives the power delivered to the load [9; 15]. The antenna effective aperture takes into account conduction dielectric losses (e_{cd}), directivity of the antenna ($D(\theta, \phi)$), polarization losses ($|\widehat{\boldsymbol{\rho}}_{\boldsymbol{w}} \cdot \widehat{\boldsymbol{\rho}}_{\boldsymbol{a}}|^2$) and impedance mismatch ($\hat{s}$).

$$A_e = e_{cd}(1 - |\hat{s}|^2)|\widehat{\boldsymbol{\rho}}_{\boldsymbol{w}} \cdot \widehat{\boldsymbol{\rho}}_{\boldsymbol{a}}|^2 \frac{\lambda^2}{4\pi} D(\theta, \phi) \quad (4.8)$$

The ***radar cross section (RCS, σ)*** is used to characterize the scattering properties of a target. RCS is defined as the area intercepting that amount of power which when scattered isotropically, produces at the receiver a power density which is equal to that scattered by the actual target [9; 15]. In simple terms, the amount of scattered power is obtained by multiplying the incident power density to the antenna with σ [9]. *RCS* is denoted usually by (4.9) for an antenna and it should also be understood as a direct measure of electrical antenna visibility.

$$\sigma = \frac{\lambda^2}{4\pi} G(\theta, \phi)^2 |1 - \hat{s}|^2 \quad (4.9)$$

The RCS term is applied during the backscattering communication from tag antenna to the reader. The probability to detect a target increases when visibility of the target (RCS) increases.

On the other hand, RCS is also used in stealth application. In this case, the RCS is optimized to be the minimum in order that radars (readers) cannot detect the object.

4.1.2 Radar range equation

The radar range equation describes the link budget between the transmitter, receiver and target. A UHF-RFID system is similar to the radar system operation because the passive tag antenna behaves as target.

The radar range equation is denoted in (4.10) [15]; and Fig. 4.2 depicts the communication power in passive UHF RFID system. The radar range equation is well explained in [15] and it is applied for the tag antenna measurement. P_t denotes the transmit power; and $e_{cdt}, D_t(\theta_t, \phi_t)$ denotes the radiation efficiency and directivity of the transmitter antenna. P_r denotes the power delivered to the load in the antenna

receiver mode; and $e_{cdr}, D_r(\theta_r, \phi_r)$ denote the radiation efficiency and directivity of the receiver antenna, R_1 is the distance between the transmitter and target, R_2 is the distance between the target and receiver, λ is the wavelength, σ is the *RCS* of the target. For a tag antenna σ is calculated using (4.9).

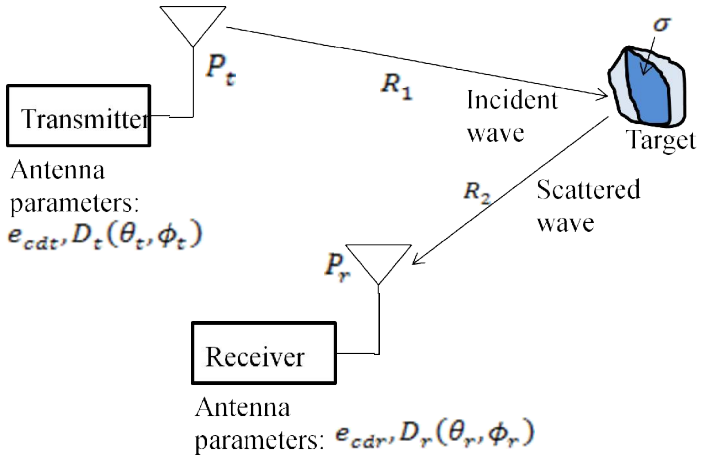

Figure 4.2. *Geometrical arrangement of transmitter, target and receiver for radar range equation [15].*

$$\frac{P_r}{P_t} = e_{cdt} e_{cdr} \sigma \frac{D_t(\theta_t,\phi_t) D_r(\theta_r,\phi_r)}{4\pi} \left(\frac{\lambda}{4\pi R_1 R_2}\right)^2 \tag{4.10}$$

This relation is applied in UHF-RFID system. The target is the tag antenna and the transmitter and receiver are placed in the same hardware called reader.

4.2 Analysis models for a rectangular microstrip antenna

The antenna analysis predicts the radiation characteristics like radiation pattern, gain, polarization, antenna impedance, radiation efficiency, etc. A good model should calculate all impedance and radiation characteristic, be accurate enough and simple [16]. There is a compromise between the simplicity of the model and accuracy. Based on this, the analytical technique and the full wave technique are the main techniques that analyze microstrip antenna.

A summary of the analytical model is taken mainly from [15; 16]. The analytical technique offers simple and analytical solutions. This analysis considers the microstrip antenna divided into interior region and exterior region as Fig.4.3. The interior region is formed by the patch conductor, the portion of the ground plane under the patch, and the walls formed by the projection of the patch periphery onto the ground plane. The exterior region is the rest of the space. The fields in the interior region are modeled as transmission line or as a cavity.

The transmission line model is studied in [16] and it analyzes the microstrip antenna as a transmission line which at the same time introduces different analysis levels and

accuracy. First, the model introduces mutual admittance term to the equivalent circuit of the antenna in order to consider the fringing field. Second, the model analyzes the non-radiating edge of the transmission line as a π-network; this assumption can be applied to any separable geometry of the antenna. Third, the model analyzes the radiation loss, dielectric loss and copper loss by increasing the dielectric loss.

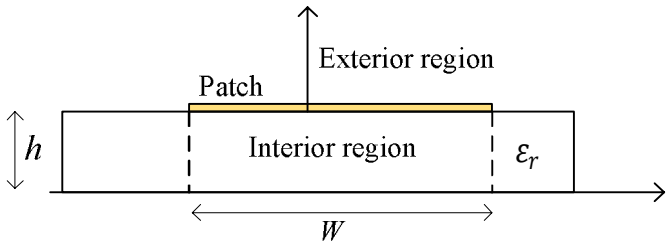

Figure 4.3. *Interior and exterior region associated with the antenna [15].*

On the other hand, the cavity model and its extension models consider the loss of the energy field due to fringing edge, radiation, conduction and surface wave, as the increase in substrate loss tangent or as the boundary edge admittance [16]. This consideration is done in order to calculate the field outside the patch antenna. The cavity model applies generally to regular patch shape. Since substrate thickness is so small with respect to wavelength there is no field variation along substrate thickness. However, the cavity model can be extended in order to include the variation field along the substrate. The cavity model assumes a magnetic wall at distance "Δ" all around the periphery of the patch in order to take into account the energy stored in the fringing fields. This assumption reduces the mathematics from the boundary conditions and the calculation of the interior electric field. The electric field can also be determined by applying the Green function to regular geometry of the patch [16].

An extension of the cavity model analyzes not regular shape patch antenna but whose geometry is non-separable. The approach of this extension model is the use of segmentation to the non-radiating edge; despite applying to arbitrary patch shape, the geometries of the segmented patches should be regular in order to use appropriately the Green's function for known geometries.

Another extension of the cavity model is the multiport network model which is also explained in [16] and it considers the "impedance boundary condition" at the periphery. The mutual coupling between edges and any discontinuity of the patch is included in the analysis. The interior region is modeled as multiport planar circuit. The fields in the exterior which includes fringing fields, radiation fields, and surface wave fields are represented by the load admittances. The fields outside the patch as fringing field at the edge, radiation field, and surface wave field are characterized as load admittance or as an Equivalent Admittance Network (EAN). The EAN consists of a capacitor and conductance. The capacitance represents the energy stored by the fringing fields and the conductance represents the power carried away by the radiation and surface wave. All

the edges are qualified to be represented as load admittance and they can be divided into a number of ports for then be connected to the multiport planar circuit.

The analytical models has some limitations like it is accurate for thin substrate, simple feed configurations, furthermore anisotropic substrates and cross polarized radiation has not been tested [16].

Full wave method is based on numerical method solutions of Maxwell's equations. This method is more rigorous and numerically intensive. It offers accurate solutions, consideration of losses in the solution, applicability for a variety of shapes and feeding techniques. Full wave method overcomes some limitations of the analytical model. Numerical methods solve Maxwell's equations and it includes integral equation analysis in the spectral domain, integral equation analysis in the space domain, and the finite-difference time-domain (FDTD). The integral equation methods, explained in [16], assume that dielectric substrate and ground plane are infinite extend; the solutions are more accurate when dielectric substrate and ground plane are several wavelengths long. However, the FDTD method is more accurate for finite sized antenna. This chapter includes a brief introduction of the FDTD method in next subchapter since one of the electromagnetic simulator software is based on this method.

4.2.1 The transmission line model

The transmission line model would lead to some quick dimensional calculus for the microstrip antenna design. The transmission line model represents the microstrip antennas as two slots separated by a transmission line of length L [15]. The main parameters of microstrip antenna are the length of the antenna (L), width of the antenna (W), dielectric thickness (h), and dielectric constant (ε_r).

The microstrip antenna has two radiating slots and two non-radiating slots. The radiating slots are the responsible for the radiation of microstrip antenna as an aperture antenna. Figure 4.5 illustrates the microstrip antenna. The field at the edges of the radiating slots of the patch overspread the radiation; this is called the fringing effect [15]. This effect influences in the resonant frequency of the antenna since the length of the antenna is electrically longer than the physical length.

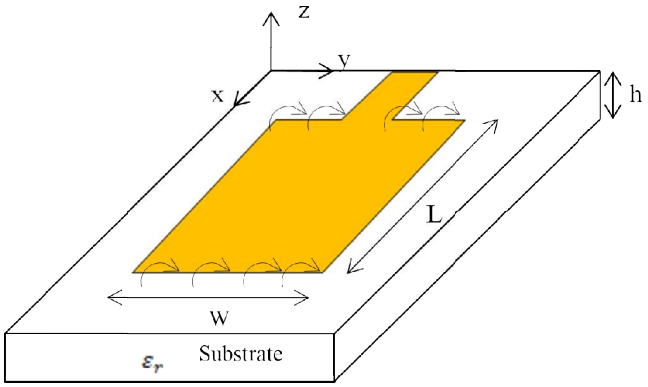

Figure 4.4. *Common microstrip antenna [15].*

The fringe effect is represented by the effective dielectric constant (ε_{eff}) and it is calculated in (4.11). As ε_{eff} approaches ε_r, the electric field lines concentrate in the substrate. This can be achieved by increasing the ratio of the antenna width respect to dielectric thickness ($W/h \gg 1$) and/or increasing the dielectric constant ($\varepsilon_r \gg 1$). The effective dielectric constant is frequency dependant. At higher frequencies, the effective dielectric constant approaches the relative dielectric constant.

$$\varepsilon_{eff} = \frac{\varepsilon_r+1}{2} + \frac{\varepsilon_r-1}{2}\left[1 + 12\frac{h}{W}\right]^{-1/2} \tag{4.11}$$

The antenna width depends on free space wavelength and dielectric constant.

$$W = \frac{\lambda_0}{2}\sqrt{\frac{2}{\varepsilon_r+1}} \tag{4.12}$$

The increase of the electrical length (ΔL) due to fringing effect is calculated as

$$\frac{\Delta L}{h} = 0.412\frac{(\varepsilon_{eff}+3)\left(\frac{W}{h}+0.264\right)}{(\varepsilon_{eff}-0.258)\left(\frac{W}{h}+0.8\right)} \tag{4.13}$$

The total electrical length and the physical length of microstrip antenna are expressed in (4.14) and (4.15), respectively.

$$L_e = \frac{\lambda_0}{2\sqrt{\varepsilon_r}} \tag{4.14}$$

$$L = L_e - 2\Delta L \tag{4.15}$$

Equations (4.11) to (4.15) are useful for designing a simple microstrip antenna at desired operating frequency.

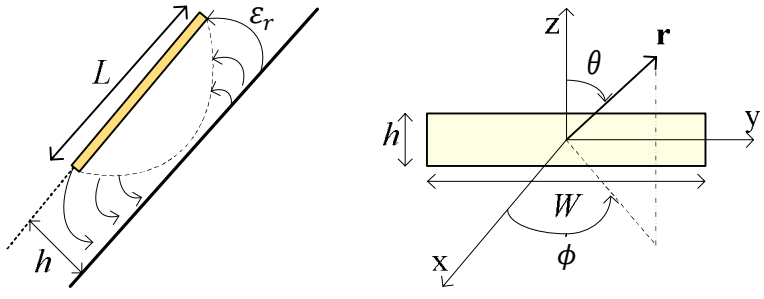

Figure 4.5. *Side views of the radiating slots (left) and coordinate system for the radiation of each radiating slot (right) that resembles an aperture antenna [15].*

4.2.2 The cavity model

The cavity model helps to explain the radiation mechanism of a microstrip patch antenna. The terms radiating and non radiating edges are well explained in this model. This model analyzes the antenna as a lossy cavity model by introducing the term effective loss tangent [16].

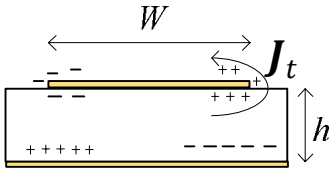

Figure 4.6. *Charge distribution and current density on microstrip patch antenna [15].*

When the microstrip patch is energized, there is a charge distribution in the patch side and the ground plane, as can be seen in Fig. 4.6. The charges on the patch repeal each other, originating electric current density $\boldsymbol{J}_t$ due to charge movement from the lower surface of the patch to the upper surface [15]. Since the patch side is a perfect conductor, electric current density within that plane is almost zero ($\boldsymbol{J}_t = 0$). The tangential current density also becomes zero since the charge movement and current flow decreases as the ratio W/h increases [15]. This approach let to define four perfect magnetic surfaces between the patch and the ground plane. Hence, microstrip antenna is modeled as a cavity formed by two conductor surface formed by the upper side patch and the ground plane and by the four perfect magnetic walls.

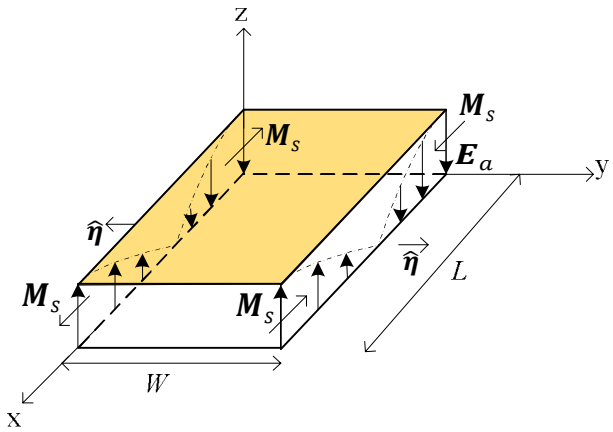

Figure 4.7. *Current densities on non radiating slots of rectangular microstrip patch [15].*

The substrate thickness is smaller compared to width and length. The electric field along the normal direction of the substrate is constant but magnetic components goes zero; as explained before. Thus, TM mode is the propagation mode. For antenna positioned like in Fig. 4.7 the mode TM_{100} is the propagation mode in which the length is half wavelength. This propagation mode causes two results. First, electric field varies up and down along L. Magnetic current densities $\boldsymbol{M} = -2\hat{\boldsymbol{\eta}} \times \boldsymbol{E}_a$ along these two walls (slots) are equal in magnitude but opposite direction. Here $\boldsymbol{E}_a$ is the electric field

formed between the patch and ground plane. As a result, the field radiated by these two slots cancels each other. These two slots are called the non radiating slots. Second, the electric field along the width is constant and the magnetic current densities along these slots have same magnitude and phase [15]. These magnetic current density form an array of two element sources that will be add in a direction normal to the patch and ground plane. These two slots are called the radiating edges. Fig. 4.8 shows the electric field and magnetic current density along *W* in both side walls. The radiation in the far field of each slot and the radiation by the contribution of both of them are represented in Fig. 4.8.

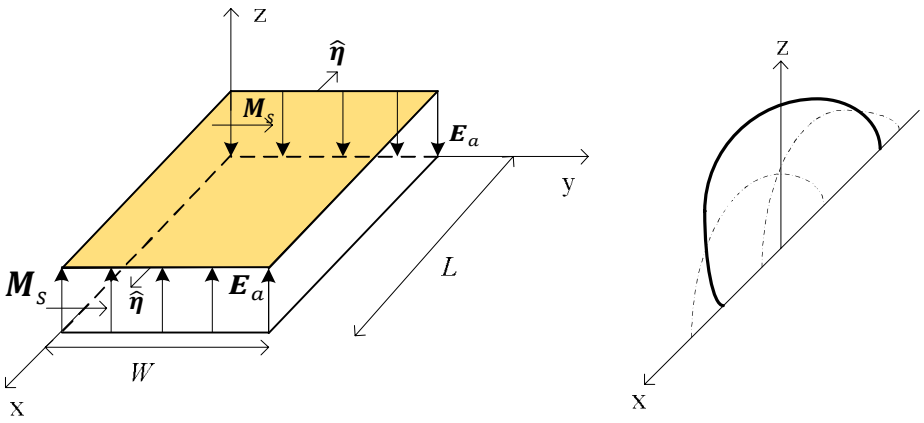

Figure 4.8. *Rectangular microstrip patch radiating slots and equivalent magnetic current densities (left) and typical radiation pattern of each microstrip patch slot and the two together (right).*

4.3 Electromagnetic modeling simulators

The Ansoft HFSS [36] and CEMS [22] software were used in the simulation for tag antenna design; both solve Maxwell's equations using different numerical methods. Ansoft HFSS uses mainly Finite Element Method (FEM) whereas CEMS uses the Finite Difference Time Domain (FDTD) method. It is the aim of this subchapter to give some introductory notes of these two methods and more descriptive information can be found in [16; 18; 22].

The electromagnetic simulators use numerical methods to solve Maxwell's equations in a transparent way for the user. It is up to the user to know the strongest of each method in order to exploit the capacity of the simulator. In general, the numerical methods solve the discretized Maxwell's equations for a discretized problem. This solution should have a finite computational time and capacity storage. Actually, there are many numerical methods. Some of these methods are based on the solution type and in the space variables, as it is described in [18].

Numerical method classified on solution domain includes frequency domain and time domain solvers. Some frequency domain solvers are the Method of Moment (MoM), Finite Element Method (FEM), Spectral Domain Method (SDM) and some commercial simulators that use this frequency domain solver are Zeland IE3D, Ansoft

HFSS, Antsoft designer, FEKO, Super NEC, Momentum ADS, EM-Slight AWR, Sonnet Suite, Microwave wizard, FEMLAB. In the same way some time domain solvers are the Finite Difference Time Domain (FDTD), Finite Integration Technique (FIT) and Transmission Line Matrix (TLM) and commercial simulators that use this time domain solver are CST Microwave Studio (CST MWS), Semcad, IMST Empire, Fidelity, QuickWave, Mefisto [17].

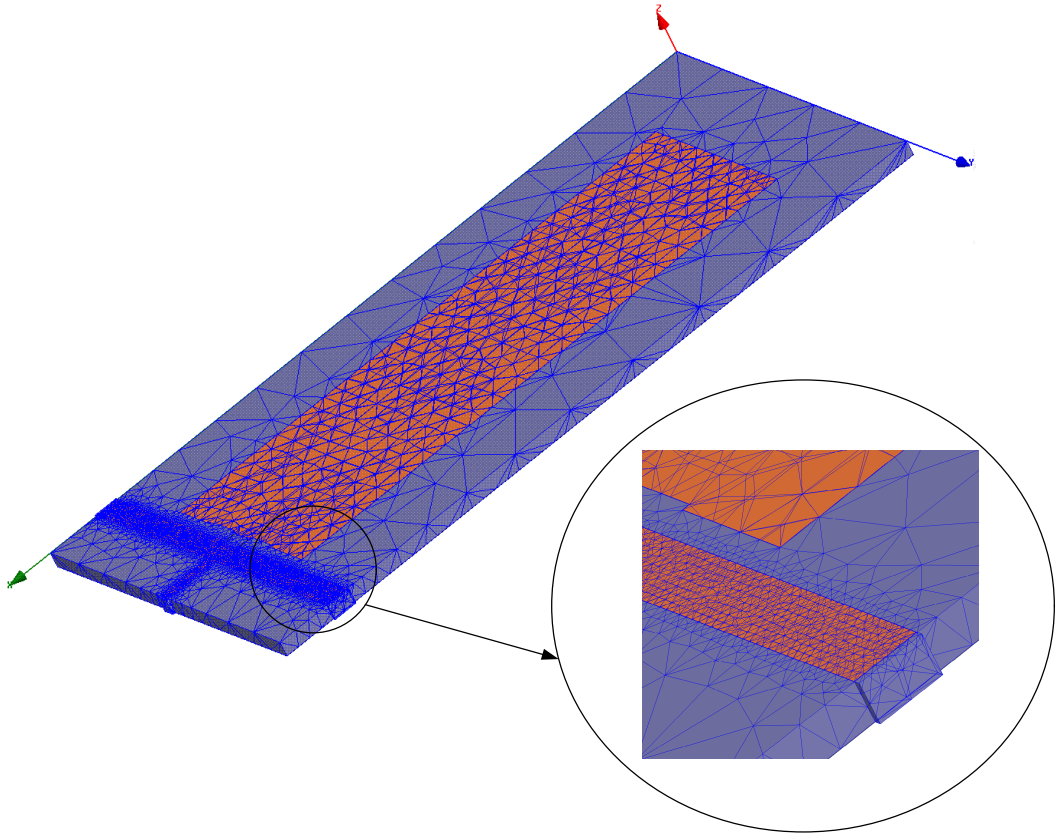

Figure 4.9. *Tag antenna mesh, using Ansoft HFSS. The tetrahedral discretization is applied in FEM method.*

The finite element method (FEM) is a numerical technique that solves the integral form of Maxwell's equation in frequency domain. This is a powerful technique for complex geometries, heterogeneous media and levels of resolution [17]. The volume is discretized using tetrahedral of different sizes as it is depicted in Fig. 4.9. The number of segments for the volume discretization affects the size of the mesh and improves the accuracy of the method. However it should be a compromise between the number of segments and solution time. Through discretization, the partial differential equations are transformed to matrix equation to be solved. At some point while solving the Maxwell equation, this matrix is a large spare matrix to invert and it requires big storage capacity [17; 18].

The unbounded region which represents the infinite free space has to be truncated in order to get finite information for processing; a special kinds of boundary property is also explained in [19; 20; 21]. A layer in which the field hits with no reflection is

assigned as absorbing boundary condition or perfect match layer. This condition also applies for the FDTD method.

The finite difference time domain (FDTD) is a numerical method that solves the Maxwell's equations by using the differential equation time domain approach. It was first proposed by Yee in 1966. The FDTD analysis starts with the volume discretization by spatial grids or cells, the simple cell is a cube of size $\Delta x, \Delta y, \Delta z$. Fig. 4.10 is an example of volume discretization in grid cell. The cell size dimension depends on the smallest feature in the problem. Next, the unbounded region or the region that represents the infinite free space is truncated by absorbing boundary condition or layer in which no reflections occur [18; 22]. Then, the electric and magnetic fields are samples at discrete points in time and space; and the partial differential equations of Maxwell's laws are approximate by finite difference form and those are applied to the discretized volume for certain time steps Δt [22]. An electromagnetic pulse excites the structure for its propagation study. An excitation source, which depends on the problem under consideration, is necessary for FDTD simulation. The source is a waveform that excites electric and magnetic fields in function of time. I.e. the Gaussian waveform is the favorite source waveform since it can be designed to contain all the frequencies up to the highest frequencies that are tied to a cell size [22]. The relation of the highest frequency wavelength to the unit cell size is known as the number of cells per wavelength.

The time and frequency domain of the structure are processed until the time domain waveform is stabilized. Furthermore, the appropriate choice of the period of sampling ($\Delta t, \Delta x, \Delta y$ and Δz) guarantees the stability and accuracy of the solution [22].

The numerical stability bounds the propagation of error during the time marching progression of the algorithm. This initial error may be due i.e. the truncation of a real number. It is demonstrated that stability condition is bounded for $\lambda \leq 1$; for values greater than 1, the error propagation increases considerable.

$$\lambda = \frac{\Delta t}{\Delta x} \tag{4.16}$$

The Courant Friedrich-Lewy (CFL) determines the numerical stability of the FDTD method [18; 22]. The CFL requires that the time increment Δt has a specific bound relative to the lattice space increments

$$\Delta t \leq \frac{1}{\sqrt{\frac{1}{\Delta x^2}+\frac{1}{\Delta y^2}+\frac{1}{\Delta z^2}}c} \tag{4.17}$$

For three dimensions and considering homogeneous dimension $\Delta x = \Delta y = \Delta z$, then CFL is expressed as $\Delta t \leq \frac{1}{\sqrt{3}c}$ [18]. For one dimension, the CFL is reduced to $\Delta t \leq \Delta x/c$. If time increment Δt is greater than the CFL limit, this leads to instability in the FDTD computation. The maximum time step is controlled by the smallest values among $\Delta x, \Delta y \; or \; \Delta z$ thus the maximum time step allowed must be smaller than

$\min(\Delta x, \Delta y, \Delta z)/c$. However this condition does not guarantee the accuracy of the solution as it is explained by examples in [22].

The discretization of the Maxwell's equation and problem space leads to a deviation solution from the original solution of the problem. This introduced error causes differing of phase velocities from the original phase velocities; this is known as numerical dispersion. Numerical dispersion error reduces when the period of sampling approach zero; however this leads to continuous wave and increment in computation capacity. The numerical distortion gives rise itself to a distortion of the waveform because waves with different frequencies propagate with different phase velocities [12; 18].

The FDTD method is capable of predicting broadband frequency domain due to the application of the Fourier transform in time domain analysis [16]. However, the frequency resolution of the method is limit. The FDTD method offers simplicity in mathematic formulation and facility to implement in computer simulator models by using parallel computation technique. Furthermore, it applies to different geometries and material properties like lossy dielectric, anisotropic plasmas, magnetized ferrites.

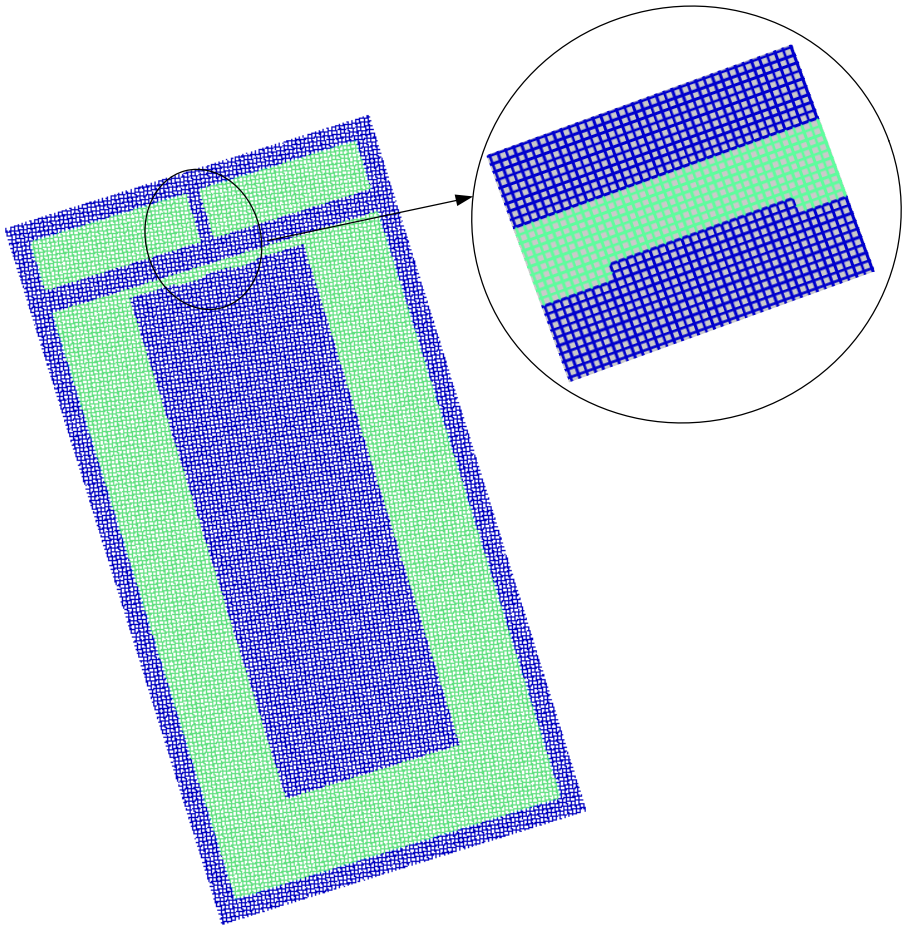

Figure 4.10. *Tag antenna mesh, using CEMS. The cube cell discretization is applied in FDTD method.*

Some differences between FEM and FDTD are listed in Table 3.1.

Table 3.1. *Some principal characteristic of numerical methods FEM and FDTD*

FEM	FDTD
Solve Maxwell's equations in frequency domain.	Finite differential are used to solve Maxwell equation in time domain.
Method applicable to time and frequency domain	Time domain is used rather than frequency domain.
Volume is discretized in tetrahedral of various sizes.	Volume is discretized into volume elements (cells). Yee cell
Automatic mesh refinement. In software application a refinement mesh of special region or the whole region can be set.	Cell size depends on the smallest dimension of the problem.

The Perfect Match Layer

As previously mentioned, the infinite space should be truncated for any electromagnetic simulator as shown in Fig. 4.11. The unbounded region represents the free space region and this should be computational truncated to have a finite time processing and reasonable computational storage capacity [20]. The Absorbing Boundary Condition (ABC) gives an approach for the truncation by using a plane or a layer in which the waves hit this layer and propagate without reflection [19]. This approach allows the propagating wave to simulate throughout the infinite space.

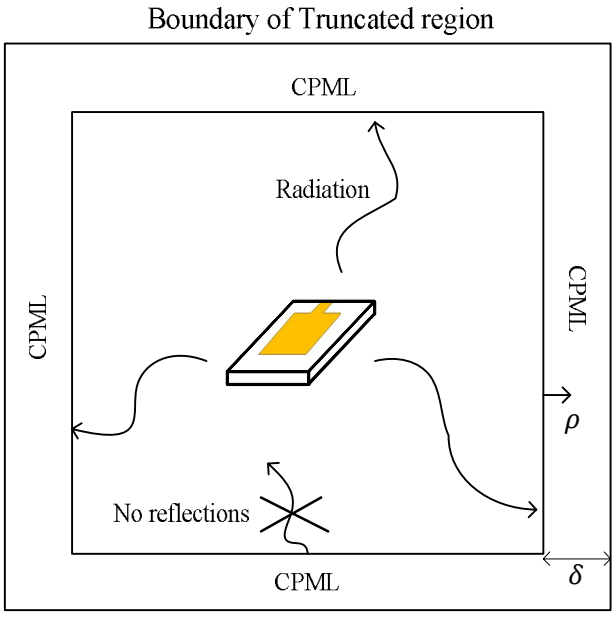

Figure 4.11. *The space is truncated to some computational region. An absorbing layer is placed adjacent to the edges of the computational region—a perfect absorbing layer would absorb outgoing waves without reflections from the edge of the absorber [19].*

There is also some classification inside ABC; like analytical, material, Perfect Match Layer (PML), etc. Analytical ABC states that there will be no reflected waves

when plane wave incidents *normal* to a perfect absorbing plane. Material ABC is another technique which introduces a *lossy medium* instead of a perfect absorbing plane. "This medium is taken to be of finite thickness and is backed by a perfect conductor" [16]. The parameters of the lossy medium are defined in way that when the wave incidents normal to this medium, there will be reflection. The Perfect Match Layer (PML) introduced by Berenger, is an extension of previous technique and it creates a nonphysical absorbing medium in the exterior region so that waves do not reflect at the interface [19; 20]. An elegant way to express the wave is to represent it in complex coordinate. The wave is transformed in sense that radiation is exponential decaying. Special cases for PML for inhomogeneous media and evanescent waves are explained in [19].

The convolutional PML (CPML) technique, which was first introduced by Kuzuoglu and Mittra [21], overcomes some limitations of PML for evanescent waves. The idea is that PML must be placed sufficiently far from the obstacle such the evanescence waves have sufficiently decayed. This is done by a different choice of the "complex stretching value", explained in [20; 21; 22].

For i.e the electric "e" complex stretching value in the "x" direction S_{ex} is updated from the PML condition to CPML condition by [21; 22]

$$S_{ex} = 1 + \frac{\sigma_{pex}}{j\omega\varepsilon_0} \rightarrow S_{ex} = k_{ex} + \frac{\sigma_{pex}}{\alpha_{ex}+j\omega\varepsilon_0}, \tag{4.18a}$$

and the complex stretching values are [22] ;

$$S_{ei} = k_{ei} + \frac{\sigma_{pei}}{\alpha_{ei}+j\omega\varepsilon_0},$$

$$S_{mi} = k_{mi} + \frac{\sigma_{pmi}}{\alpha_{mi}+j\omega\varepsilon_0}, \; i=x, y \; or \; z. \tag{4.18b}$$

Where k_{ei}, α_{ei} are the two new different parameters added from the already proposed PML. k_{ei} and k_{mi} are obtained by [22]

$$k_{ei} = 1 + (k_{max} + 1)\left(\frac{\rho}{\delta}\right)^{n_{pml}},$$

$$k_{mi} = 1 + (k_{max} + 1)\left(\frac{\rho}{\delta}\right)^{n_{pml}}. \tag{4.19}$$

Where n_{pml} is the order of the propagation, ρ is the distance from the computational domain-PML interface to the position of the field component, δ is the thickness of the CPML layer as it is expressed in Fig. 4.11. The conductivity profile scaling is expressed as [22]

$$\sigma_{pei}(\rho) = \sigma_{max}\left(\frac{\rho}{\delta}\right)^{n_{pml}},$$

$$\sigma_{mei}(\rho) = \frac{\mu_0}{\varepsilon_0}\sigma_{max}\left(\frac{\rho}{\delta}\right)^{n_{pml}}. \quad (4.20)$$

where $\sigma_{max} = \sigma_{factor} \times \sigma_{opt}$, here σ_{opt} is calculated by $\sigma_{opt} = \frac{n_{pml}+1}{150\pi\sqrt{\varepsilon_r}\Delta i}$; and the α_{ei} and α_{mi} are expressed as [22]

$$\alpha_{ei} = \alpha_{min} + (\alpha_{max} - \alpha_{min})\left(\frac{\rho}{\delta}\right),$$

$$\alpha_{mi} = \frac{\mu_0}{\varepsilon_0}\left[\alpha_{min} + (\alpha_{max} - \alpha_{min})\left(\frac{\rho}{\delta}\right)\right]. \quad (4.21)$$

From those equations, it is observed that the remaining unknown values in order to get the complex stretching value are k_{max}, n_{pml}, σ_{factor}, α_{max}, δ. Thus those scaling CPML parameters should be chosen in order to reduce the reflection error of evanescent modes [22]. The common range is σ_{factor}: 0.7 – 1.5; k_{max}: 5-11; α_{max}: 0-0.05; n_{pml} = 2,3 or 4; tickness of CPML (δ): 8 layers. α should not be zero in front of boundary interface but should decrease to zero away from the boundary interface to absorb purely propagating modes at low frequency [22].

CPML algorithm is independent of the material medium and can be extended for: dispersive media, anisotropic media, or nonlinear media [19]. This technique is used for CEMS simulator.

For the initialization of CEMS, two main processes occur: the definition of the problem and the initialization routine of FDTD; as it is well described in [22].

a) Definition of the problem

Parameters of the object, boundary and source are defined for the electromagnetic problem in order to create a data structure.

- Geometry of the objects in the problem space
- Materials type
- Electromagnetic properties of these material types
- Types of source and waveform
- Types of simulation results sought from the FDTD computation
- Types of boundary of the problem space.

b) Initialization

It permits initialize the problem space and FDTD parameters

- Number of time steps is the total number of time steps that the FDTD time-marching iteration will last.
- Number of cells per wavelength is a parameter by which the highest frequency in the Fourier spectrum of a source waveform is determined for a certain accuracy level.

- Courant factor is a factor that determines duration of time step with respect to the CFL limit.

Most of these values are set for the simulation running of the tag antenna in CEMS. They are summarized for this patch tag design of this thesis in Appendix 2.

4.4 Design considerations for a rectangular patch antenna

The thickness of the substrate (h), the dielectric constant (ε_r), and dimension of the antenna, width (W) and length (L) are the main parameters that determine the microstrip antenna design performance like radiation power, directivity, bandwidth, radiation efficiency [15; 16]. The improvement of one parameter in a microstrip antenna radiation may deteriorate another radiation parameter. Thus a compromise between antenna radiation parameters and the target of the design should be defined before and during the antenna dimension and dielectric setting. Figure 4.12 shows the counteract effect that dimension or dielectric constant of microstrip antenna may induce.

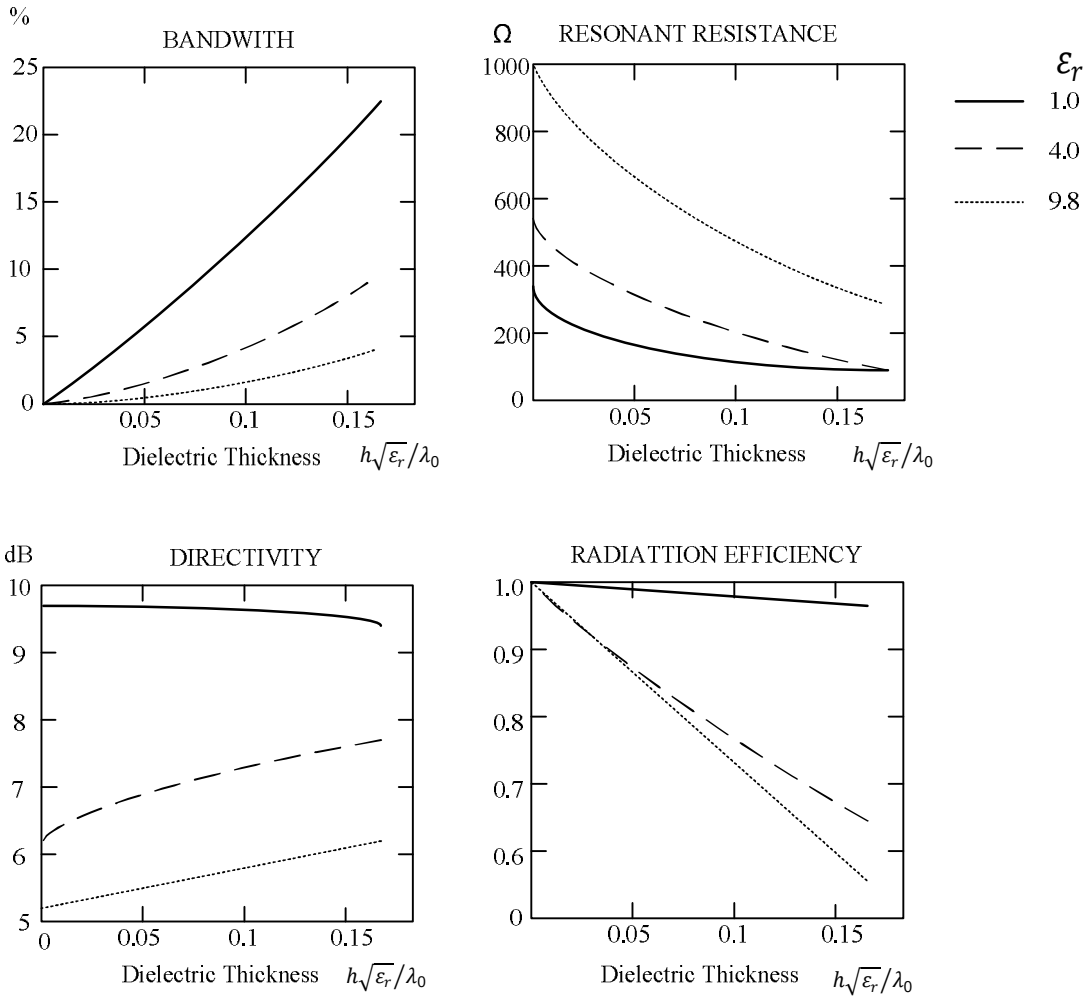

Figure 4.12. *Dependence of bandwidth, resonant resistance, directivity and radiation efficiency respect to thickness and dielectric constant [16].*

A resume of the dependence of some important radiation parameters of microstrip antenna is described and Fig.4.11 and it is described also in [15; 16]. The directivity varies inversely proportional to beamwidth. Directivity diminishes with lower *h* and *W*; whereas, beamwidth improves for decreasing *h, W,* and *L*. The radiated power diminishes when *h, W* decreases; whereas, radiation resistance increases because it varies inversely proportional to the radiated power. The bandwidth can be increased by increasing *h, W/L* or by decreasing ε_r. The radiation efficiency of the antenna may also be improved by increasing *h* and decreasing ε_r.

For example a microstrip antenna with small dielectric constant, the antenna dimension is large, even though the bandwidth can be improved by increasing the dielectric thickness; the radiation efficiency decreases. A compromise between antenna dimension and radiation parameters is done during antenna design and electromagnetic software helps to analyze those parameters for non-regular microstrip antenna design as it is the case of this thesis.

5. PASSIVE FAR FIELD RFID TAG

This chapter describes the operation process of passive RFID UHF far field system, the matching impedance between the tag antenna and the IC, and the link budget applied to the measurement of passive UHF tag antennas. The communication of this system is based on backscattering modulation; the tag antenna scatters the incoming signal at different levels by switching the impedance state of IC. For the matching analysis, the tag antenna should be the complex impedance conjugate of the IC impedance. The power reflection coefficient (PRC) is an indicator of impedance matching respect to frequency. The link budget in a UHF RFID system is used in the measurement analysis. The radar cross section and effective definitions are used for the communication link and some formulas such as transmitted power, maximum read range are also exposed. Those parameters and equations will be used directly for the measurement of the UHF patch tag antenna described in Chapter 7.

5.1 Operation of far field RFID system

The operation process of passive UHF RFID system is based on backscattering modulation. The first backscatter communication was described by H. Stockman and it dates from 1948 [80]. Through the years this communication type has evolved and it is actually applied for RFID system operation.

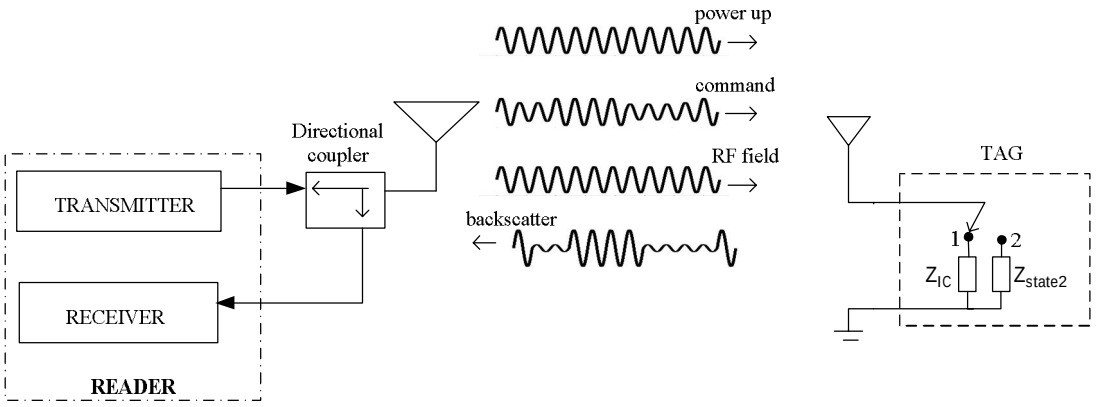

Figure 5.1. *Passive UHF RFID system operation between reader and tag antenna. RFID radio use coupler or circulator to detect only reflected signal [4; 30].*

The operation of UHF RFID system as illustrated in Fig. 5.1 is summarized in three steps as follows [2]:

- The tag rectifies the signal emitted by the reader in order to power up the IC.
- The reader sends the modulated and codified information to the tag.
- The tag sends information to the reader by switching the impedance state connected to the tag antenna between IC impedance (Z_{IC}) and an arbitrary load impedance (Z_{state2}) in order to modulate the continuous incoming RF wave from the reader. This process is called backscattered modulation.

The communications link between reader and tags is half-duplex, so tags shall not be required to demodulate reader's commands while backscattering [8].

The IC needs a constant voltage source to start operating. The reader sends to the tag antenna a continuous wave (CW), which is an electromagnetic wave with constant frequency and peak amplitude. The tag receives this CW and rectifies the induced voltage to power up the IC [8; 29; 31].

The rectification process of the sinusoidal wave is depicted in Fig. 5.2, as it is observed the rectification is mainly done by diode and capacitor (junction and/or stocky). The diode operates as a switch, letting pass the received input voltage (V_{in}) bigger than the operating diode voltage (V_{on}). The capacitor stores the voltage between RF cycles giving as output the ideal continuous source [8].

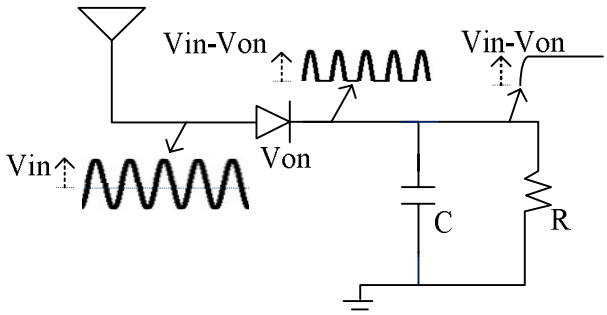

Figure 5.2. *RF signal rectification scheme in a passive tag IC. Principle for power up with constant voltage source [8].*

The tag IC needs around 1V to 2V [8] to run and common diode needs 0.5 V to operate; however, the final induced voltage in the tag antenna is lower than 0.5 V; thus a very common approach for obtaining higher voltage from a rectifier is the use of a number of diodes connected in stages (pump) in order to increase the output voltage of the array. The *voltage doubler* and *Dickson charge pump* are kinds of these array diodes structure, explained in [8]; however, the increase number of stages decrease the efficiency of the pumps, since all the DC current must flow through all the DC diodes in series and more power is wasted in turning on voltage of the diodes. A compromise between desired increase in output voltage and pump efficiency is done by IC designer company like [23; 24].

The reader modulates and encodes the information to be sent to the tag; the modulation format and data rate are fixed by the reader. The tag demodulates the signal through a similar circuit used for rectification to track the changes in the envelope

voltage of the RF signal to be decoded [8]. A passive tag does not have a mixer that allows channel filtering, then all received signal at RFID frequency band are converted to baseband. The air interface standard for the communication between reader and tag antenna are summarized in table 2.2.

A tag communicates to the reader by using backscatter modulation. The tag IC generates the binary coded information back to the reader in states of "1" and "0" that reflect certain voltages. A transistor also forms part of the IC circuitry and these voltage levels determine the transistor biasing of the transistor. The on/off states induce the transistor to work as a switcher between the IC impedance and the arbitrary load, matched to the tag antenna; hence, the reflected power is different for each state [29; 30; 31]. While the tag antenna is sending the information back, the reader sends a continuous wave (CW) to continue power up the IC; this CW signal modulated by the on/off state of the transistor is known as backscattering modulation. The tag vendor selects the modulation format and the reader should be able to demodulate any modulation of tag IC specified by the ISO/IEC 18000-6 [1].

5.2 Matching Impedance and Power Reflection Coefficient

The equivalent circuit component values of the IC chip are specified in data sheet of the manufacturer [23], it is generally formed by a resistor (R_P) and capacitor (C_P). The IC attachment (strap) to the tag antenna adds some stray capacitance (C_{strap}) and stray inductance (L_{strap}) to the IC chip impedance [35]. The strap is used for a simple attachment of the IC to the antenna design.

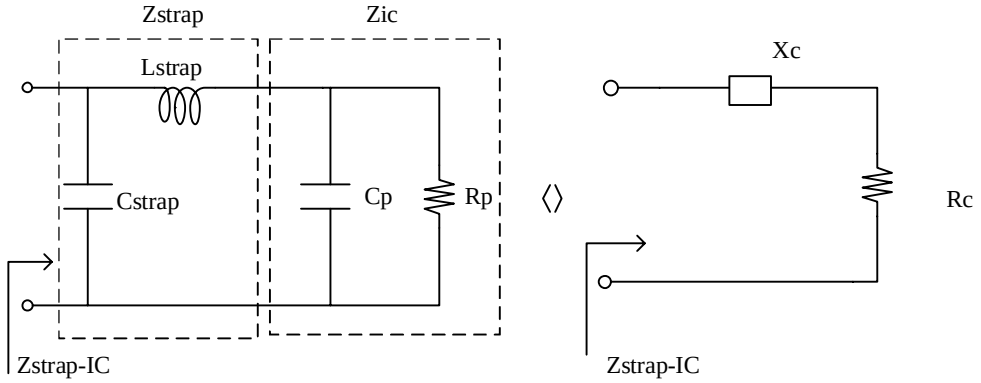

Figure 5.3. *The IC and strap equivalent circuit. The IC equivalent circuit is a parallel resistor R_P and capacitor C_P [35].*

Table 5.1. *Electrical properties of the Higgs-3[23] and strap capacitor*

Description	Value	Unit	Comments
Operating frequency	860-960	MHz	
Sensitivity during reading	-18	dBm	During reading
Equivalent input parallel resistance (R_p)	1500	Ohms	At -14dBm input power
Equivalent input parallel capacitance (C_p)	0.85	pF	At -14dBm input power
Strap capacitance (C_{strap})	0.25	pF	
Strap inductance (L_{strap})	0.45	nH	

The strap and IC generate the new equivalent impedance $Z_{strap+IC}$, which is going to be used as a parameter for the antenna design. The capacitance and inductance of the strap are taken from [35].

$$Z_{strap+IC} = Z_{strap} // Z_{IC}$$

$$Z_{strap+IC} = \frac{1}{jwC_{strap}+\frac{1}{jwL_{strap}+Z_{IC}}} = R_c + jX_c \qquad (5.1)$$

The impedance matching between the IC-strap and tag antenna is analyzed by the power reflection coefficient (PRC) term. This term is described along [26; 27; 28; 29] and here a summary of those references are explained. Fig. 5.4 will let start the analysis. In the circuit below, the generator source (E_0) has an internal impedance (Z_i). Where V_i and I_i are the voltage and current flowing into the *i-port*. The internal impedance, current and voltage at *i-port* define the incident and reflected power waves a_i and b_i.

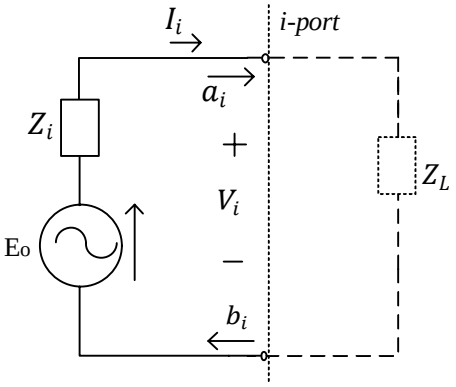

Figure 5.4. *The equivalent circuit of linear circuit explains the incoming and outcoming voltage wave [26].*

The incident and reflected power waves a_i and b_i introduced by Penfield [25] are defined by

$$a_i = \frac{V_i + Z_i I_i}{2\sqrt{|Re\{Z_i\}|}}$$

$$b_i = \frac{V_i - Z_i^* I_i}{2\sqrt{|Re\{Z_i\}|}}. \qquad (5.2)$$

The ratio of reflected power wave (b_i) respect to the incident power wave (a_i) defines the power wave reflection coefficient ($\hat{s}$). Equation (5.3) expresses the power wave reflection coefficient in terms of the load impedance and internal impedance of generator. The power wave concept can also be applied to N-port network arising to the *S*- matrix [22].

$$\hat{s} = \frac{b_i}{a_i},$$

$$\hat{s} = \frac{Z_L - Z_i^*}{Z_L + Z_i}. \tag{5.3a}$$

The power reflection coefficient ($|\hat{s}|^2$) introduced by Kurokawa [26], is used in the general case when the internal impedance of generator and load impedance are complex and no lossless transmission line connects them [28]. This concept is valid and applied to tag antenna because there is not a transmission line connection between the IC and the tag antenna. The strap connected to IC could be traded as a transmission line; but the length of the strap is really short (at most 2mm) that it is neglected.

$$|s|^2 = \left|\frac{Z_L - Z_i^*}{Z_L + Z_i}\right|^2 \tag{5.3b}$$

The power reflection coefficient shows what fraction of the maximum available power from generator is not delivered to the load. The goal is the maximum transfer of available power from generator to load [8; 28]. This occurs when PRC is zero.

Fig. 5.5 shows the circuit state when tag antenna is connected to IC-strap and the induced voltage (V_0) due to the electromagnetic waves that impinge the tag. This circuit is similar to the circuit in Fig. 5.4; then, a parallel analysis of PRC is applied. The PRC for the circuit of a tag antenna and the load IC impedance is described in equation (5.4). The PRC is zero when tag antenna impedance is complex conjugate to IC-strap impedance ($Z_{antenna} = Z_{STRAP-IC}{}^*$).

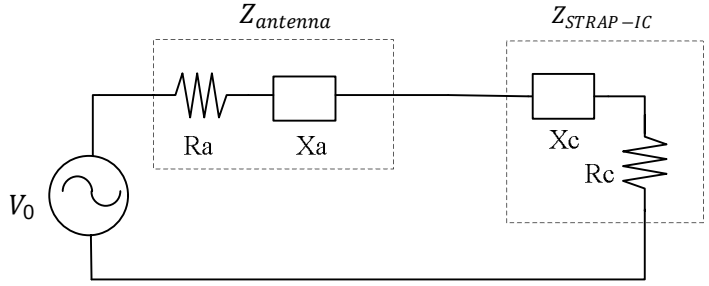

Figure 5.5. *The antenna and strap-IC equivalent circuit [8].*

$$s = \frac{Z_{strap-IC} - Z_{antenna}^*}{Z_{strap-IC} + Z_{antenna}}$$

$$|s|^2 = 1 - \frac{4R_cR_a}{(R_c+R_a)^2+(X_c+X_a)^2}$$

$$PRC\ (dB) = 10\log(|s|^2) = 10\log\left(1 - \frac{4R_cR_a}{(R_c+R_a)^2+(X_c+X_a)^2}\right) \tag{5.4}$$

Eq. (5.4) is the parameter to be optimized in the design of a tag antenna in the HFSS simulation process. The idea is to design a tag antenna whose impedance is equal to the complex conjugate of the IC-strap.

For certain application where the power relations are of main concern, the power waves are more suitable quantities than the conventional traveling waves. The traveling wave concept is more closely related to the voltage or current along the line than the power in the stationary state [26]. At this point, the main difference between traveling wave reflection coefficient and power wave reflection coefficient is that the second focus on complex impedance mismatch and power relation at certain common port. They have the same definitions when the load impedance is real and positive [25, 26].

Fig. 5.6 illustrates how the tag antenna communicates to the reader by modulating the backscattered RF field. The tag antenna sends information to the reader by modulating the incoming RF field. The information generated in the IC (tag circuitry) is digital codified and an array of "0" and "1" enters to the transistor. The transistor behaves as a switcher by switching the connection to the tag antenna between the IC impedance and the impedance on state 2 [7; 8].

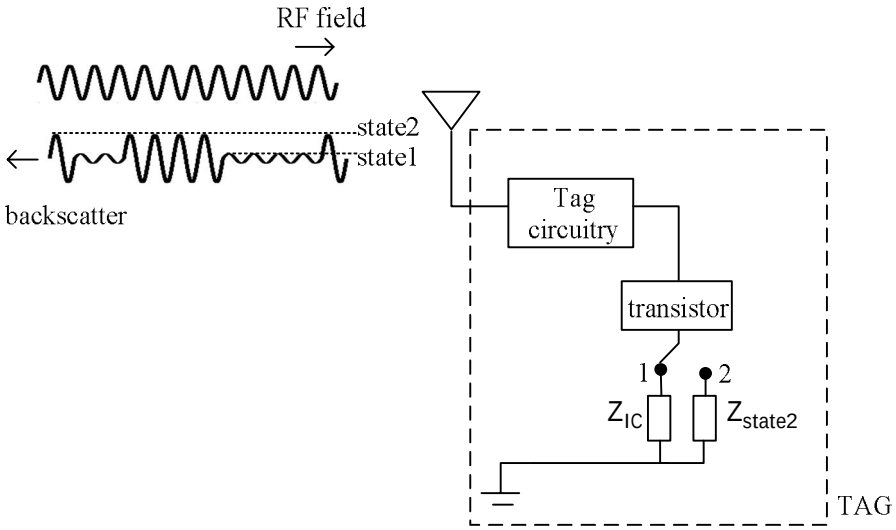

Figure 5.6. *Backscattering modulation used during communication from tag to reader*

The effective area modulated (A_e^m) depends mainly on both states impedances connected to the tag antenna. This dependence is represented on the power reflection coefficient between the tag antenna impedance connected to IC impedance ($\hat{s}_1$), and between the tag antenna connected impedance connected to state 2 impedance ($\hat{s}_2$) [9]. The gain of tag antenna is slow variant respect to frequency then the effective area modulated depends mainly on the impedance mismatch state and it is expressed as [9]

$$A_e^m = \frac{G_{tag}\lambda^2}{4\pi}\left(1 - \frac{1}{2}\left[|s_1|^2 + |s_2|^2\right]\right), \tag{5.5}$$

where:

$$\hat{s}_1 = \frac{Z_{IC} - Z_{antenna}^*}{Z_{IC} + Z_{antenna}},\ \hat{s}_2 = \frac{Z_{state2} - Z_{antenna}^*}{Z_{state2} + Z_{antenna}}.$$

The amount of scattered power depends on the impedance state connected to the antenna. This is known as the modulated backscattering radar cross section (σ^m). It

depends on the contribution of signal scattering at carrier frequency (σ_0) and the scattering at the harmonic components (σ_m) as it is demonstrated in [9]. Modulated backscattering radar cross section (σ^m) is also known as the differential radar cross section [30] and it depends on the difference of two complex RCS due to each impedance state connected to tag antenna [29; 31]

$$\sigma^m = \sigma_0 + \sigma_m$$

$$\sigma^m = \frac{G_{tag}{}^2\lambda^2}{4\pi}\left|1 - \frac{1}{2}(s_1 + s_2)\right|^2 + \frac{G_{tag}{}^2\lambda^2}{16\pi}|s_1 - s_2|^2. \quad (5.6)$$

A contradiction between good matching and high modulation emerges. The higher the difference between the modulation states, the higher the scattered power is, but the lower the power transferred to the IC [9].

5.3 Link budget applied to measurement setup

The link budget in any UHF RFID system describes the power compensation along the communication between the reader and tag antenna. Fig.5.7 illustrates the link budget for a general UHF RFID system. The reader [32; 33] generates the signal at certain power (P_{tx}) and frequency. This signal is emitted to the space by the antenna transmitter. The electromagnetic wave, which is traveling in the space, undergoes losses due the distance between reader and tag antenna and wavelength; this is called the path loss. The captured power in the tag antenna is delivered to the IC. This accepted power to the IC (P_{IC}) should be at least equal to the reader sensitivity of the IC ($P_{IC}{}^0$). The sensitivity of the IC is a manufacturer characteristic [23; 24]. The tag antenna radiates power back to the reader; this scattered power depends on tag antenna RCS and the power density that arrives to the tag antenna. The backscattered signal undergoes again to path loss in order to reach the receiver antenna. Finally, the received signal power (P_{rx}) in the receiver should be higher than the reader sensitivity.

Generally, the maximum achievable distance between the reader and tag antenna depends on forward link, since the sensitivity of the IC is higher than the reader sensitivity. For example, the sensitivity of Higgs 3 IC is -18dBm; whereas the sensitivity of Tagformance reader is -80dBm.

The link budget is used in the measurement of tag antenna. Fig. 5.8 and Fig. 5.9 describe the link budget in the forward link (communication from reader to tag) and backward link (communication from tag to reader), respectively. The setup of the system is based on Voyantic test bed [32] and this is used in the RFID Lab.

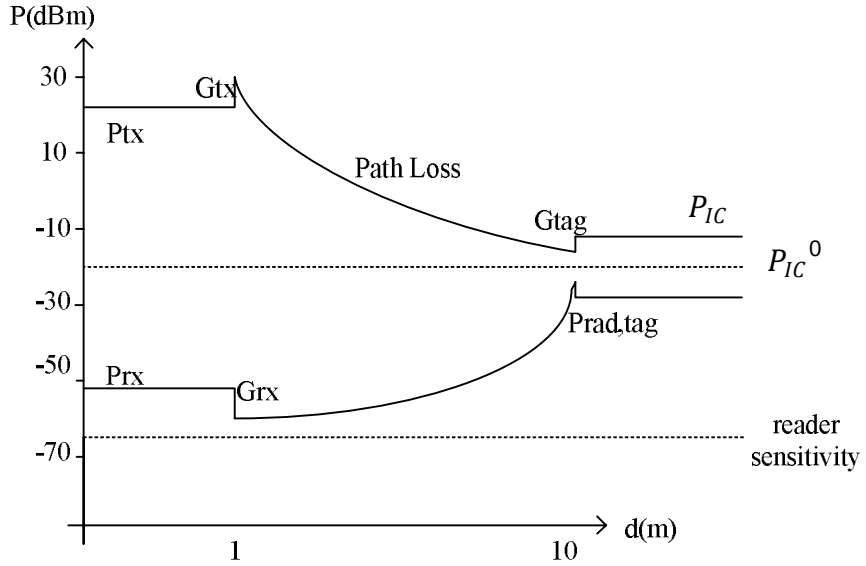

Figure 5.7. *Link budget in common UHF RFID system.*

The link budget in forward direction:

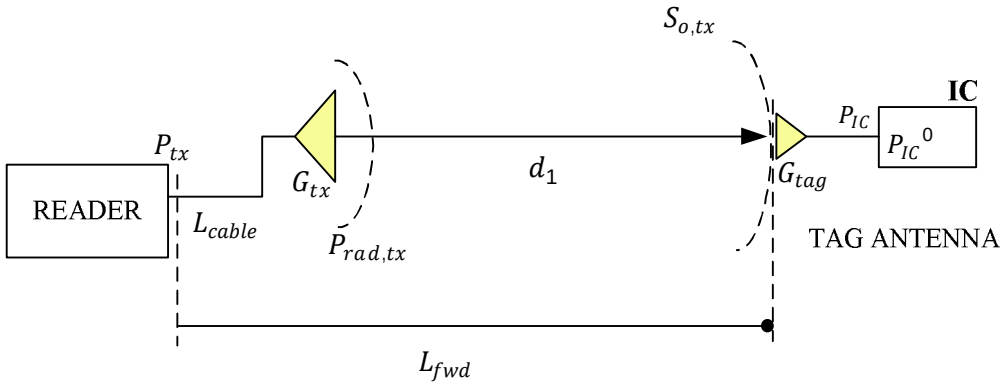

Figure 5.8. *Link budget in the forward link*

The radiated power ($P_{rad,tx}$) emitted by the reader is the result of the transmitted power generated by the reader (P_{tx}) multiplied by the cable loss (L_{cable}) that connects the reader and transmitter antenna; and by the transmitter antenna gain (G_{tx}), a similar construction can be found in [27]

$$P_{rad,tx} = P_{tx} L_{cable} G_{tx} \,. \tag{5.7}$$

The average power density ($S_{o,tx}$) arrives to the tag antenna. This tag is located at certain distance from the reader (d_1). Assuming an isotropic transmitter antenna, the average power density is calculated as [15; 31]

$$S_{o,tx} = \frac{P_{rad,tx}}{4\pi {d_1}^2} \,. \tag{5.8}$$

The accepted power to the IC (P_{IC}) is calculated as the power in the antenna load

$$P_{IC} = A_{e,tag} S_{o,tx} \,, \tag{5.9}$$

where the effective area of the tag is represented by $A_{e,tag}$.

When the accepted power to the IC (P_{IC}) is equal to the sensitivity of the IC ($P_{IC}{}^{0}$), the threshold power ($P_{tx,th}$) is defined [79]. Threshold power is the minimum transmitted power to active the IC at certain distance [27; 28; 29].

"Commonly, the sensitivity of the IC refers to its read sensitivity, i.e. to the minimum power required to reply to the EPC Gen2 protocol's *query* command. This is the most common and expectedly the least power consuming task for the IC, since the tag's reply to *query* consists only of its ID number" [79]. The reading sensitivity of the Higgs3 is -18dBm.

$$P_{IC}{}^{0} = \frac{\lambda^2}{4\pi} G_{tag} (1 - |\hat{s}|^2) \frac{P_{tx,th} L_{cable} G_{tx}}{4\pi {d_1}^2} \tag{5.10}$$

Calibration of the system is done before the measurements; the path loss in the forward (L_{fwd}) and in the backward (L_{bwd}) directions are calculated by the Tagformance. The forward path loss is expressed as

$$L_{fwd} = \frac{L_{cable} \lambda^2 G_{tx}}{(4\pi d_1)^2} \,,$$

and finally the reading sensitivity of the IC may also be expressed as

$$P_{IC}{}^{0} = P_{tx,th} L_{fwd} G_{tag} (1 - |s|^2) \,. \tag{5.11}$$

The realized gain is obtained from measurement as

$$G_{realized}(\text{dB}) = P_{IC}{}^{0}(\text{dBm}) - P_{tx,th}(\text{dBm}) - L_{fwd}(\text{dB}). \tag{5.12}$$

The maximum distance that tag antenna can be placed from reader occurs when the maximum allowed power, the "Equivalent Isotropic Radiated Power (EIRP)" is radiated ($EIRP = P_{tx} L_{cable} G_{tx}$). The read range is sensitive to: the tag antenna orientation, the material attachment, and the propagation characteristic of the surrounding environment. An equivalent analysis for the maximum read range based on the measurement threshold power is also explained in [27; 28; 29].

$$d_{max} = \frac{\lambda}{4\pi} \sqrt{\frac{EIRP G_{tag} (1 - |s|^2)}{P_{IC}{}^{0}}} \,,$$

$$d_{max} = d_1 \sqrt{\frac{EIRP}{P_{tx,\text{th}} G_{tx} L_{cable}}} \,. \tag{5.13}$$

Link budget in the backward direction:

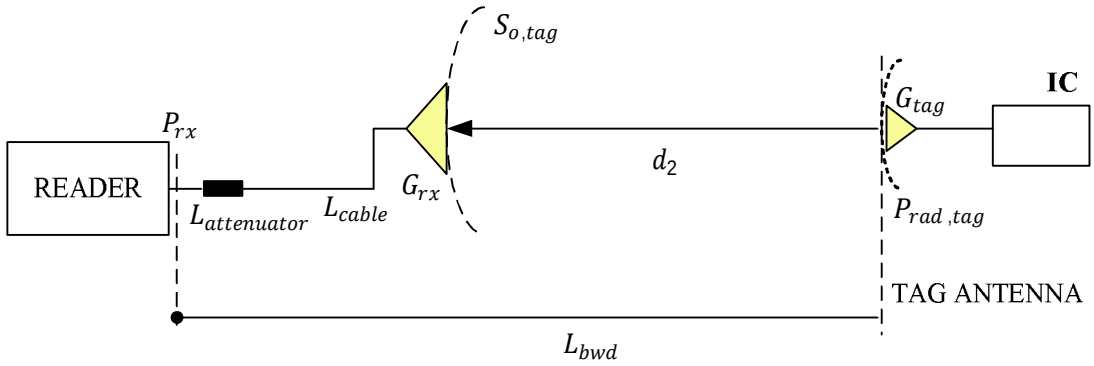

Figure 5.9. *Link budget in the backward link.*

The power radiated by the tag ($P_{rad,tag}$) is the scattered power by the tag antenna, and it is equal to the radar cross section of the tag antenna (σ) multiplied by the power density emitted by the reader ($S_{o,tx}$) [29; 31]

$$P_{rad,tag} = S_{o,tx}\sigma \,, \tag{5.14}$$

$$S_{0,tag} = \frac{P_{rad,tag}}{4\pi {d_2}^2} \,. \tag{5.15}$$

The power density radiated by the tag ($S_{0,tag}$) multiplied with the effective area of the reader antenna ($A_{e,tx}$) gives the power in the cable load. This received power at the reader (P_{rx}) should be at least equal to the reader sensitivity and it is calculated as

$$P_{rx} = \left(A_{e,tx}S_{o,tag}\right)L_{cable}L_{attenuator},$$

$$P_{rx} = \left(\frac{\lambda^2}{4\pi}G_{rx}\frac{\sigma}{4\pi {d_2}^2}\frac{P_{tx}L_{cable}G_{tx}}{4\pi {d_1}^2}\right)L_{cable}L_{attenuator}.$$

The attenuator is placed in order to prevent saturation in the reader. If the transmitter and receiver antenna are the same, then $G_{rx} = G_{tx}$ and $d_1 = d_2 = d$. Besides, assuming that for the Tagformance the path loss in the forward direction is expressed as $L_{bwd} = \frac{L_{cable}L_{attenuator}\lambda^2 G_{rx}}{(4\pi d_2)^2}$, the received power by at reader is also calculated by

$$P_{rx} = \left(\frac{\lambda^2}{4\pi}\sigma\frac{P_{tx}L_{cable}{G_{tx}}^2}{4\pi^2 \mathrm{d}^4}\right)L_{cable}L_{attenuator}$$

$$P_{rx} = L_{fwd}L_{bwd}\frac{\sigma}{\lambda^2}\frac{P_{tx}}{L_{attenuator}} \,. \tag{5.16}$$

6. METAL SURFACE EFFECTS ON UHF PATCH TAG ANTENNA

UHF RFID passive tag antennas are widely used in the industrial services for many applications. However, the identification of tag antennas near or on top of metal surfaces is one of the challenging topics for the antenna design; due to metal surface alters antenna properties and degrades its performance.

When electromagnetic waves impinge on any object, the waves undergo through reflection and transmission. A special case occurs when the object is a perfect electric conductor (PEC); the incoming waves reflect completely with phase reversal. Only the normal component of electric field and the tangential component of the magnetic field exist on the PEC boundary. Thus, it is recommendable to look for antenna that does not depend on the tangential electric field component and normal magnetic field component [75] in order that electric and magnetic components are not directly affected when metal surface is nearby.

Metal surface, which resembles a finite in size PEC, alters the radiation properties of the antenna: input impedance, radiation pattern, radiation efficiency, and resonance frequency [12; 15; 76]. The antenna performance degrades on the presence of metal surface or conductive material in general due to reflections; for example, directivity and input impedance oscillates near metal surface [15].

This chapter includes some solutions to overcome the metal surface and a survey of most used design procedure for UHF patch tag antenna based on open literature.

6.1 Solution proposals

The following list of ideas is compiled and proposed to overcome the effect of metal surface on antenna performance [2; 75; 76]:

i. Use of perfect magnetic conductor.
ii. Place the metal surface at the nodes of the standing electric field.
iii. Increasing the frequency of operation in order to reduce the wavelength.
iv. Insertion of dielectric between the antenna and metal surface.
v. Insertion of magnetic material.
vi. Use metal surface as part of the antenna structure operation.

It is described each of the cases:

i. Theoretically when the wave impinges on Perfect Magnetic Conductor (PMC), the electric field is reflected without phase change. There is an average power flow in the direction normal to the boundary and constructive interference of the electric field. The idea is to use this PMC between the antenna and the metal surface. In practice EBG antenna structure and High Impedance Surface (HIS) structure mimic PMC.

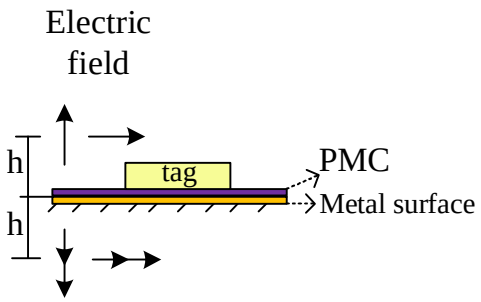

Figure 6.1. *Perfect Magnetic Conductor between the tag antenna and the metal surface*

ii. Metal surface is a good reflector but when the wave impinges on it, the incident wave is reflected complete with phase shift π and destructive interfering. The antenna should be placed at quarter wave length from the metal surface in order that the total round trip from the antenna to the metal surface, and back to the antenna, equals to one complete cycle and the waves adds constructively [78].

$$z = \frac{\lambda}{4} \tag{6.1}$$

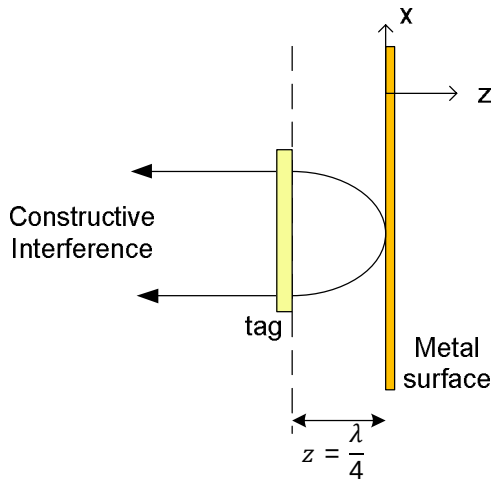

Figure 6.2. *Quarter wavelength separation respect to metal surface in order to create constructive interference.*

iii. Increasing operating frequency of the wave reduces the wavelength; reduction of wavelength means that the wave has to travel more periods to reach a same physical distance. As it is expressed in equation (6.2), the operating frequency is denoted by f_o and ε_r, μ_r are the constant relative permittivity and permeability, respectively.

$$\lambda = \frac{c}{f_o\sqrt{\varepsilon_r\mu_r}}. \quad (6.2)$$

I.e. in UHF band the wavelength at 915MHz in free space is $\lambda = 0.32\text{m}$ but at 2.4GHz in free space, the new wavelength is now $\lambda = 0.125\text{m}$, so the wave has to travel longer distance in order to reach the metal surface.

iv. Inserting dielectric material between the antenna and metal surface increases the electromagnetic distance between them because the wavelength gets shorter.

In practical case, the permeability of the dielectric is unity because most of dielectrics in the market are not magnetic ($\mu_r = \mu_{r,dielectric} = 1$). I.e. in UHF band the wavelength at 915MHz in free space is $\lambda = 0.32\text{m}$, and for a dielectric $\varepsilon_r = 4.4$ the wavelength is now $\lambda = 0.15\text{m}$. As Fig. 6.3 illustrates, the wave has to travel at least twice to reach the same distance.

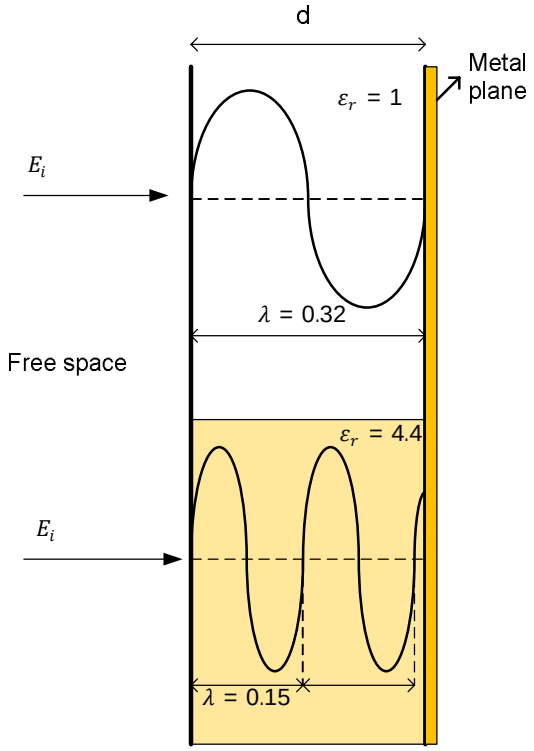

Figure 6.3. *Wavelength due in different mediums. In free space and on dielectric.*

Nevertheless, the traveling wave in free space undergoes reflection when it impinges on dielectric material in similar fashion as it impinges on metal surface. The reflection due a wave incident on the interface between free space and on dielectric is expressed in (6.3). The impedance of a medium is denoted by $\hat{n} = \sqrt{\frac{\mu_0\mu_r}{\varepsilon_0\varepsilon_r}}$. Here, the relative permittivity and permeability of air are equal to unity ($\varepsilon_{r,free} = 1; \mu_{r,free} = 1$).

$$\hat{\Gamma} = \frac{\hat{n}_{dielectric} - \hat{n}_{free}}{\hat{n}_{dielectric} + \hat{n}_{free}},$$

$$\hat{\Gamma} = \frac{\sqrt{\frac{\mu_{r,dielectric}}{\varepsilon_{r,dielectric}}}-1}{\sqrt{\frac{\mu_{r,dielectric}}{\varepsilon_{r,dielectric}}}+1}. \quad (6.3)$$

If permeability of the material is equal to one ($\mu_{r,dielectric} = 1$); then, the absolute value of reflection coefficient increases as material permittivity increases. See (6.4) and Fig. 6.4

$$\hat{\Gamma} = \frac{\frac{1}{\sqrt{\varepsilon_{r,dielect}}}-1}{\frac{1}{\sqrt{\varepsilon_{r,dielect}}}+1}. \quad (6.4)$$

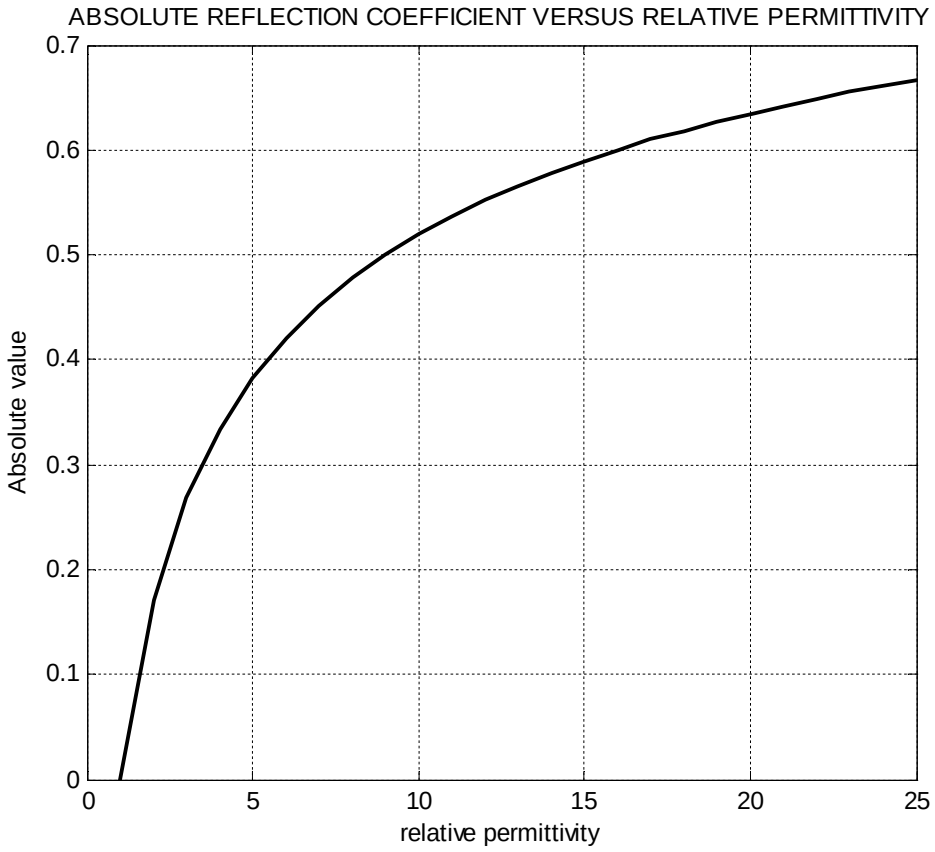

Figure 6.4. *Absolute value of reflection coefficient vs. permittivity.*

Prothro et al. [2] studied the insertion of dielectric material to reduce the vulnerability of the antenna on metal surface. And it was experimental demonstrated that the use of dielectric material reduces even more the impedance of folded dipole instead of increasing and hindering the ability of the antenna to radiate properly.

v. Inserting magnetic material between the antenna and ground plane lead to increasing the permeability of the material. Two main approaches can be achieved. First, the dielectric constant may increase freely in order that the ratio between permeability and permittivity is one; and the reflection coefficient is zero from Eq. (6.3)

$$\frac{\mu_{r,dielectric}}{\varepsilon_{r,dielectric}} = 1 \rightarrow \hat{\Gamma} = 0$$

So, the signal impinging this material not reflects. Second, the wavelength gets shorter since permeability increases freely.

vi. In order to improve the performance of tag antenna on metal surface different tag antenna designs had been explored. These antenna designs take an advantage from metal surface; i.e. patch antenna, Inverted F-Antenna (IFA), planar –IFA (PIFA) antenna structures. Those antennas use the metal plane as its own ground plane that forms part of the whole antenna design to work properly. For example, the excitation currents in IFA results in the excitation of currents in the ground plane. However, IFA antennas exhibit power loss, negligible radiation, and lower efficiency. Then, improvement of this antenna is achieved by placing a conductive plate instead of the folded wire.

Matching the tag antenna impedance to the high resistance equivalent circuit of the IC diminish the impedance mismatch sensitivity. Despite using this approach, the metal surface effect may continue degrading the tag antenna performance. It is recommendable to design a tag antenna with high resistance and opposite value than IC reactance. This approach is used in [61] and some experimental results are explained in [71].

Some other aspects like the size and shape of metallic plane and the polarization of reader also determine the capability of tag detection. Those effects are studied in [76] by the read range and read rate measurement method. It is concluded that non uniform metal plane and bigger metal planes decreases even more the tag antenna identification and decrease the read range. Longer read range is achieved by a linear polarized antenna reader due to lower polarization mismatch when it is aligned to the linear polarized tag antenna.

6.2 Review of different RFID patch tag antenna designs

Patch antennas overcome the near metal boundary effects because they need a ground plane to work properly. This subchapter is based on the review of different patch tag antenna designs and its approach to overcome the metal surface effect.

Some approaches of proper patch antenna designs *without using a cross-layer structure* are based on a balanced antenna structure [42; 72], capacitive coupling structure [40] and radiating U-T slot [41]. The cross-layer structure is more complex to construct; however, it is widely used to improve even more the performance of tag antenna on metal surface, design examples are shown through [45-68].

Patch tag antenna *without a cross-layer structure* could be the simplest and cheapest way for an antenna design; however, it suffers from narrow bandwidth and frequency

sensibility to metal surface. The balanced feed structure is used for the tag antenna design in [42; 72]. Eunni et al. [42] uses the balanced feed approach as a matching circuit in order to eliminate any reference to zero ground. The tag works independent of the ground plane; despite achieving narrow bandwidth. In the same way, Mohammed et al. in [72] used the balanced feed approach to propose a patch antenna without ground plane that behaves as dipole in free space but when it is placed on metal surface; it works as an efficient microstrip tag antenna with even 6dBi gain. Then, Liu et al. [50] uses a capacitive coupling structure and a coplanar waveguide (CPW) in the antenna design; the antenna exhibits a read range of 7m when it is placed on metal surface 300x270 mm^2. CPW structure supports quasi-TEM modes of propagation, it is a center conductor strip separated by a gap from the adjacent conductor planes and mounted on dielectric substrates. There is a capacitive effect due to the gap between the center strip and the conductor planes [77]. Finally, for broadband antennas, higher harmonic order should be exploited in the antenna structure by parasitic elements such slots or stubs in order to tune the frequency. It is Tang et al. [41] that use a U-slot and T-slot approach to increase the bandwidth. The tag antenna was constructed to work in the microwave RFID frequency around 2.45GHz and it exhibits a good performance. The -10dB PRC bandwidth is 10% and gain 2.1dBi; this idea may also be used for the UHF-RFID band application.

Many patch tag antenna designs uses the *cross layer structure* by via hole or by a strip wall in order to improve bandwidth and insensitivity to metal surface. In this sense, IFA, PIFA and grounded patch antennas are introduced as possible tag antenna design for metal surface improvement. A study of the PIFA and the effects of different sizes of ground planes are issued in [43] in which an infinite, perfect conductor and plane (perfect ground plane) improves the electric performance of PIFA. PIFA is designed to operate with a ground plane and this ground plane is part of the whole antenna design. PIFA is an antenna shorted to ground plane. Hirvonen et al. [44] use this PIFA approach to construct UHF PIFA tag antenna achieving good immunity to ground platforms and read ranges of 7m. A survey of some common patch tag antenna shorted to ground plane use:

- Loop matching,
- T-matching,
- GND-IC-patch structure,
- High Infinite Surface (HIS) structure, and
- Stuck lumped components.

All those cases are briefly explained below, taking on main consideration the geometry structure of the patch tag antenna design. A detailed comparison of these different patch tag antennas: dimension, bandwidth, read range is found in Appendix 1.

The IC is matched to the tag antenna by *the loop matching*. This induces proximity coupled feeding to the physical separated radiating patch. No additional matching

network is required. The separation gap and the length of the loop affect mainly the resonant frequency for the whole cases [46; 48; 49; 59]. Kim et al. [59] models the patch radiator and the feeding loop as a transformer structure. The antenna resistance varies direct proportional to the mutual inductance of the gap. The loop length influences mainly the reactance. The feeding loop is shorted in order to minimize the antenna length at resonance frequency. Fig. 6.5d represents the final design for [59]. Another approach is presented by Yu et al. [48] and Kim et al. [49] in which the radiating patch is shorted to ground plane. In [48], two separated radiating patches are shorted to ground in order to achieve more balanced current distributions and electric coupling between those two adjacent radiators. Figure 6.5b represents this final design approach. Another approach is the use of two shorted plane in each side of the patch which help to sweep the antenna resistance; this is illustrated in Fig. 6.5a and Fig.6.5c, respectively from [46; 49].

A *T-matching network* may also be used as a feeding structure in a patch tag antenna. T-matching offers facility to manipulate the input impedance and more bandwidth can be achieved. Xu et al. [47] uses a T-matching network attached to two symmetrical radiating patches shorted to ground plane. Fig.6.6 illustrates this approach. The antenna structure is similar to Fig.6.5c but the feeding loop is replaced by the T-matching [49]. The electrical coupling is generated around the gap between two patches, generating more balanced current distribution.

The *GND-IC-patch* structure consists: one side of the IC shorted to GND and the other connected to the radiating patch through microstrip line. High radiation efficiency and peak gain are achieved by using shorting strip. The feed line resembles a coplanar waveguide that matches the high impedance of the patch with the low impedance from the IC. This is the main approach observed in [45; 57; 58; 60]. Um et al. [45] uses a high dielectric thickness to improve the gain and make the antenna less metallic sensitive. Fig. 6.7a illustrates the final design of [45]. In the same way, Parl et al. [57] achieves really high bandwidth, small dimension antenna but short read range. Figure 6.7d represents the three different approaches of [57] and the three exhibits similar results. Lee at al. [58] introduces a low profile antenna with good read range but lower bandwidth than [57] which is illustrated in Fig. 6.7b. Finally Mo et al. [60] make use of U-slot to achieve larger wideband design and acceptable read range of 3.8 m in metal surface. See Fig. 6.7c.

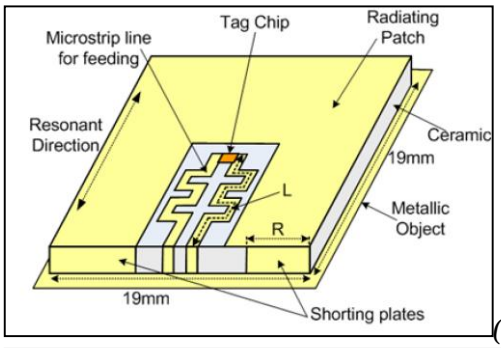

(a)

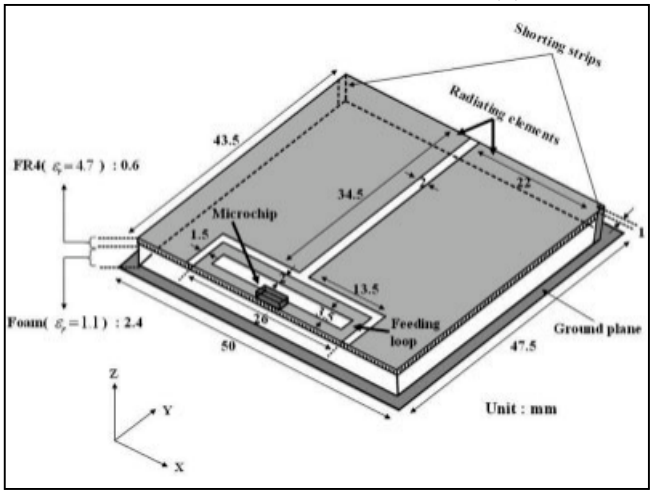

(b)

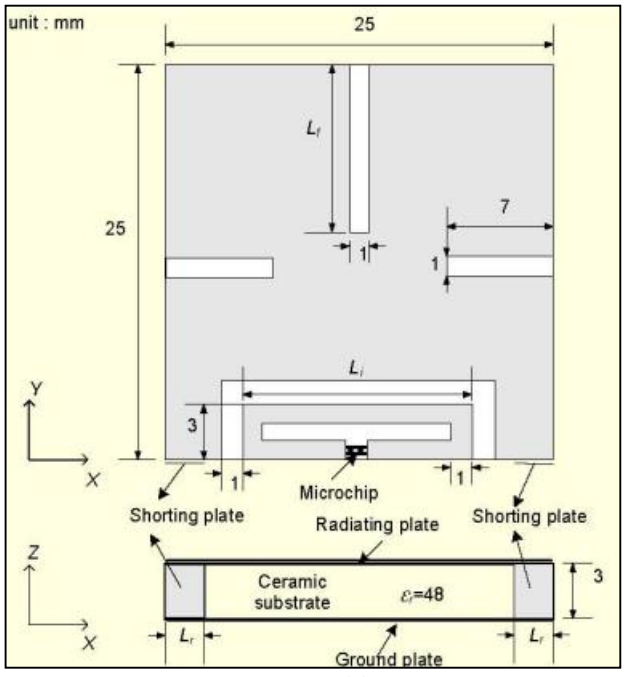

(c)

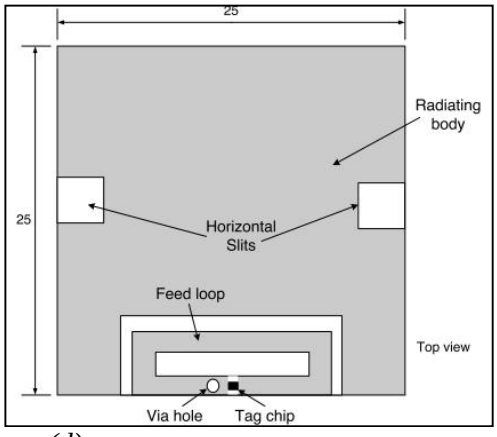

(d)

Figure 6.5. *Feed loop directly to IC and separated to the patch radiator. It works like a proximity coupling structure. (a)The shorted plates tune the antenna resistance and the length of the loop tunes the antenna reactance [46]. (b) Two radiating patch separated by a gap to increase the coupling; both patches are grounded [48]. (c) The radiating patch has three slot slits to tune antenna impedance [49]. (d) The feeding loop is shorted to minimize antenna dimension [59].*

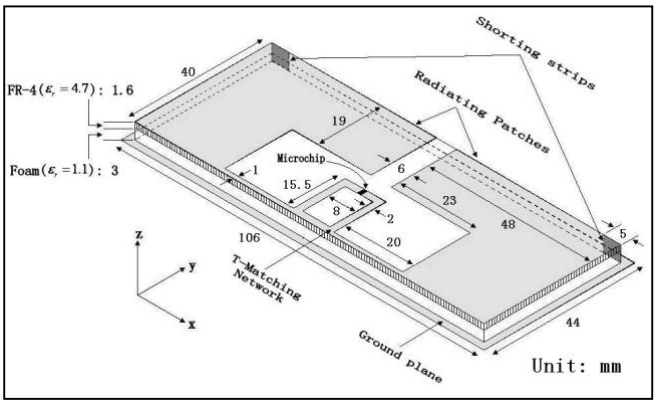

Figure 6.6. *T-matching network connected to IC, the radiation patch, matching network and IC are all connected together [47].*

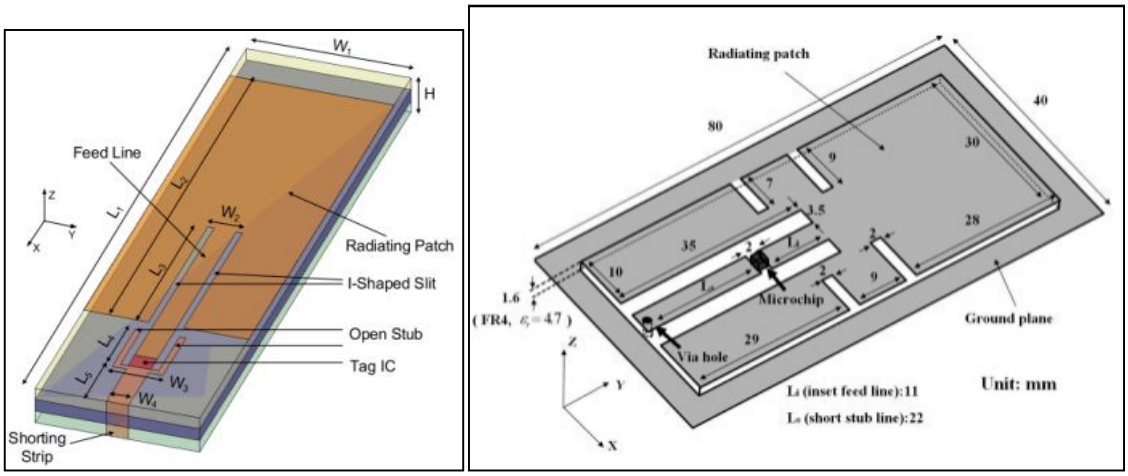

(a) *(b)*

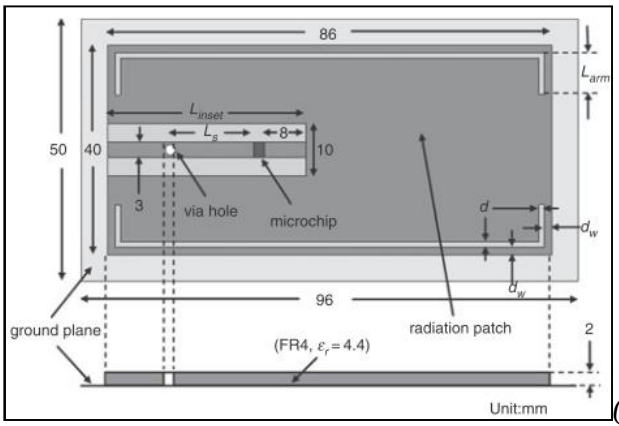

(c)

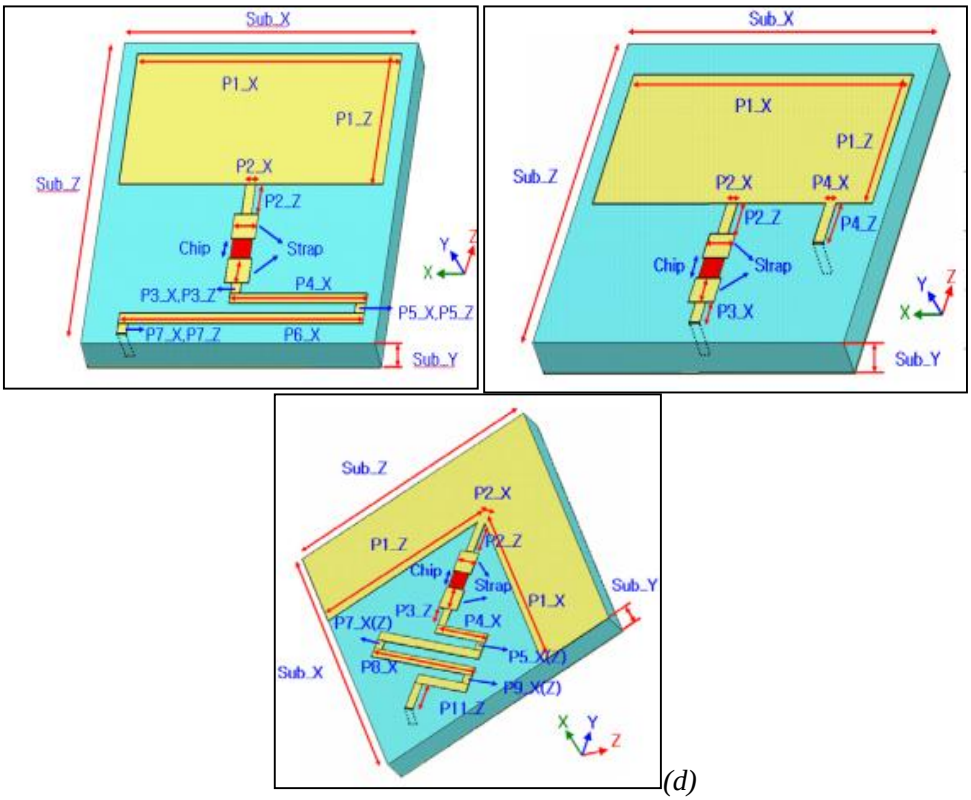

(d)

Figure 6.7. *The GND-IC-patch tag antenna structure. It probably offers the best performance compared to other approaches. (a) The higher dielectric thickness improves the immunity to metal surface [45]. (b) Low profile antenna with slot for antenna tuning [58]. (c) U-slots are added in order to improve the bandwidth [60]. (d)Three different designs exhibit similar radiation characteristics and small dimensions. [57].*

Some tag antenna designs are based on a simple High Impedance Surface [HIS] unit cell [50; 51; 53; 54; 56; 61]. The HIS is based on two adjacent rectangular patch electrically connected via ground plane. The patches, via to ground and ground plane resemble an inductor which is parallel connected to the capacitor represented by the gap between the two adjacent patches. This parallel resonant circuit formed by the inductor and capacitor behaves as a filter where for certain radiofrequency the antenna structure has high impedance and does not allow this frequency band to propagate [78]. References [51; 56; 61] are the direct representation of HIS surface; size reduction and acceptable bandwidth is achieved. Figure 6.8b, Fig.6.8e, Fig.6.8f represent the HIS structure when the radiator patch are shorted. The reference [54] is represented in Fig. 6.8d. It uses HIS approach and inserts a conductor layer between the radiating patch and ground plane in order to increase the capacitance and to reduce the total length at high inductance. However less read range is achieved and Higg2 is used for this experiment. Chen et al. [53] introduce two antenna designs using the same approach and it is experimental demonstrated that the position of the shorting pins near the IC and additional appropriate matching stubs to the IC may improve the bandwidth. This is because the excitation of surface current on two patches is on same phase. The final antenna designs of [53] are represented in Fig. 6.8c. Finally, a similar HIS approach is studied in [50], an improvement in antenna gain and reduction in spurious radiation is

achieved by using a coplanar waveguide (CPW) in the design. See this approach in Fig. 6.8a.

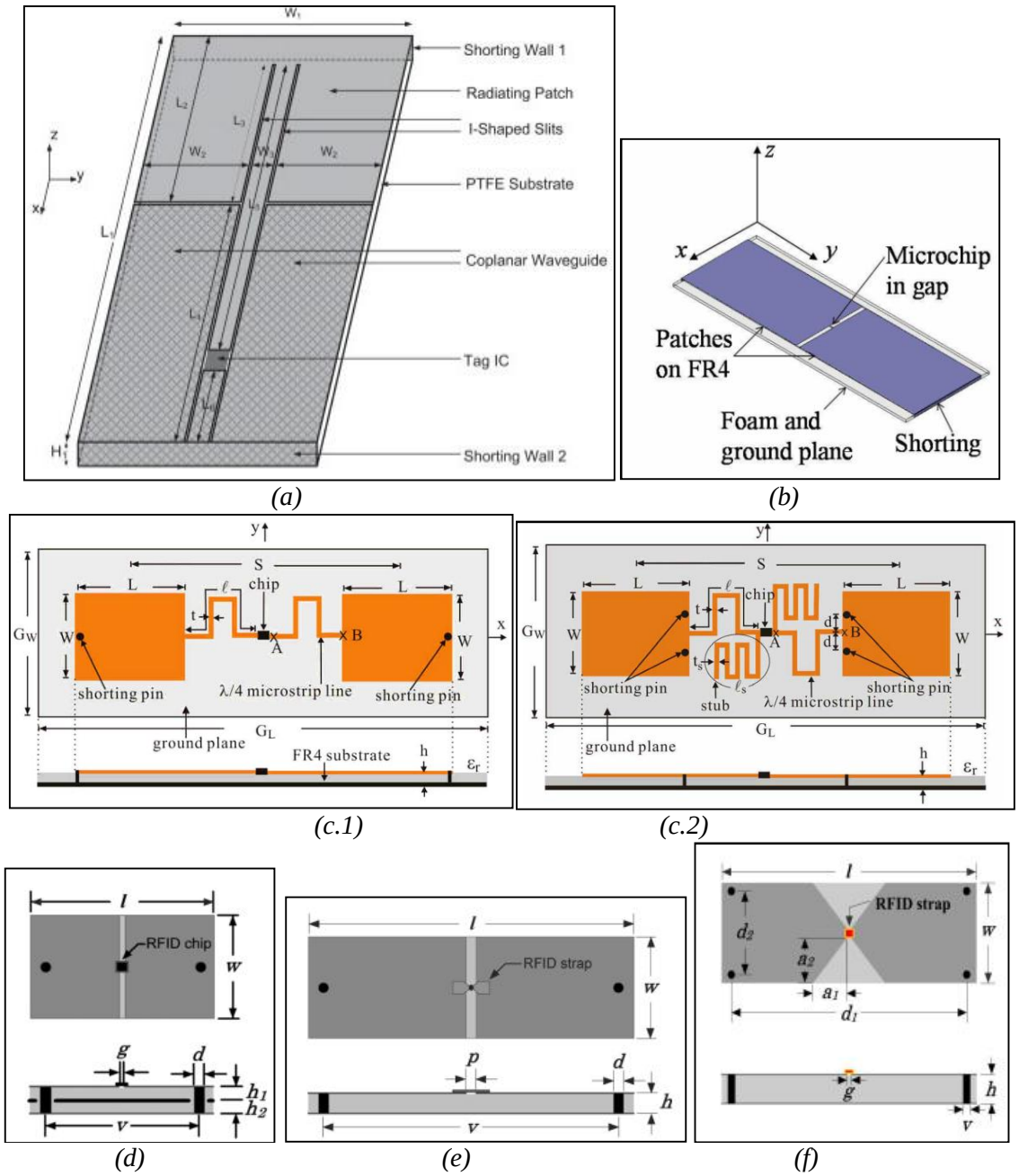

Figure 6.8. *Common HIS structure to reduce the interference originated by the metal surface. (a) The patch tag includes coplanar waveguide to reduce spurious radiation and improves capacitive coupling to the feed [50]. (b) Common HIS patch tag antenna structure [51]. (c.1) The shorting pins are connected at the end of the radiating patch [53]. (c.2) Shorting pins are located near the IC and additional stubs improve matching [53]. (d) A parallel plate is located between the top and bottom of the patch; this reduces the antenna dimensions [54]. (e) Common HIS structure implementation [56]. (f) Four total shorting pins are used the current balance. The radiating patches ends on a point to increase the induction current to IC [61].*

The use of lumped components emerges as an alternative to match the IC impedance [52; 55; 62]. Some design antenna uses lumped capacitor; however, the antenna gain becomes lower and the design cost increases. Popugaev et al. [62]

introduces the use of distributed capacitors instead of lumped capacitor by using slots; this improves relatively the bandwidth. The designed antennas using this approach are showed in Fig. 6.9.

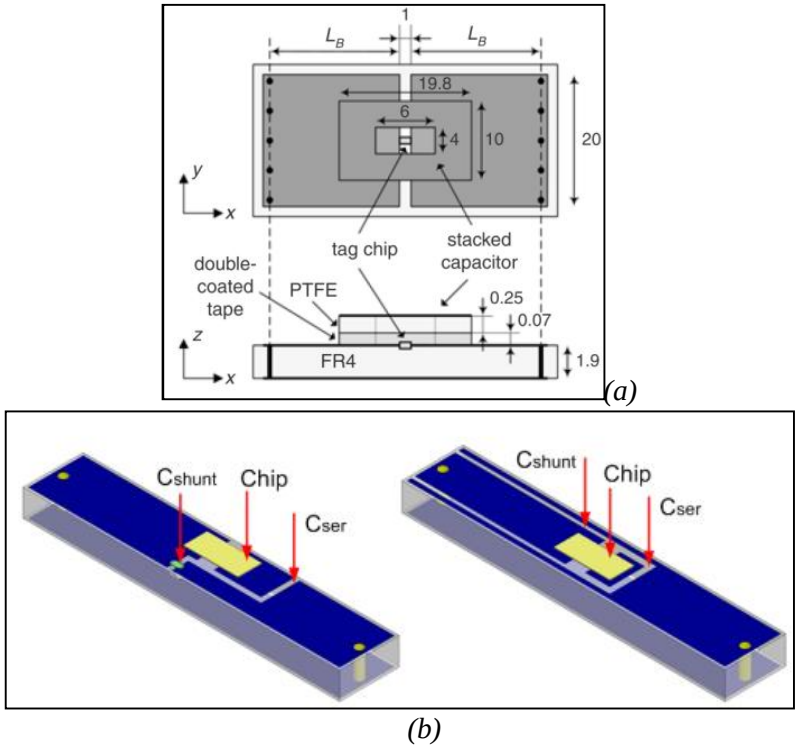

Figure 6.9. *Lumped components are stuck on the antenna design for tuning antenna impedance. (a) A lumped capacitor is used for matching in this design [52; 55]. (b) The antenna designs improve if a lumped capacitor is replaced by slot [62].*

Another approach is the design of tag antenna that can be placed inside a metal surface; lower read range had been achieved in the study [63-68] and this topic continues to be under research.

Miniaturization or size reduction of the antenna leads to degradation in radiation efficiency and bandwidth. For size reduction of tag antenna some possibilities exist. Shorted fractal design exhibit more size reduction than shorted patch and fractal patch but also smaller bandwidth between them. Monti et al. in [74] proposes the shorted fractal patch tag antenna approach. And, as it is pointed out in [73] by meandering and using inverted F-structure, it is possible to reduce even more the antenna size. Another option is the use of EBG plane which mimic a PMC plane. “EBG structures are defined as artificial periodic (or sometimes non periodic) objects that prevent/assist the propagation of the electromagnetic waves in a specific band of frequency for all incident angles and all polarization states” [69]. EBG improves radiation efficiency and gain due to suppression of surface wave [70; 78]; it needs a periodic structure of design and manufacturer. This increases the cost production of the antenna.

Based on microstrip antenna design parameters explained on chapter 4; a high permittivity substrate reduces the interference from the metallic surface but reduces the radiation efficiency. The designs in [46; 49; 59] uses high permittivity for antenna

construction. A low tangential constant reduces the losses of the material; however, the antenna cost increases, some patch tag antennas use this approach in [52; 55; 57; 62]. Two different dielectric layer approaches are also used in antenna design. The upper layer is made of higher dielectric constant in order to reduce the antenna size. The lower layer has lower dielectric constant and higher thickness in order to increase the bandwidth and reduce reflections between the free space and dielectric; those designs are expressed in [48, 51, 52].

7. EXPERIMENTAL UHF PATCH TAG ANTENNA

A passive UHF patch tag antenna that overcomes the performance on metal surface effect is designed and constructed. The antenna is first designed using HFSS [36] (High Frequency Structure Simulator) and later using CEMS [22] (Computational Electromagnetic Software). The simulation result (antenna impedance, total gain) among both software is compared in free space and on metal surface, showing similar results. Besides, the minimum transmitted power to active the tag antenna is measured in Tagformance. The maximum read range at which the tag antenna can be activated is measured in real environment with a RFID reader gateway and linear and circular polarized antenna by using the read rate method. Finally, the realized gain is measured and compared with the simulation results. The tag antenna shows a good performance on metal mainly at YZ plane.

7.1 Antenna Design Process

The UHF patch tag antenna has initial dimension (length, height, width) based on the formulas described for the microstrip antenna. The design is first simulated by the electromagnetic simulator HFSS v.12 and then it is corroborated by CEMS.

The target of the design is the immunity of tag antenna performance when it is placed on metal surface. Even though, it is recommendable to have the minimum dimension of tag antenna as possible; it is not the main objective of this design. The dimensions are settled in order to get a good impedance matching between tag antenna and IC and good tag antenna gain.

From different commercial dielectric materials available in Rauma Research Unit, the dielectric material is chosen of low permittivity (Rogers RT5880 [39], ε_r = 2.2, $\tan\delta$ =0.0004) in order to obtain a high bandwidth and radiation efficiency; however, tag antenna dimension increases. The dielectric thickness (h=3.18 mm) is not low profile since as ticker it is, bandwidth increases but efficiency decreases.

The antenna design is inspired in [45] due to the high bandwidth achieved. However, the patch tag antenna proposed in this thesis has lower dielectric thickness and better immunity to metal surface. One side of the IC-strap is shorted to ground via a three strips, these strips resemble an inductor and the inductance improves to the IC feeding. The other side of the antenna is connected to patch radiator, which is not perfect rectangular. The patch radiator has two main gaps near the feeding IC that tune the antenna impedance. Besides, the two shorted-feeding strips inductively high couple to the patch radiator. There is an intentionally dielectric distance between the patch

radiator and the edge of the upper side of the microstrip. As this distance increases, the metal surface approaches to infinite space and the performance of the patch improves on metal surface. If the distance is at least $\lambda/20 = 16mm$, the ground plane of the patch simulates infinite ground plane [16].

The patch tag antenna was constructed on milling machine "LPKF ProtoMat c100/HF" controlled by software interface CAD/EDA CircuitCAM [81]. The final design is observed in Fig. 7.1.

The initial tag antenna design had minimum PRC at 915MHz. After the construction it exhibits shorter dimensions (about 0.5mm) furthermore the thickness was reduced to 2.7mm. Due to these changes in dimension, the lowest PRC of the tag antenna is shifted to 932MHz in free space. It is observed (in simulation) that variation of strip dimensions in the feeding zone and dielectric thickness are the main parameters that leads to the frequency shifted in this design. The simulation was redone based on the constructed dimension of the tag antenna and this will be called "the simulated tag antenna" in order to compare simulation and measurement results.

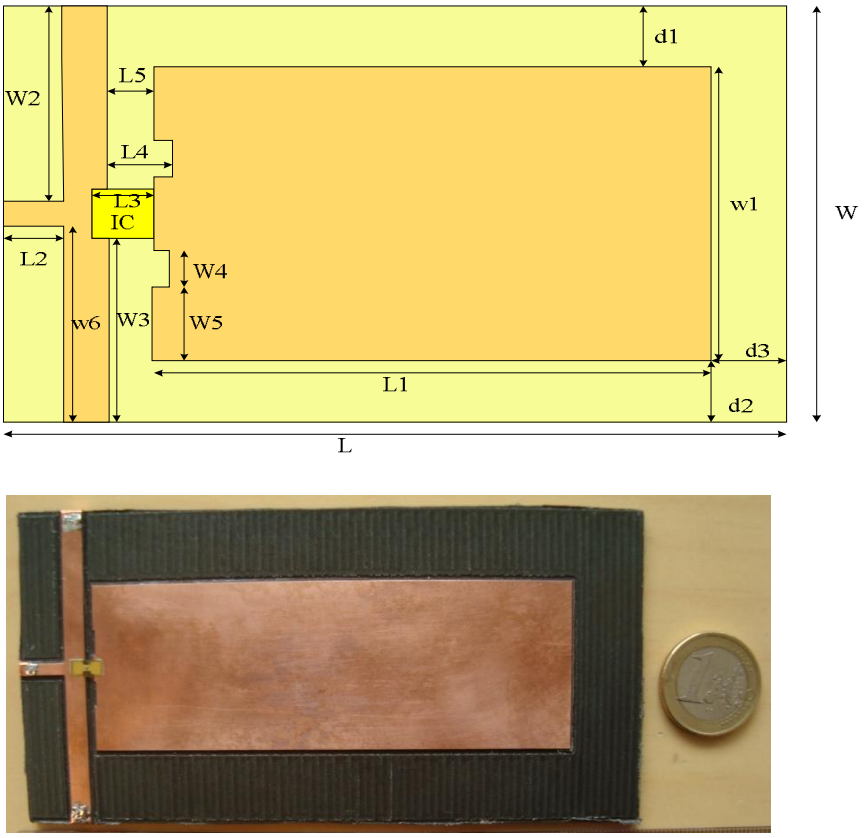

Figure 7.1. *Dimensions of the fabricated UHF patch tag antenna 135mmx67mmx2.7mm (upper),* $\varepsilon_r = 2.2$*, h=2.7mm with Higgs3. Final Fabricated antenna (bottom).*

Dimension of the constructed tag antenna are shown in table 7.1. The total gain in dB at 935 MHz is illustrated in Fig.7.2 for free space and on metal surface. The radiation of backside of the tag antenna shows lower gain than in free space due to the metal surface effect.

Table 7.1. *Dimension of the constructed antenna*

Parameter	Length(mm)	Parameter	Length(mm)
W	67	L	135
W1	35.5	L1	102.5
W2	32	L2	10
W3	31.5	L3=L4	2.5
W4	5.5	L5	2
W5	9.5	d1	15.5
W6	32.5	d2=d3	16

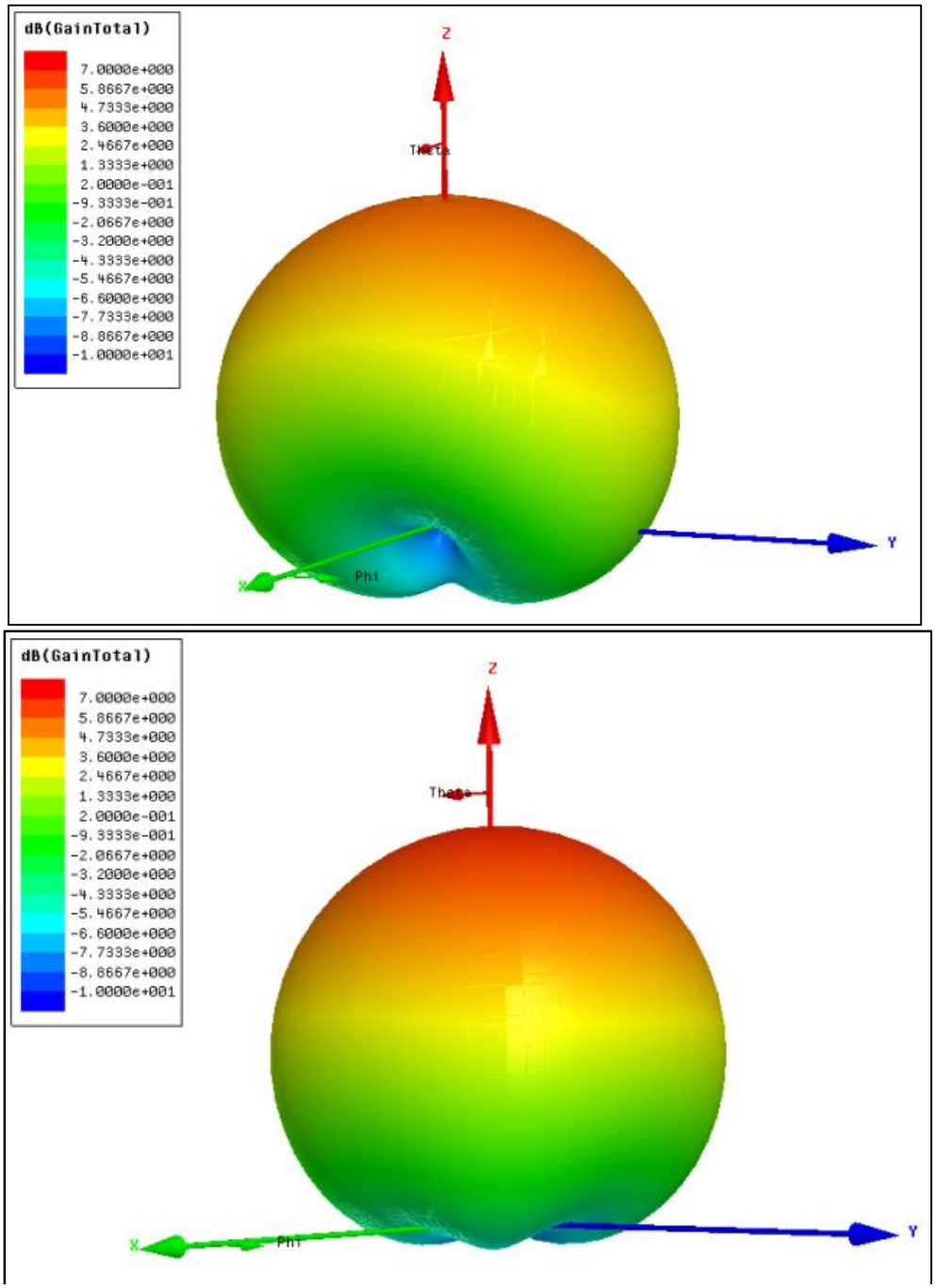

Figure 7.2. *The simulated 3D-total Gain at 935MHz of UHF patch tag antenna in free space (up) and on metal surface 200x200 mm^2 (down) in HFSS.*

The simulated surface current density is lower in metal surface than the antenna in free space. When this patch tag antenna is placed on the metal surface, the surface waves are conducted through the shorting strips to the metal plane and travels until the bound of the metal surface to scatter. This strip grounded approach reduces the effect of metal surface on the this patch tag antenna

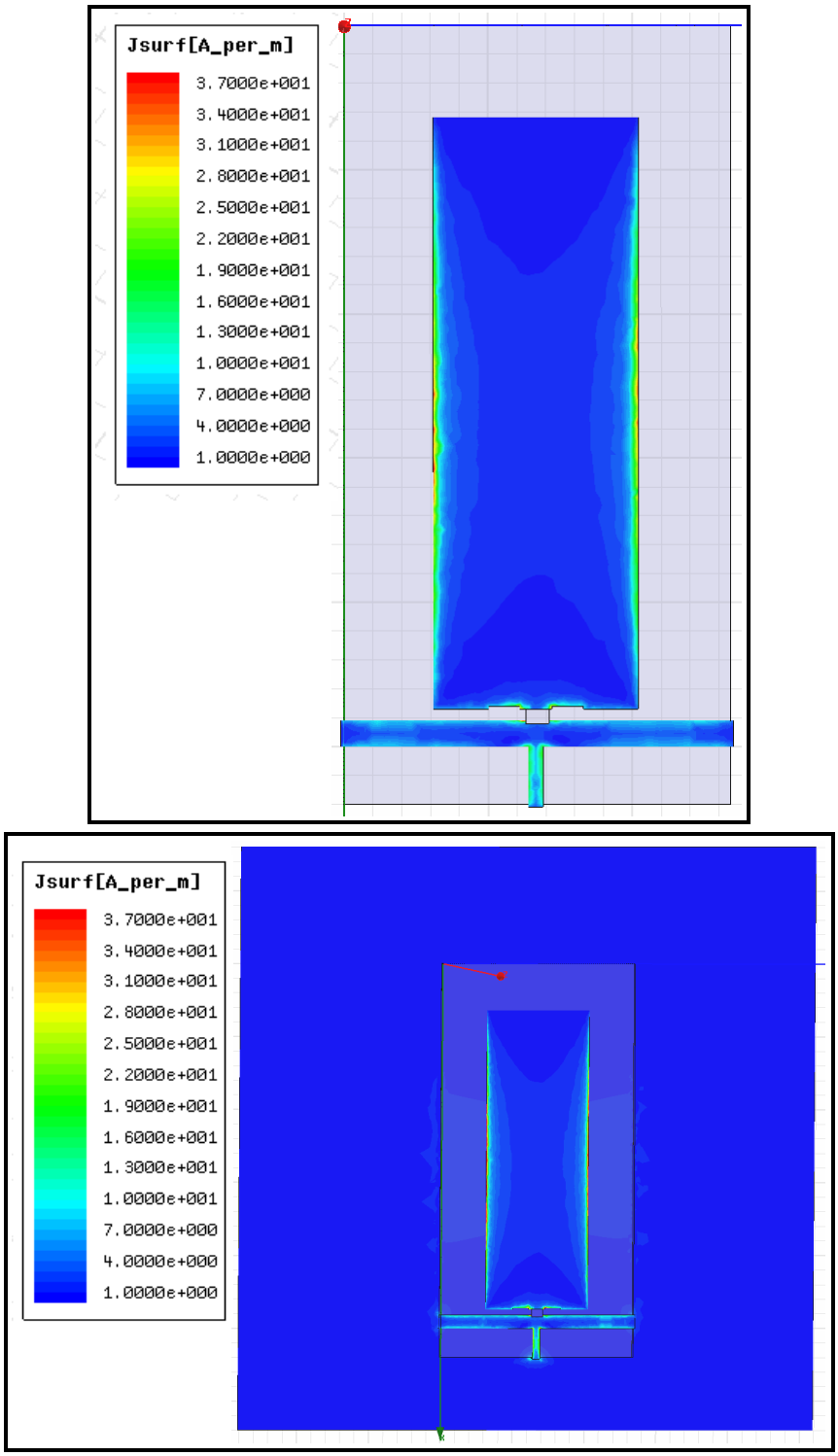

Figure 7.3. *Surface current density in free space(upper) and on metal surface(down) at 935MHz, and phase=80°.Simulation from HFSS.*

The radiation efficiency of the patch tag antenna in metal surface decreases respect to free space.

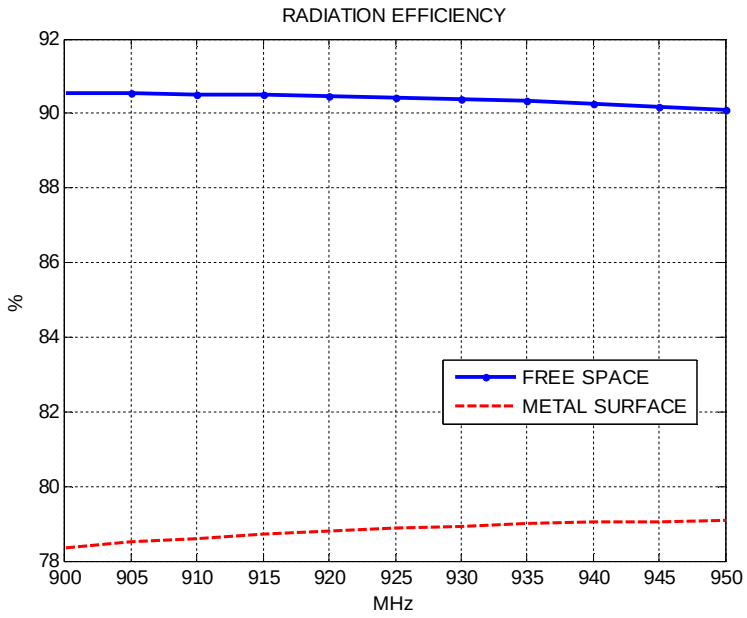

Figure 7.4. *Radiation Efficiency in free space and on metal surface 200x200mm^2. Simulation results from HFSS*

A resume table of simulation performance of patch tag antenna design can be found in Appendix 4.

7.2 Simulation results in CEMS and HFSS

The tag antenna is simulated in CEMS using the same dimension that the constructed antenna. Each software use different numerical methods to solve the simulation process. HFSS is commercial software that uses Finite Element Method (FEM) and CEMS uses Finite Difference Time Domain (FDTD) method. It is of interest how the antenna is simulated in both methods and how well the simulation results agree between them. The antenna impedance and total gain at 935MHz in the far field are the two main simulation results to be compared in this thesis.

In CEMS it should be set: the definition of problem space parameter, boundary condition, cell size, material type, CPML absorbing boundary condition, output parameter in frequency domain and far field. Appendix 2 shows the table of all these parameters for the design in free space and on metal surface.

For practical antenna construction-simulation in CEMS, the gap in the feed antenna is filled by the IC conductor strap side as it can be observed in Fig. 7.5. So, the whole feeding side attached to the IC is straight. This is a real observation in the construction of the antenna and it should be applied in simulation in CEMS simulation in order to smooth the computation capacity and improve the accuracy of the results. Reduction of cell size provides accuracy simulation results despite increasing computational capacity.

The tag antenna is simulated in both software and they exhibit similar results in free space and on metal surface 107x175 mm^2. When the tag antenna is placed on metal surface the tag antenna resistance is more affected (decreases) than the reactance tag antenna.

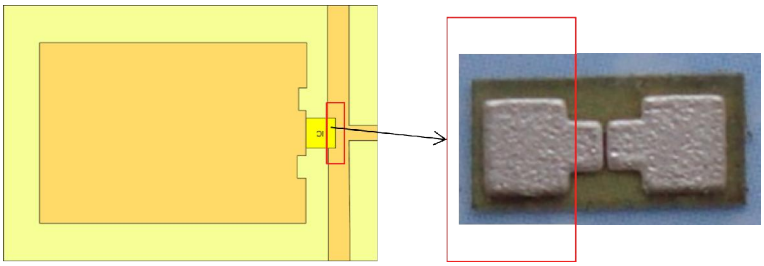

Figure 7.5. *Practical antenna view in CEMS. The conductive sides of the strap connected to the IC filled the gap in the feeding design.*

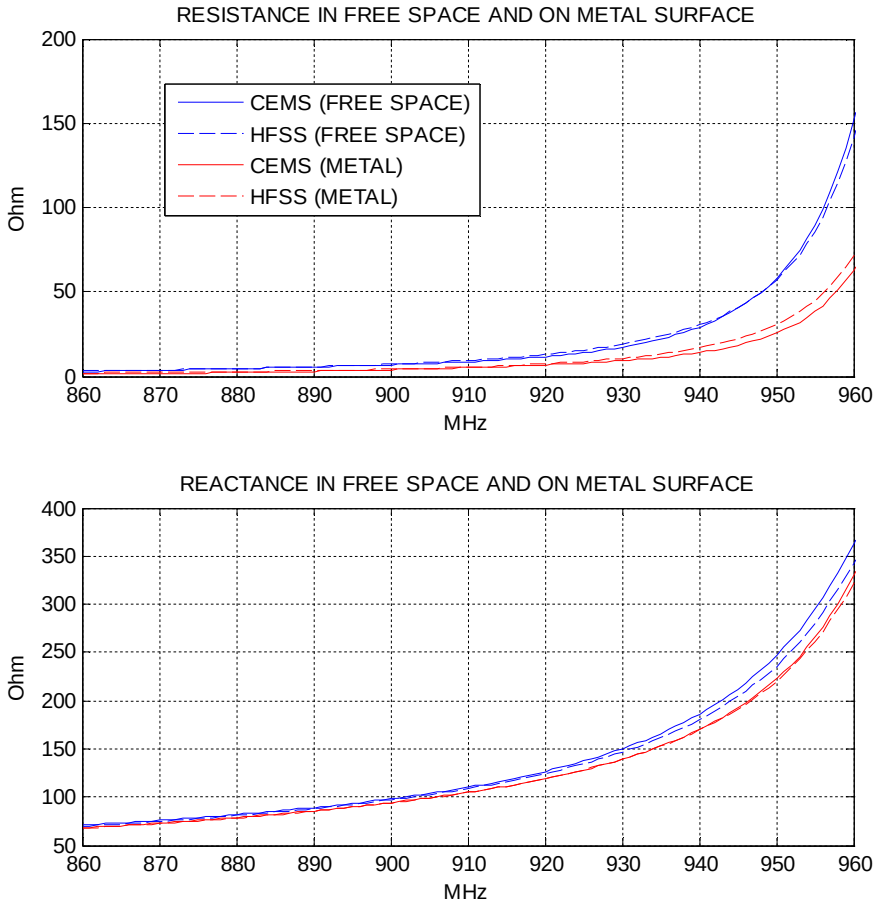

Figure 7.6. *Simulation, antenna impedance comparison between HFSS and CEMS in free space and on metal surface 107x175 mm^2.*

Both simulators confirm that frequency, at which minimum PRC occurs, is slow affected by the metal surface. There is not a complete immunity, and the frequency is shifted 3MHz when the tag antenna is placed on metal surface.

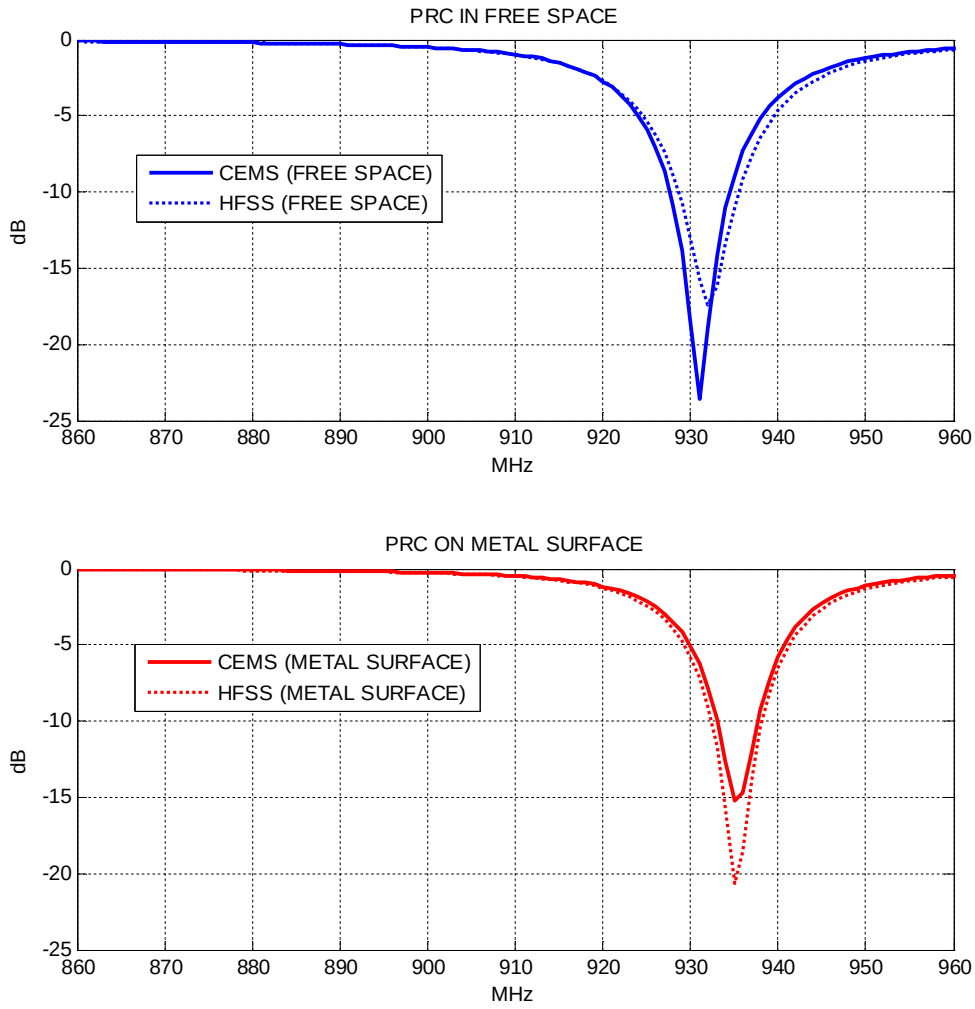

Figure 7.7. *Simulation of Power Reflection Coefficient in free space and on metal surface 107x175 mm^2 in HFSS and CEMS.*

The total gain in dBi at 935 MHz is simulated in free space and on metal surface, both simulators agree that metal surface affects gain antenna, mainly in the XY plane. The XZ and YZ planes are more immune to metal surface effect and even show an improved performance on metal surface for the front side of tag antenna.

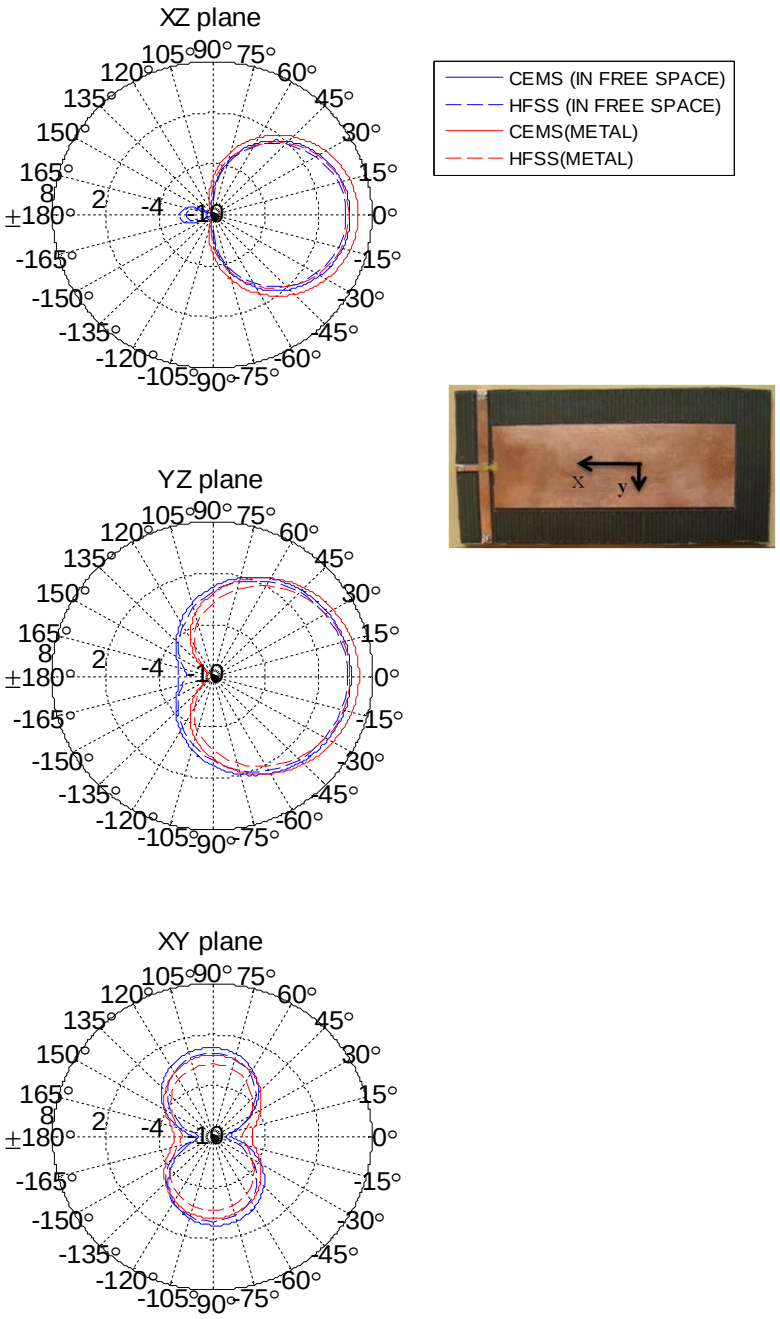

Figure 7.8. *Simulation, total gain in dBi at 935MHz between HFSS(--) and CEMS(-) in free space (blue) and on metal surface 107x175 mm^2 (red)*

It should be highlighted that CEMS simulation is providing faster computational time than HFSS; and HFSS and CEMS show good agreement in simulation results comparison.

7.3 Simulation and measurement results

The tag antenna is measured in the RFID Tagformance [32] measurement system that includes the anechoic chamber "cabinet", reader, reader antenna [34], and software that controls the measurement. The minimum transmitter power necessary to activate the tag antenna (threshold power) at 0.45m and the maximum read range are measured and plotted in Fig.7.10 and Fig. 7.11. For the measurement and simulation result, the metal surface has dimension 200x200 mm^2. It is observed in HFSS simulation, that the increase in metal surface dimension, does not lead to big changes in tag antenna performance simulation results.

7.3.1 Transmitted power and read range measurement

The measurement test bed is show in Fig. 7.9.

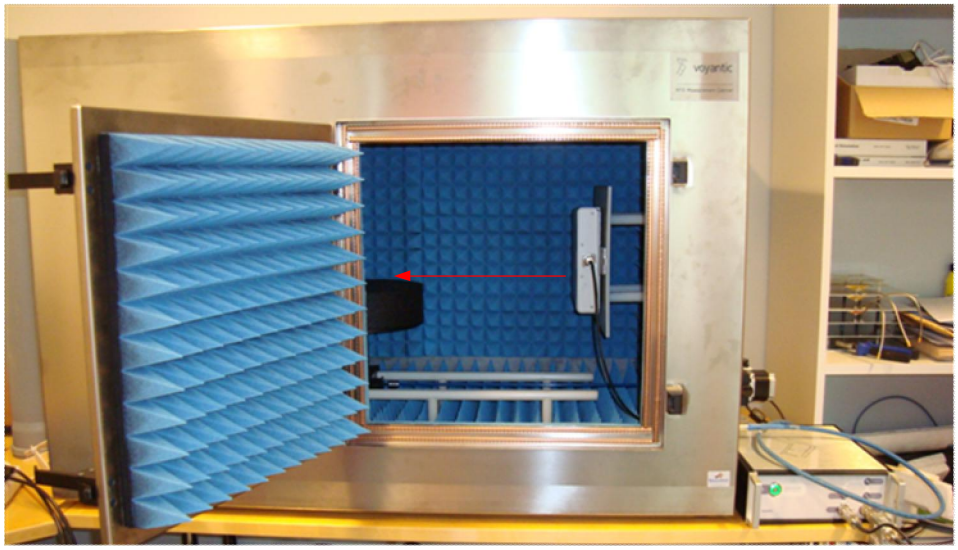

Figure 7.9. *Tagformance measurement test bed of the UHF patch tag antenna in RFID cabinet*

The threshold power is the minimum required power that the reader needs to communicate with the tag antenna and it is measured when the tag antenna is positioned ($\phi = 0^0, \theta = 0^0$) and at 0.45m from the reader. The tag antenna has better performance in metal surface than free space. The threshold power depends on tag antenna gain and PRC. The tag antenna gain is slow frequency dependent whereas the PRC varies for the frequency range. Then, the threshold power respect to frequency is a matching impedance indicator between tag antenna and IC. The frequency at which minimum PRC occurs is shifted from 932MHz (free space) to 935 MHz (metal surface).

The read range is one of the most important attribute of the tag antenna. The Tagformance calculates the theoretical maximum read range by using the threshold power for the initial fixed distance.

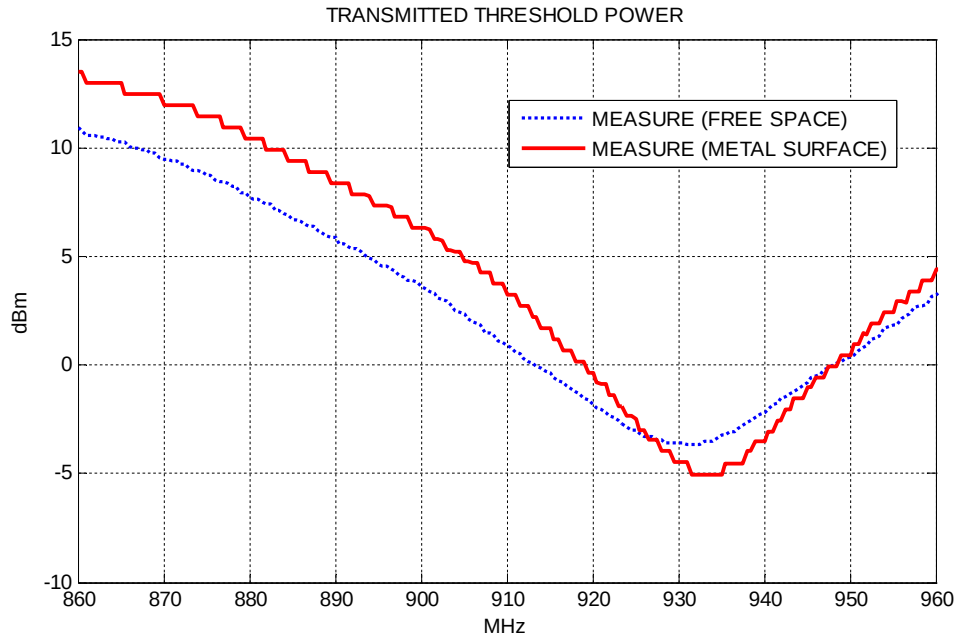

Figure 7.10. *Tagformance measurement, minimum transmitted power to activate the UHF patch tag antenna versus frequency in free space and on metal surface 200x200mm^2. There is 3MHz frequency shifted when the antenna is placed on metal surface. Tag antenna position is along Z ($\phi = 0, \theta = 0$). At 932MHz, tag antenna transmits more power to the IC in metal surface than in free space.*

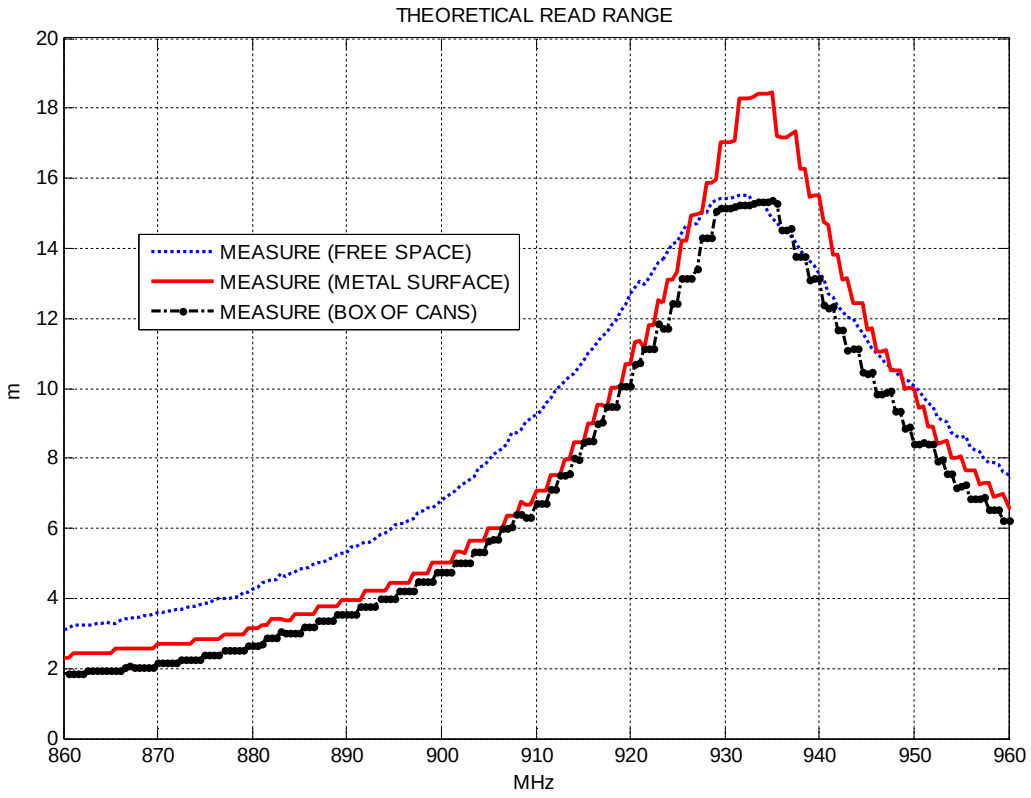

Figure 7.11. *Tagformance measurement of theoretical maximum read range versus frequency of the UHF patch tag antenna in free space and on metal surface 200x200mm^2,for $\phi = 0, \theta = 0$, EIRP=3.28W.*

Table 7.2. *Tagformance measurement of maximum theoretical read range for EIRP=3.28W at 935MHz in free space, on metal surface and box of cans.*

Frequency	Maximum read range (m) In free space	Maximum read range (m) On metal surface	Maximum read range (m) On box of cans
935 MHz	14.8 m	18.5 m	15.4 m

Theoretical maximum read range is measured for EIRP=3.28 W, which is the power used for European UHF RFID system. The tag antenna is placed in free space, on metal surface 200x200mm^2 and on box of cans. Probably, due to reflections there is increase in harvesting power to the IC and the tag antenna shows better performance in metal surface than free space at 935MHz. The performance on non planar metal surface (box of cans) decreases with respect to planar metal surface although good read range is also achieved.

Figure 7.12. *RFID Gateway reader ALR 8800 from Alien technology used for measurement in real environment.*

The read range of the designed antenna was measured on real environment (open area) again in free space, on metal surface 200x200mm^2 and on box of cans. The measurement was done using Alien RFID Gateway ALR 8800 [38] at 866MHz and the linear antenna [37] and circular reader antenna.

The gateway is a high performance EPC Gen 2 reader, with ERP 2W and operating frequency 865.6MHz at 867.6MHz. The EIRP of the gateway and Tagformance is almost the same 3.28W so both measurements are comparable when linear reader antenna is used; results are shown in Table 7.3. The read range measurements with circular polarized antenna and different attenuation are shown in Appendix 3.

The maximum reliable read range is defined by the distance where the reader detects the tag continuously without interruption [51, 79]. The read rate varies when the tag is placed at the maximum reliable read range. When the tag is moved beyond the maximum reliable read range, the read rate starts to drop occasionally to zero immediately [79].

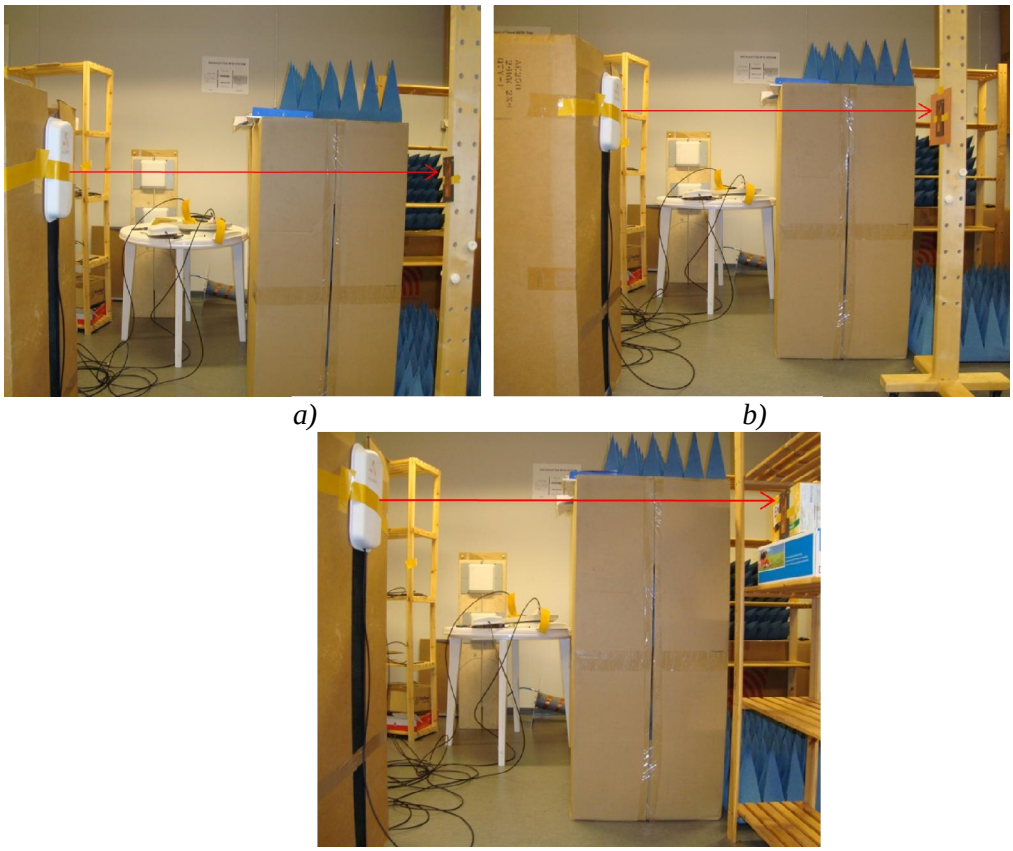

a) *b)* *c)*

Figure 7.13. *Read range measurement setup of the UHF patch tag antenna a) in free space b) on metal surface 200x200 mm^2 c) on box of cans (irregular metal surface). The tag is located in* $\phi = 0, \theta = 0$.

Table 7.3. *Maximum reliable read range measurement at 866 MHz with linear polarized antenna, EIRP=3.28W.*

Boundary	**Tagformance at 866MHz**	**Alien RFID gateway at 866 MHz with linear polarized antenna**
On free space	3.4 m	4.50 m
On metal surface200x200mm^2	2.5 m	4.30 m
On box of cans	2.0 m	3.85 m

It is observed that the read range on real environment is larger than the measured by Tagformance. Probably, due to the increase of reflections in the real environment which are constructive rather than destructive. The harvesting power in IC is higher and the tag antenna can be detected at longer distances.

7.3.2 Realized gain and radiation pattern result

The realized gain is the parameter that can be accurately compared between the Tagformance measurement and HFSS simulation. It is perhaps the most useful definition of RFID tags. The gain is nevertheless only slightly frequency dependent and therefore the bandwidth performance is mainly affected by the impedance matching. Stability of realized gain over frequency gives the range-width of the reader-tag system [73]. The realized gain is the result of transmitter coefficient and gain. Figure 7.14 shows this dependence.

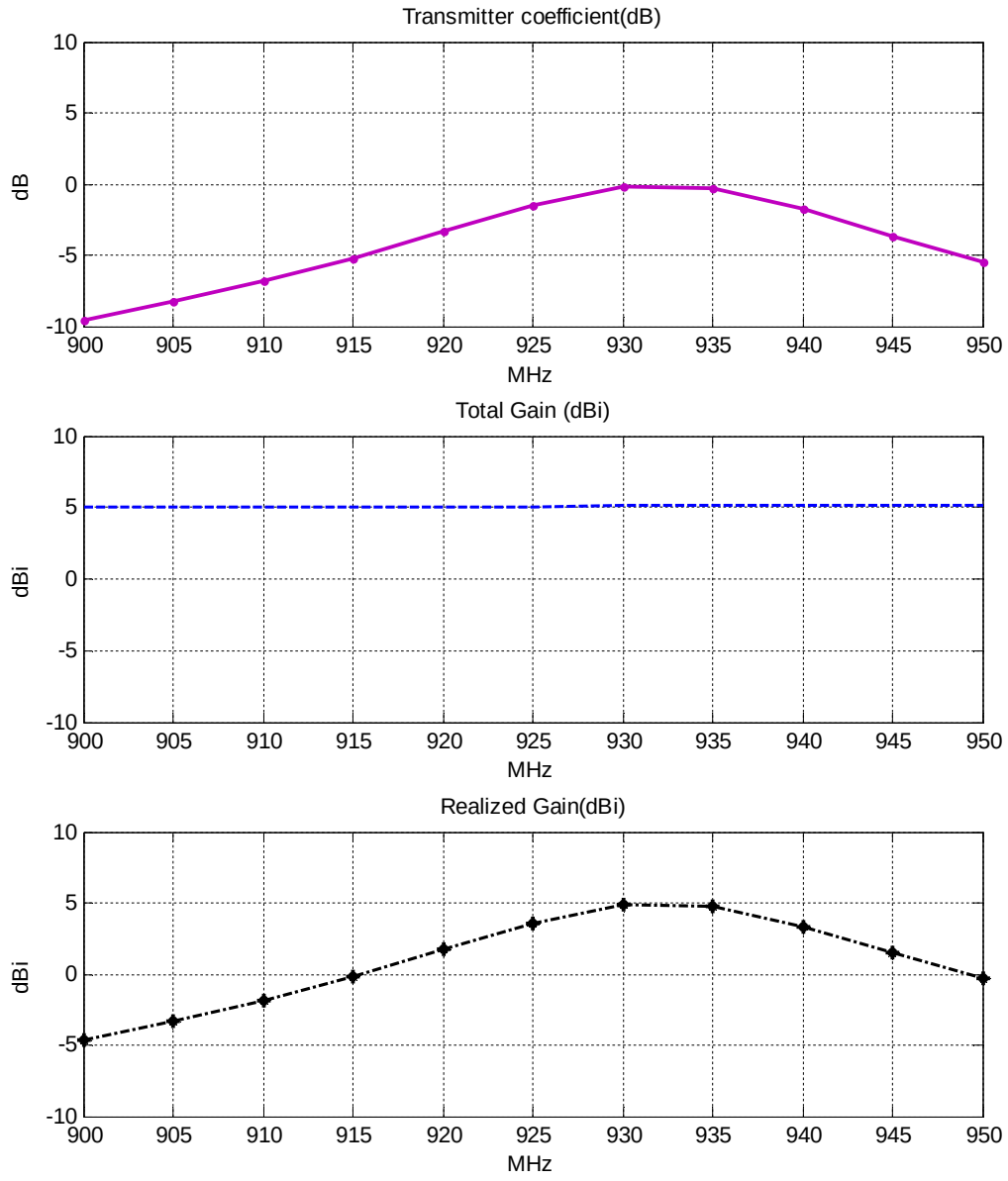

Figure 7.14. *Transmitter coefficient, total gain and realized gain simulation in free space for the tag antenna position* $\phi = 0, \theta = 0$ *in the HFSS simulator. The realized gain over frequency depends mainly of matching impedance between tag antenna and IC. The total gain is almost constant over the frequency.*

The realized gain is the parameter that can be accurately compared between the Tagformance measurement and HFSS simulation. It is perhaps the most useful definition for RFID tags. The gain is nevertheless only slightly frequency dependent and therefore the bandwidth performance is mainly affected by the impedance matching. Stability of realized gain over frequency gives the range-width of the reader-tag system [73]. The realized gain is the result of transmitter coefficient and gain. Fig.7.14 shows this dependence.

$$G_r = G_{tag}(1 - |s|^2) \tag{7.1}$$

The realized gain respect to frequency is compared between measurement and simulation. The realized gain, when tag is placed on metal surface, is lower than that of the free space at position $\phi = \pi/2, \theta = \pi/2$. The realized gain at ($\phi = 0, \theta = 0$), when tag is placed on metal surface, improves with respect to free space for frequency higher than 930 MHz due to the improvement of transmitter coefficient at those frequency and high total gain.

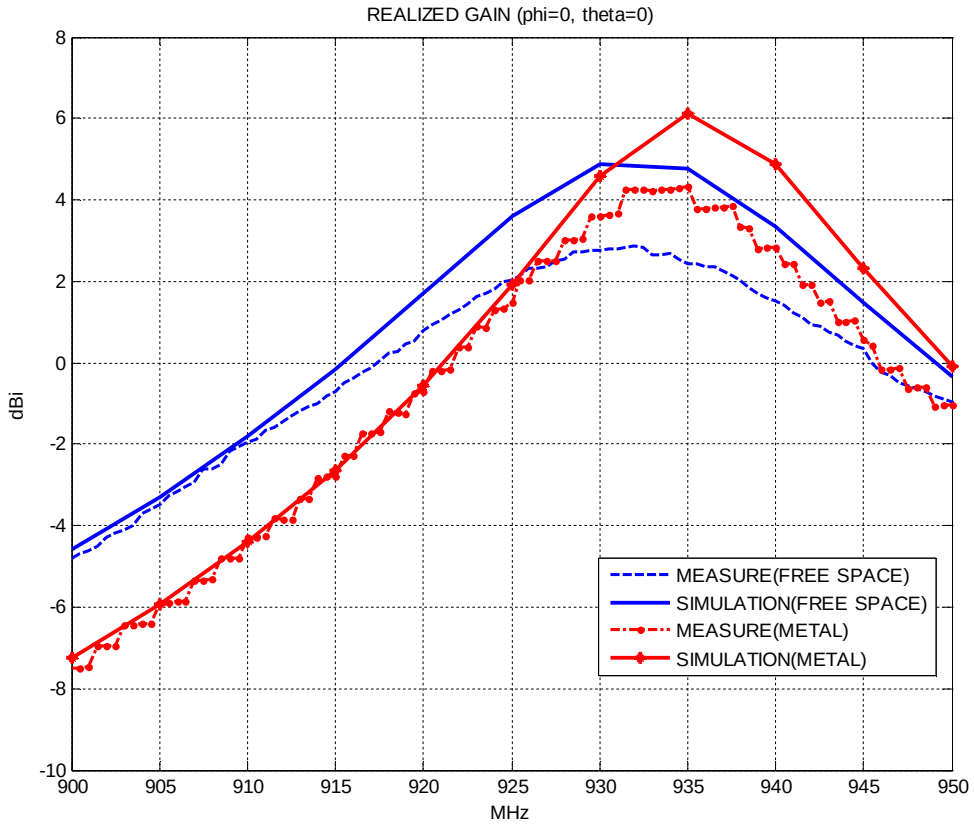

Figure 7.15. *Realized gain, comparison between Tagformance measurement and HFSS simulation, when the tag antenna is located at* $\phi = 0, \theta = 0$ *(right) in free space and on metal surface 200x200 mm*^{2}.

Finally, the normalized gain in dB is also compared between measurement and HFSS simulation in free space (Fig. 7.16) and on metal surface (Fig.7.17) for the XZ, YX, and XY planes. The agreement is fairly good mainly in the XZ, YZ plane for the upper side of the tag antenna radiation.

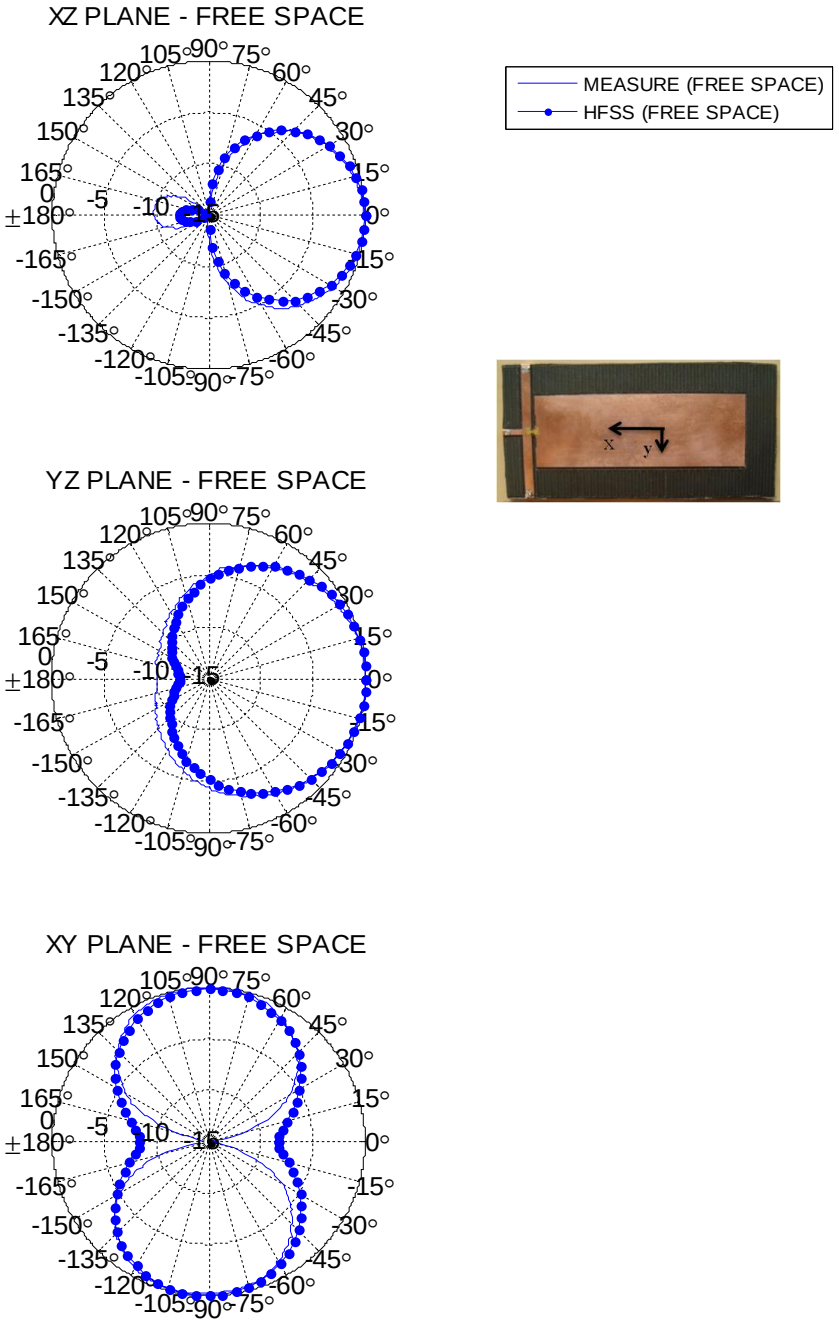

Figure 7.16. *Radiation pattern of normalized gain (dB) at 935 MHz, comparison between Tagformance measurement and HFSS simulation in the XZ, YZ and XY plane in free space.*

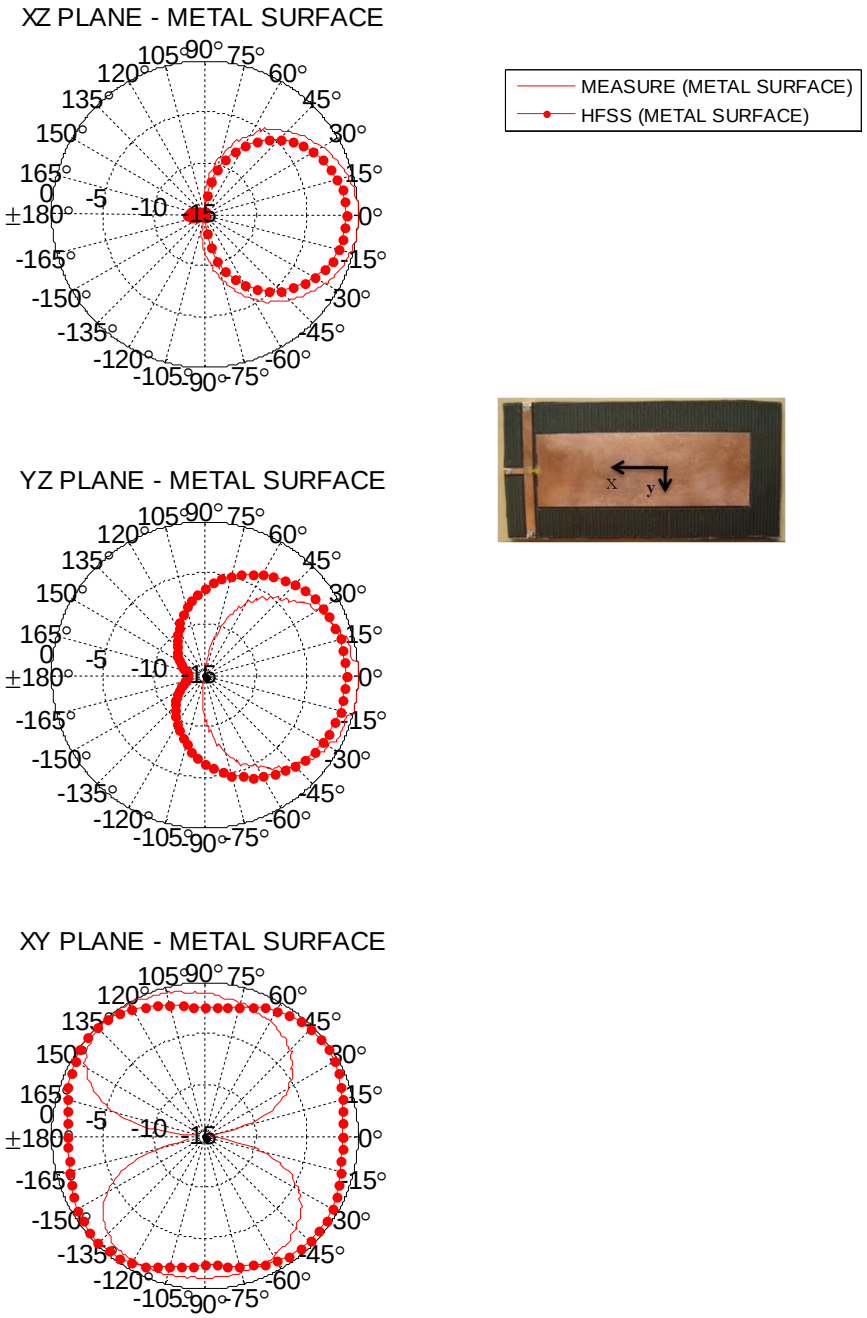

Figure 7.17. *Radiation pattern of normalized gain (dB) at 935 MHz, comparison between Tagformance measurement and HFSS simulation in the XZ, YZ and XY plane on metal surface 200x200 mm^2.*

8. CONCLUSIONS

Passive UHF RFID technology is the most used system for object identification. This system may reach longer read range of identification (in the order of meters) compared to electric and magnetic coupling (<1m). Besides, a passive system offers cheaper cost compared to active system, in which a battery is required. The simplicity of the construction of the tag antenna, the ideal durability of the tag, and the cheaper cost of components makes the passive UHF RFID tag antenna an ideal choice for object identification.

Many applications required to indentify object formed by metal surface. However this type of material degrades the performance of passive UHF tag antennas. Metal surface is an ideal perfect conductor medium. As it is review in this thesis, when an electromagnetic wave impinges on conductor medium, all the wave reflects with a phase shift of 180 degrees. The incoming and the reflected waves create a standing wave. Reflections are the main responsible for the variation in the tag antenna radiation pattern, antenna impedance, bandwidth, efficiency; unfortunately, degrading the tag antenna performance.

A list of solutions to overcome the metal surface effect on arbitrary tag antenna is listed in this thesis. It is concluded that, the use of material with high and equal value of permittivity and permeability should be placed between the tag antenna and metal surface. The reflection of incoming signal impinging on this dielectric-magnetic material is zero. However, this type of material solution is not of wide accessibility in the market as there are dielectric materials. This solution is not applied in this thesis.

Through the years and from the open literature, a patch tag antenna and it is variants are used as the tag antennas to overcome the metal surface effect. Patch antennas needs of metal surface to work properly and radiates. They even work better for infinite metal surface. However, infinite metal surface is an ideal condition since the size of tag antenna depends on the object and application.

Patch tag antenna is the reference for tag antenna design. And, as it is reviewed in this thesis, there are many designs based on path tag antenna on the open literature that enhances the performance of this antenna through different methods. The most common methods are: shorting to ground the radiating patch, the use of feed loop and coupling the radiating patch, the use of coplanar waveguide and high impedance surface, etc. In addition, the use of U-slots improves the bandwidth of patch tag antenna and the matching impedance between the patch tag antenna and the high impedance of IC, leads to a better immunity of impedance mismatch.

From different methods used to improve the immunity of the patch tag antenna on metal surface; it is chosen: one side of the IC shorts to ground and the other side connect to the patch radiator. A passive UHF patch tag antenna based on this model is designed and constructed. The simulation results exhibits encouraging results. The patch tag antenna is first designed in HFSS and tested on CEMS electromagnetic simulator based on the final tag antenna dimensions obtained from the HFSS simulator.

In the same way, CEMS simulator based on Finite Difference Time Domain (FDTD) method is compared to HFSS based on Finite Element Method (FEM). The comparison between them is made through comparing the simulation results in free space and on metal surface 107x175 mm^2 like: patch tag antenna impedance, power reflection coefficient and total gain. Both electromagnetic simulators agree on results and CEMS greatly satisfied the simulation results. This enhances the reliability of the designed antenna. It is worth to note that CEMS took less processing time.

The constructed passive UHF patch tag antenna has good performance on free space and on metal surface. This tag antenna is almost immunity to metal surface. From measurement; when the tag antenna is placed on metal surface 200 x 200 mm^2, the maximum read range is 18m and realized gain is 5dBi at 935MHz. The transmitted power EIRP during measurement is 3.28W, which is the allowed EIRP power used in the European region. Besides, the UHF RFID frequency at minimum power reflection coefficient (PRC) in free space is 932MHz; whereas, it is shifted 3 MHz when tag antenna is placed on the metal surface. This tag antenna works in good performance for the whole UHF RFID frequency band (860MHz-960MHz).

This new tag antenna design is applied for the identification of metal surface objects. For example, containers, car platform, ships, etc. However, this design is limited to regular metal surface. For irregular metal surface like a box of cans, a reduction to 14m in maximum read range at 935MHz is noticed. Besides, the total dimension of this design is 135x67mm^2. This dimension limits the application range. Even, the operating frequency of this tag antenna, at which best performance characteristic occurs, is not applicable for a specific country or region; this tag works in good performance in the whole UHF RFID frequency band.

For future work, it is recommended to work on diminish the dimension of the designed tag antenna. Miniaturization of this tag antenna would increase the demanding applications and compact of the design. The miniaturization may be lead by increasing the dielectric constant of the microstrip; by introducing a U-slot in the radiating slots in way that wider bandwidth may be achieved. Those two initial ideas do not give straight forward and successful results. Computation time, review of literature and after running many simulation designs would lead to the proper new miniaturized passive UHF patch tag antenna mountable con metal surface.

REFERENCES

[1] ISO/IEC 18000-6: Information Technology-Radio Frequency Identification for Item Management- Part 6: Parameter for Air Interface Communications at 860 MHz to 960 MHz, website www.iso.org, ISO, 2004.

[2] J. Prothro, "Improved Performance of a Radio Frequency Identification Tag Antenna on Metal Ground Plane," Master of Science Thesis, Georgia Institute of Technology, 2007.

[3] L. Wiebklimg, M. Korpela, M. Nikkanen and K. Pentillä, "WP1-Roadmap Working Draft 1.3 Final Report," state of art of RFID system, 2007.

[4] K. Penttilä, "Studies towards Improving RFID Reader Performance," Doctoral Thesis, Tampere University of Technology, publication 603, pp. 1-31, 2006.

[5] EPC Radio Frequency Identification Protocols: Class-1 Generation-2 UHF RFID, Protocol for Communication at 860-960 MHz, version 1.2.0, website www.epcglobalinc.org, EPCglobal, 2006.

[6] K. Finkenzeller, *RFID Handbook: Fundamentals and applications in Contactless Smart Cards and Identificaiton,* 2nd Ed., John Wiley & Sons, England, 2003.

[7] EPC Global 1: Tag classification definition, website www.epcglobal.org, 2007.

[8] D. Dobkin, *The RF in RFID: Passive UHF RFID in practice*, Elsevier, USA 2008.

[9] P. Pursula, "Analysis and Design of UHF and Millimeter Wave Radio Frequency Identification," VTT Publication 701, pp. 9-48, 2008.

[10] European Telecommunications Standards Institute, www.etsi.org, 2006.

[11] Rules and Regulations. Federal Communications Commission (FCC) Part 15: Radio Frequency Device, website: www.fcc.gov, 2009.

[12] C. Paul, K. Whites and S. Nasar. *Introduction to Electromagnetic Fields*, 3rd edition, McGraw-Hill, 1998, pp. 287- 575.

[13] D. Cheng, *Fundamentals of Engineering Electromagnetics*, Addison-Wiley, 1994, pp. 228-327.

[14] IEEE Std. 145-1983: Standard Definitions of Terms for Antennas, June 1983.

[15] C. Balanis, *Antenna Theory Analysis and Design*, 3rd edition, Wiley, New York, 2005.

[16] R. Garg and P. Bhartia, *Microstrip antenna design handbook,* Artech House, London. pp 1-314, 2000

[17] P. Hazdra, M. Polivka and V. Sokol. "Microwave Antennas and Circuits Modeling using Electromagnetic Field Simulator," Department of electromagnetic field, Czech Technical University, Volume 14, number 4, December 2005.

[18] D. G. Jr. Swason and W. J. R Hoefer, *Microwave Circuit Modeling Using Electromagnetic Field Simulation,* Artech House, London, 2003, pp. 125-171.

[19] S. G. Johson , "Perfectly matched layers (PMLs)," Notes for the course 18.369 and 18.336 at MIT, March 2010.

[20] J. Roden and S. Gedney, "Convolutional PML (CPML): An efficient FDTD Implementation of the CFS-PML for arbitrary media," Submitted to Microwave and Optical Technology Letters, 2000.

[21] M. Kuzuoglu and R. Mittra, "Frequency dependence of the constitutive parameters of causal perfectly matched anisotropic absorbers," *IEEE Microwave and Guided Wave Letters*, Vol.6, pp. 447-449, 1996.

[22] A. Elsherbeni and V. Demir, *The Finite-Difference Time-Domain Method for Electromagnetics with Matlab Simulations,* SciTech Publishing, 2009.

[23] Alien Technology, web site http://www.alientechnology.com

[24] Impinj web site, web site http://www.impinj.com/

[25] P. Jr. Penfield, "Noise in negative resistance amplifiers," *IRE Trans. on Circuit Theory*, Vol. CT-7, pp. 166-170, June 1960.

[26] K. Kurokawa, "Power waves and the scattering matrix," *IEEE Trans. Microwave Theory and Techniques*, Vol. MTT-13, No. 3, pp. 194–202, March 1965.

[27] K. V. S. Rao, P. V. Nikitin and S. F. Lam. "Antenna Design for UHF RFID Tags: A Review and Practical Application," *IEEE Transactions on Antenna and Propagation*, Vol.53, Issue 2, pp.3870-3876, 2005.

[28] P. V. Nikitin, K. V. S Rao, S. F. Lam, V. Pillai, R. Martinez and H. Heinrich. "Power Reflection Coefficient Analysis for Complex Impedances in RFID Tag Design," *IEEE Transactions on Microwave Theory and Techniques*, Vol.53, Issue 9, pp.2721-2725, 2005.

[29] P. V. Nikitin and K. V. S. Rao, "Antennas and Propagation in UHF RFID Systems," *2008 IEEE International Conference on RFID*, USA, pp. 277-288 April 2008.

[30] P. V. Nikitin, K. V. S. Rao and R. D. Martinez. "Differential RCS of RFID Tag," *IET Journals Electronic Letters*, Vol.43, No.8, pp.431-432, April 2007.

[31] P. V. Nikitin and K. V. S. Rao, "Theory and Measurement of Backscattering from RFID Tags," *IEEE Journals on Antennas and Propagation Magazine*, Vol.48, Issue 6, pp.212-218, 2006.

[32] RFID cabinet provider, Voyantic webpage http://www.voyantic.com/

[33] Mercury 4 RFID reader, web site http://www.thingmagic.com/

[34] Reader antenna used in the measurements with Tagformance, Data sheet website http://www.hubersuhner.com

[35] J. Virtanen, "Tulostettava Kosteusanturi UHF-Alueen RFID-Järjestelmiin," Master of Science Thesis, Tampere University of Technology, pp.72, 2009.

[36] HFSS software, web site http://www.ansoft.com/products/hf/hfss/

[37] Linear polarized antenna, data sheet http://www.aifos-solutions.com/pdf/ALR 8610Lesp.pdf

[38] Alien RFID reader data sheet http://www.alientechnology.com/docs/products/DS_ALR_8800.pdf

[39] Dielectric material provider Rogers RT5880, Rogers web site http://www.rogerscorp.com

[40] H.-W. Liu, Y.-S. Lin, K.-H. Wu and C.-F. Yang. "A Metal Mounting Tag for Passive UHF RFID applications," *IEEE Antennas and Propagation Society International Symposium*, pp. 1769-1772, 2007.

[41] Z.-J. Tang and Y.-G. He, "Broadband Microstrip Antenna with U and T slots for 2.45/2.41 GHz RFID tag," *IEEE Electronics Letters*, Vol.45, No.18, pp.926-928, August 2009.

[42] M. Eunni, M. Sivakumar and D. Deavours. "A Novel Planar Microstrip Antenna Design for UHF RFID." *Journal of Systemics, Cybernetics and Informatics*, Vol. 5, No. 1, pp. 209-203, January 2007.

[43] M.-C. Huynh and W. Stutzman, "Ground Plane effects on Planar Inverted-F Antenna(PIFA) performance," *IEE Proc.-Microw. Antennas Propag.*, Vol. 150, No 4, pp. 209-213, August 2003.

[44] M. Hirvonen, P. Pursula, K. Jaakola and K. Laukanen. “Planar Inverted-F antenna for Radio Frequency Identification,” *IEEE Electronic Letters*, Vol.40, No.14, July 2004.

[45] Y. Um, U. Kim, W. Seong and J. Choi. “A Novel Antenna Design for UHF RFID Tag on Metallic Objects,” *PIERS Proceedings*, Prague, pp. 158-161, August 2007.

[46] W. Choi, J. Kim, J.-H. Bae and G. Choi. “A Small RFID Tag Antenna to Identify Metallic Object,” in *IEEE APS International Symposium*, 2008, pp. 1-4.

[47] L. Xu, L.-B. Tian and B.-J. Hu. “A Novel Broadband UHF RFID Tag Antenna Mountable on Metallic Surface,” in *International Conference on Wireless Communications, Networking and Mobile Computing*, September 2007, pp. 2128-2131.

[48] B.-Y Yu, S.-J. Kim and B. Jung. “RFID Tag Antenna Using Two-Shorted Microstrip Patches Mountable On Metallic Objects,” *Microwave and Optical Technology Letters*, Vol.49, No.2, pp. 414-416, February 2007.

[49] J.-S. Kim, W. Choi, G.-Y. Choi, C.-S. Pyo and J.-S. Chae. “Shorted Microstrip Patch Antenna Using Inductively Coupled Feed for UHF RFID Tag,” *ETRI Journal*, Vol. 30, No. 4, pp. 600-603, August 2008.

[50] Y. Um, U. Kim and J. Choi. “Design of a Compact CPW-FED UHF RFID Tag Antenna for Metallic Objects,” *Microwave and Optical Technology Letters*, Vol. 50, No. 5, pp. 1439-1943, May 2008.

[51] T. Koskinen and Y. Rahmat-Samii, “Metal-Mountable Microstrip RFID Tag Antenna for High Impedance Microstrip,” in *3rd EuCAP Conference*, 2009, pp. 2791-2795

[52] H.-W. Son, “Design of RFID Tag Antenna for Metallic Surfaces Using Lossy Substrate,” *IEEE Electronics Letters*, Vol. 44, No. 12, pp. 711-713, June 2008.

[53] H.-D. Chen and Y.-H. Tsao, “Low-Profile PIFA Array Antennas for UHF Band RFID Tags Mountable on Metallic Objects,” *IEEE Transactions on Antennas and Propagation*, Vol.58, No.4, pp. 1087-1092, April 2010.

[54] S.-L. Chen, “A Miniature RFID Tag Antenna Design for Metallic Objects Application,” *IEEE Antennas and Wireless Propagation Letters*, Vol.8, pp. 1043-1045, 2009.

[55] H.-W Son, W.-K. Choi and G.-Y Choi. “Radiation Efficiency Improvement Method of RFID Tag Antenna for Metallic Objects Printed on Lossy Substrate,” in *APM Microwave Conference Asia-Pacific*, 2008, pp. 1-4.

[56] S.-L. Chen and K.-H. Lin, "A Slim RFID Tag Antenna Design for Metallic Object Applications," *IEEE Antennas and Wireless Propagation Letters*, Vol.7, pp. 729-732, 2008.

[57] Y.-K. Parl, S.-G. Lee, J.-K. Kan and Y.-C. Chung, "Various UHF RFID Tag for Metallic Object," in *IEEE Antennas and Propagation Society International Symposium*, 2007, pp. 2285-2288.

[58] B. Lee and B. Yu, "Compact Structure of UHF Band RFID Tag Antenna Mountable on Metallic Objects," *Microwave and Optical Technology Letters*, Vol. 50, No. 1, pp. 232-234, January 2008.

[59] J.-S. Kim, W. Choi and G.-Y. Choi. "Small Proximity Coupled Ceramic Patch Antenna for UHF RFID Tag Mountable on Metallic Objects," *Progress in Electromagnetics Research C*, Vol. 4, pp. 129-138, 2008.

[60] L. Mo, H. Zhang and H. Zhou. "Broadband UHF RFID Tag Antenna with a pair of U-Slots Mountable On Metallic Objects," *IEEE Electronic Letters*, pp. 1173-1174, September 2008.

[61] S.L. Chen and R. Mitra, "A Long Read Range RFID Tag Design For Metallic Objects," in *European Conference on Antenna and Propagation*, Barcelona, 2010, pp. 1-3.

[62] A. Popugaev and R. Wansch, "A Small High Performance Metal-Mountable RFID Tag Antenna," in *European Conference on Antenna and Propagation*, Barcelona, 2010, pp. 1-4.

[63] S.-H. Jeong, H.-W. Son and J. Yeo. "A Low-Cost, Wideband RFID Tag Antenna on Metallic Surfaces Using Proximity-Coupled Feed," in *IEEE Microwave conference- Asia Pacific*, 2009, pp. 2409-2411.

[64] J.-S. Kim, W. Choi and G.-Y. Choi. "UHF RFID Tag Antenna Using two PIFAs Embedded in Metallic Objects," *IEEE Electronics Letters*, Vol. 44, No. 20, pp. 1181-1182, September 2008.

[65] H.-W. Son, G.-Y. Choi and C.-S. Choi. "Design of wideband RFID Tag Antenna for Metallic Surface," *IEEE Electronics Letters*, Vol. 42, No. 5, pp. 263-265, March 2006.

[66] J.-S. Kim, W. Choi and G.-Y. Choi. "Ceramic Patch Antenna for UHF RFID Tag Embedded in Metallic Objects," in *IEEE Ant. Propag. Soc. Int. Symposium*, June 2009, pp. 1-4.

[67] H.-W. Son and G.-Y. Choi, "Orthogonally Proximity-Coupled Patch Antenna for a Passive RFID Tag on Metallic Surfaces," *Microwave and Optical Technology Letters*, Vol. 49, No. 3, March 2007.

[68] W. Choi, H.-W. Son and J.-H. Bae. “An RFID Tag Using a Planar Inverted-F Antenna Capable of Being Stuck to Metallic Objects,” *ETRI Journal*, Vol. 28, No.2, pp. 216-218, April 2006.

[69] F. Yang and Y. Rahmat-Samii, *Electromagnetic Band Gap Structures in Antenna Engineering*, Chapter 1: Introduction, Cambridge University Press, 2009.

[70] B. Gao and M. Yuen. “Passive UHF RFID with Ferrite Electromagnetic Band Gap (EBG) Material for Metal Object Tracking,” in *IEEE 58th Electronic Components and Technology Conference*, May 2008, pp. 1990-1994.

[71] L. Ukkonen and L. Sydänheimo, “Impedance Matching Considerations for Passive UHF RFID Tags,” in *IEEE Asia Pacific Microwave Conference*, December 2009, pp. 2367- 2330.

[72] N. Mohammed, M. Sivakumar and D. Deavours. “An RFID Tag Capable of Free-Space on Metal Operation,” in *IEEE Radio and Wireless Symposium*, 2009, pp. 63-66.

[73] G. Marroco, “The Art of UHF RFID Antenna Design: Impedance Matching and Size-Reduction techniques,” *IEEE Antennas and Propagation Magazine*, Vol. 50, N.1, pp. 66-79, January 2008.

[74] G. Monti, L. Catarinucci and L. Tarricone. “Compact Microstrip Antenna for RFID Applications,” *IEEE Progress in Electromagnetics Research Letters*, Vol.8, pp. 191-199, 2009.

[75] B. Yu, F. Harachiewicz and B. Lee. *Radio Frequency Identification Fundamentals and Applications Design Methods and Solutions: RFID Tag Antennas Mountable on Metallic Plataforms*, INTECH, February 2010, pp. 1-16.

[76] L. Sydänheimo, L. Ukkonen and M. Kivikoski. “Effects of Size and Shape of Metallic Objects on Performance of Passive Radio Frequency Indentification,” in *The International Journal of Advanced Manufacturing Technology*, Springer London, Vol. 30, Number 9-10, pp. 897-905, October 2006.

[77] R. Simons, *Coplanar Waveguide Circuits: Advantages of coplanar waveguides, Components and Systems*, Chapter 1: Introduction, Wiley-Interscience, 2001.

[78] D. Frederic, “High Impedance Electromagnetic Surface,” Dissertation for the degree of Doctor Phylosophy, University of California, Los Angeles, 1999.

[79] T. Björninen, L. Ukkonen, L. Sydänheimo et al. “Wireless Measurement of UHF RFID tag chip impedance”, Atlanta USA, to be appear soon in Antenna Measurement Techniques Association AMTA October 10-15, 2010.

[80] H. Stockman, “Communication by Means of Reflected Power,” *Proceedings of the Institute of Radio Engineers*, Vol. 36, No. 10, 1196-1204, 1948.

[81] Milling machine LPKF ProtoMat c100/HF data sheet. http://www.lpkfusa.com/RapidPCB/CircuitboardPlotters/c100hf.htm

APPENDIX 1: SURVEY OF DIFFERENT PATCH ANTENNA MOUNTABLE ON METALIC OBJECTS

	Ref.	Dimension (mm^3)	Dielectric constant and height (mm.)	-3dB Bandwidth (MHz)	Read range(m) [2]
Feed loop	[46]	19x19x3	er=22, h=3	895-925	4
	[48]	47.5x50x3	er=4.7, h=0.6 er=1.1, h=2.4	904-930	4.5
	[49]	25x25x3	er=48, h=3	904-925	5
	[59]	25x25x3	er=48, h=3	910-920	6.6
T-matching	[47]	106x40x4.6	er=4.7, h=1.6 er=1.1, h=3	862-872 921-938	
GND-IC-Patch	[45]	100x5.5x6	er=4.4, h=6	696-978	4.75
	[57]	30x30x3.18	er=2.2, h= 3.18 RT duroid 5880	625-1300 400-1070 600-1200	1.7 0.85 1.9
	[58]	80x40x1.6	er=4.7, h=1.6	900-930	4.2
	[60]	96x50x2	er=4.4, h=2	842- 975	3.8
HIS	[50]	39x26x2.2	er=3.2, h=2.2, tanδ=0.0036	904-914	4.5
	[51][1]	140x50x1.8	er=4.4, h=0.4 er:vacuum, h=1.4	970-1000	4
	[53]	130x45x0.8 127x 52x0.8	er=4.4, h=0.8	901-936	1.5 2.4
	[54][1]	32x18x3.2	er=4.2, h1=1.6 er=4.2, h2=1.6	898-954	1.5
	[56]	65x20x1.5	er=4.2, h=1.5	902-960	3.1
	[61]	70x24x3	er=4.2, h=3	917-970	2.8
Add lumped capacitor	[52,55]	39x20x2.22	er=4.3, h=1.9, tanδ=0.017. er=2.6, h= 0.07 er=3.5,h=0.25, tanδ=0.0018	900-930	*
	[62]	a. 45x15x5 b. 37x7x3.2	er=3.55,h=3.1, tanδ=0.0027	865-870 865-956	5[3] 2[3]

[1]Study based on Higg2.
[2]Common read range taken in metal surface.
[3]At European bandwidth
*not mention

APPENDIX 2: THE PROBLEM PARAMETERS DEFINITION IN CEMS.

SETUP DEFINTION	In free space	On metal surface 107x175 mm^2
Define the problem space parameter		
Courant factor	0.95	0.95
Number of time steps	30000	30000
Dimension of Cell size (Δx, Δy, Δz) in mm	0.245; 0.245; 0.27	0.25; 0.25; 0.27
Boundary condition		
Boundary type xp	CPML	CPML
Boundary air buffer, number of cells xp	8	9
Boundary CPML, number of cells xp	8	8
Boundary type xn	CPML	CPML
Boundary air buffer, number of cells xn	8	9
Boundary CPML, number of cells xn	8	8
Boundary type yp	CPML	CPML
Boundary air buffer, number of cells yp	8	9
Boundary CPML, number of cells yp	8	8
Boundary type yn	CPML	CPML
Boundary air buffer, number of cells yn	8	9
Boundary CPML, number of cells yn	8	8
Boundary type zp	CPML	CPML
Boundary air buffer, number of cells zp	8	9
Boundary CPML, number of cells zp	8	8
Boundary type zn	CPML	CPML
Boundary air buffer, number of cells zn	8	9
Boundary CPML, number of cells zn	8	8
Material type		
Air		
ε_r =	1	1
μ_r =	1	1
σ^e =	0	0
σ^m =	0	0
Copper		
ε_r =	1	1
μ_r =	1	1
σ^e =	5.8e7	5.8e7
σ^m =	0	0
RT5880 (dielectric)		
ε_r =	2.2	2.2
μ_r =	1	1
σ^e =	0.0001	0.0001
σ^m =	0	0

Continue next page…

SETUP DEFINTION	**In free space**	**On metal surface 107x175 mm^2**
CPML _ABC		
n_{pml}	3	3
σ_{factor}	1.3	1.3
K_{max}	7	7
α_{min}	0	0
α_{max}	0.05	0.05
CPML layer in term of cells	8	8
Output parameters		
Frequency domain parameters		
Frequency start (GHz)	0.5	0.5
Frequency end (GHz)	1.5	1.5
Frequency step (GHz)	0.001	0.001
Far field frequencies		
Frequency (GHz)	0.935	0.935

APPENDIX 3: UHF PATCH TAG ANTENNA MEASURED WITH LINEAR AND CIRCULAR POLARIZED ANTENNA

Appendix 3. Table 1*. Comparison of the linear and circular polarized antenna used in the measurement setup.*

Description	**Linear polarized antenna**	**Circular polarized antenna**
Model	ALR- 8610-L	ALR-9610-BC
Company	Alien technology	Alien technology
Working frequency	865.6MHz-867.6MHz	915MHz
Gain	6dBi	6dBi
Polarization	Linear	Circular

Appendix 3. Table 2. *Read range comparison in different environments using Alien RFID gateway and linear polarized antenna.*

Attenuation	**Free space**		**On metal surface 200x200 mm^2**		**On box of cans**	
	Average* (read/s)	Maximum reliable distance	Average* (read/s)	Maximum reliable distance	Average* (read/s)	Maximum reliable distance
0dB	169	4.50 m	170	4.30 m	169	3.85 m
6dB	169	2.30 m	170	2.20 m	172	1.25 m
10dB	172	1.26 m	168	1.20 m	171	0.88 m

The attenuation affects the total radiated power from the gateway. The attenuation may represent any loss not considered during the measurement, i.e. connections, cable loss. The average read per second is the amount of times the tag is reading per second until it is not more identified. The maximum reliable distance is the maximum distance at which the tag will respond.

Appendix 3. Table 3. *Read range comparison for circular polarized antenna using Alien RFID gateway using circular polarized antenna.*

Attenuation	**Free space**		**On metal surface 200x200 mm^2**		**On box of cans**	
	Average* (read/s)	Maximum reliable distance	Average* (read/s)	Maximum reliable distance	Average* (read/s)	Maximum reliable distance
0dB	173	2.05 m	172	1.90 m	171	1.55 m
6dB	170	1.40 m	169	1.25 m	173	0.75 m
10dB	168	0.80 m	172	0.73 m	172	0.42 m

*the average read varies from 169/175 in general for all the measurements.

APPENDIX 4: SIMULATION PERFORMANCE RESULT FROM HFSS OF PATCH TAG ANTENNA IN FREE SPACE AND ON METAL SURFACE

Figure of merit	In free space	On metal surface 200x200mm^2	Comments
-10dB PRC BW [MHz]	929-935	932.5-938	
Total Gain	5dBi	6.25 dBi	Average from 900MHz to 950MHz, for tag located at $\theta = 0, \varphi = 0$
Realized Gain	4.77 dBi	6.12 dBi	Maximum value, tag located at $\theta = 0, \varphi = 0$, 935MHz.
Radiation efficiency	90.5%	79%	Average from 900MHz-950MHZ